Jerzy Haber Institute of Catalysis and Surface Chemistry
Polish Academy of Sciences

Surface and interface properties of metal- oxide magnetic nanostructures

by

Ewa Młyńczak

Supervisor: prof. dr hab. Józef Korecki

This work was accomplished within the Krakow Interdisciplinary PhD-Project in Nanoscience and Advanced Nanostructures which is operated within the Foundation for Polish Science MPD Programme co-financed by the EU European Regional Development Fund

Kraków, 2013

Contents

Preface

This thesis is based on the experimental work carried out in Jerzy Haber Institute of Catalysis and Surface Chemistry, Polish Academy of Sciences, in close collaboration with the Department of Solid State Physics, AGH University of Science and Technology, both located in Kraków, Poland. An important part of the research was also conducted in the National Center on nanoStructures and bioSystems at Surfaces (S3) CNR-INFM in Modena, Italy.

I am grateful to my supervisor, prof. dr hab. Józef Korecki, for introducing me to the field of surface science. Thank you for your support and guidance during preparation of this thesis. I am also very grateful to dr hab. Nika Spiridis, who shared with me the wide knowledge of the UHV and surface science techniques. I had a great pleasure of working with dr Ewa Madej, Barbara Figarska, Magdalena Szczepanik- Ciba, Kinga Freindl, Tomasz Giela, dr Dorota Wilgocka-Ślęzak, dr Michał Ślęzak, dr Tomasz Ślęzak, Anna Kozioł- Rachwał, Barbara Matlak, Krzysztof Matlak, dr Robert Socha and dr Jacek Gurgul. Thank you all.

I would like to express my gratitude to prof. Sergio Valeri, who gave me the opportunity to conduct part of my work within his research group in Modena, which gave me invaluable experience.

I am indebted to dr Paola Luches, who was supervising my work in Modena. You gave me the best example of how to conduct the valuable research keeping the work- life balance. Thank you for your patience and willingness to explain everything I was asking for.

I would also like to thank all the other people from the SESAMo and SUP&RMAN labs in Modena, who were very helpful and kind for me, especially dr Alessandro di Bona, dr Stefania Benedetti and dr Alberto Rota. Thank you.

Abstract

This thesis investigates the relation between structure and magnetism of epitaxial bilayers composed of Fe and oxides of the rock salt crystal structure i.e. MgO, FeO, CoO and NiO. The bilayers were prepared in ultrahigh vacuum conditions using molecular beam epitaxy (MBE) to assure the reproducibility of the structures of high crystalline quality. Standard surface science techniques: low energy electron diffraction, Auger electron spectroscopy and x-ray photoelectron spectroscopy were applied to characterize the samples *in- situ*. The special attention was paid to the chemical structure of the interface between Fe and an oxide. The interface structure was examined using ^{57}Fe conversion electron Mössbauer spectroscopy. The magnetic properties of the bilayers were investigated *ex- situ* using the magnetooptic Kerr effect. The effects of the diverse conditions, which affect the multilayer properties, i.e. the deposition order, crystal orientation and the layers thicknesses were studied systematically.

The deposition order was studied for the Fe-MgO system, where it was found to highly influence the chemical and atomic structure of the interface. The interface was found to be partially oxidized for both Fe/MgO (iron deposited on MgO) and MgO/Fe (MgO deposited on iron), where 86% and 63% of the interfacial Fe atoms, respectively, formed bonds with oxygen. MgO/Fe interface was found to be highly defected, in contrast to Fe/MgO.

Furthermore, the method to prepare polar oxide films by oxidation of single metallic atomic layers was developed and applied to the growth of FeO(111) on MgO(111). The stable FeO(111) film as thick as 16ML was obtained. The Mössbauer measurements revealed its similarity to the bulk FeO in terms of the electronic and magnetic properties. Using the same method for the growth of CoO, the influence of the crystal orientation on the exchange bias in the Fe/CoO bilayers was studied. It was shown that despite the close similarities between the crystalline quality and stoichiometry of the CoO sublayers, as well as the similar chemical structures of the interfaces between Fe and CoO, the

exchange bias was ten times larger for Fe/CoO(111) as compared to Fe/CoO(001). This high exchange bias for Fe/CoO(111) was attributed to the combination of the magnetically uncompensated CoO(111) structure and the Fe layer of low magnetic anisotropy.

Finally, the NiO/Fe bilayers of different thicknesses were studied. The exchange bias, which exhibited the training effect was observed for 100ML NiO/24ML Fe, while no loop shift was detected for 50ML NiO/50ML Fe. For both samples, the magnetization reversal mechanism was studied and was found to be related to the occurrence of the exchange bias. The Mössbauer measurements allowed identification of the approximately 30 Å – thick, magnetically frustrated iron oxide interfacial layer of $Fe^{3+}_4Fe^{2+}_1O_7$ stoichiometry, which was responsible for the training effect and complex magnetic anisotropy observed in the NiO/Fe bilayers.

Streszczenie

Tematyka niniejszej pracy doktorskiej obejmuje badania struktury oraz właściwości magnetycznych epitaksjalnych dwuwarstw złożonych z Fe oraz tlenków o strukturze krystalicznej typu NaCl (B1): MgO, FeO, CoO oraz NiO. Dwuwarstwy zostały wytworzone w warunkach ultra wysokiej próżni (UHV) metodą epitaksji z wiązek molekularnych (MBE), co zapewniło powtarzalność próbek o wysokiej jakości struktury krystalicznej. Standardowe techniki charakteryzacji powierzchniowej w warunkach UHV, takie jak dyfrakcja elektronów niskoenergetycznych, spektroskopia elektronów Augera oraz spektroskopia fotoelektronów zostały zastosowane *in situ*. Szczególną uwagę zwrócono na chemiczną strukturę warstwy granicznej pomiędzy Fe i tlenkiem. Struktura ta była badana za pomocą spektroskopii mössbauerowskiej elektronów konwersji czułej na izotop żelaza ^{57}Fe. Właściwości magnetyczne dwuwarstw określono za pomocą magnetooptycznego efektu Kerra, mierzonego *ex situ*. Przeprowadzono systematyczne badania wpływu kolejność depozycji, orientacji krystalicznej oraz grubości podwarstw na właściwości układów dwuwarstwowych.

Kolejność nanoszenia była badana w układzie Fe-MgO, gdzie pokazano jej znaczący wpływ na strukturę atomową oraz chemiczną warstwy granicznej. W obu konfiguracjach: Fe/MgO (żelazo naniesione na MgO) oraz MgO/Fe (MgO naniesione na żelazie) warstwa graniczna okazała się być częściowo utleniona. 86% oraz 63% atomów Fe, odpowiednio dla Fe/MgO oraz MgO/Fe, wytworzyło w warstwie granicznej wiązania z tlenem. Stwierdzono, że warstwa graniczna MgO/Fe jest znacząco zdefektowana, w przeciwieństwie do Fe/MgO.

Opracowano metodę wytwarzania polarnych warstw tlenkowych poprzez utlenianie pojedynczych warstw atomowych metalu, którą zastosowano do wzrostu FeO(111) na MgO(111). Otrzymano stabilny film FeO(111) o grubości 16 ML. Pomiary mössbauerowskie pozwoliły na określenie jego właściwości elektronowych oraz magnetycznych, bardzo zbliżonych do litego FeO. Stosując podobną metodę preparatyki dla CoO, zbadano wpływ orientacji krystalicznej

na sprzężenie wymienne typu ‘exchange bias’ (EB) w dwuwarstwach Fe/CoO. Pokazano, że pomimo zbliżonej jakości struktury krystalicznej oraz stechiometrii podwarstw CoO, jak również struktury chemicznej warstwy granicznej pomiędzy Fe i CoO, wielkość efektu EB była dziesięciokrotnie większa dla Fe/CoO(111), niż dla Fe/CoO(001). Tak duża wartość EB dla Fe/CoO(111) została wytłumaczona w oparciu o współdziałanie dwóch efektów: magnetycznego nieskompensowania warstwy CoO(111) oraz niewielkiej anizotropii magnetokrystalicznej warstwy Fe.

Ostatnim dyskutowanym tematem jest wpływ grubości podwarstw w układzie NiO/Fe na efekt EB. Efekt ten, podlegający zjawisku treningu został zaobserwowany dla układu 100ML NiO/24ML Fe, podczas gdy dla 50ML NiO/50ML Fe nie wykryto żadnego przesunięcia pętli histerezy. Dla obu próbek, badano mechanizm przemagnesowania, który okazał się być zdeterminowany efektem EB. Pomiary mössbauerowskie pozwoliły na identyfikację granicznej warstwy tlenku żelaza o stechiometrii $Fe^{3+}{}_4Fe^{2+}{}_1O_7$ i grubości około 30 Å, której zaburzona struktura magnetyczna odpowiedzialna jest za efekt treningu oraz za złożoną anizotropię magnetyczną dwuwarstw NiO/Fe.

List of Publications

The main findings of this thesis are described in the following papers:

I. ‘*Epitaxial MgO/Fe(001) and Fe/MgO(001): structures of the interfaces*’, E. Młyńczak, K. Freindl, N. Spiridis, J. Korecki, J. Appl. Phys. 113, 024320 (2013)

II. ‘*Layer-by-layer epitaxial growth of polar FeO(111) thin films on MgO(111)*’, J. Gurgul, E. Młyńczak, N. Spiridis, J. Korecki, Surf. Sci. 606, 711 (2012)

III. ‘*Fe/CoO(001) and Fe/CoO(111) bilayers: the effect of crystal orientation on the exchange bias*’, E. Młyńczak, B. Matlak, A. Kozioł- Rachwał, J. Gurgul, N. Spiridis and J. Korecki, Phys. Rev. B, (2013), accepted

IV. ‘*NiO/Fe(001): magnetic anisotropy, exchange bias and interface structure*’, E. Młyńczak, P. Luches, S. Valeri, and J. Korecki, J. Appl. Phys. 113, 234315 (2013)

Publications related to, but not included in the thesis:

1. ‘*Growth and electronic and magnetic structure of iron oxide films on Pt(111)*’, N. Spiridis, D. Wilgocka- Ślęzak, K. Freindl, B. Figarska, T. Giela, E. Młyńczak, B. Strzelczyk, M. Zając and J. Korecki Phys. Rev. B 85, 075436 (2012)
2. ‘*Magnetic properties of the Fe-MgO interface studied by Mössbauer spectroscopy*’, J. Balogh, I. Dézsi, Cs. Fetzer, J. Korecki, A. Kozioł-Rachwał, E. Młyńczak, A. Nakanishi, Phys. Rev. B 87, 174415 (2013)

1. Introduction

The emergence of the ultra high vacuum (UHV) technology in the 1970' opened a new route of the experimental research devoted to surface science, which combines chemistry, physics and materials research. The possibility to obtain atomically clean surfaces and to analyze them using electron - based methods opened new opportunities of fabrication and characterization of the nanoobjects having properties unknown in the bulk phases. Nanoparticles of the noble metals that show high catalytic activity [1] or metallic multilayer structures, where giant magnetoresistance (GMR) occurs [2] are some of the most striking examples. The novel properties of the nanostructures are related to their size, comparable with the length scales of the phenomena involved, e.g. the mean free- path of electrons, spin diffusion length or the magnetic domain wall widths [4]. What is more, with the reduction of size, the role of surface, and interfaces, becomes more and more important. The chemical and physical properties of surfaces are so much different from the bulk phases, that surfaces are often called “a different state of matter” [5].

Among the ultrathin layered nanostructures, a group of the metal- oxide magnetic nanostructures stands out as exhibiting the magnetic phenomena like tunneling magnetoresistance (TMR) or exchange bias (EB), which are intriguing from the point of view of basic research and are also applied in magnetic tunnel junctions (MTJ), which find wide applications in the fields of magnetic sensing and data storage. MTJ is a trilayer structure, where an ultrathin (approximately 1 nm) isolating layer is sandwiched between the two ferromagnetic layers. Thanks to the tunneling effect, current can flow through this kind of structure, and the resistivity of the structure depends on the relative orientation of the magnetizations in two ferromagnetic electrodes, being maximum where the two are antiparallel and minimum when they are parallel. This property is called TMR. MTJ can be switched between the high- and low- resistance states if the magnetization directions in the two electrodes can be independently switched, for example when the magnetization of one of the electrodes is pinned. Pinning is realized using the EB effect, where the magnetic hysteresis loop of one of the ferromagnetic electrodes becomes wider and shifted relative to the zero field thanks to the proximity of an additional antiferromagnetic layer.

The magnetic properties of the multilayers, like TMR and EB crucially depend on the chemical, atomic and spin structure of the interfaces between the layers. However, the relations between the structure and magnetism are often elusive due to the complexity of the systems or controversial due to the diversity of preparation and characterization methods of the nominally similar systems. Therefore, there is strong demand for the experimental research on the model nanostructures prepared under the precisely controlled conditions, which facilitates the interpretation of the experimental results and allows the general conclusions to be drawn.

Monoxides of the rock salt crystal structure: MgO, FeO, CoO and NiO are well suited for the model investigations. Besides the simple crystal structure, they are stable mechanically and chemically. The late transition metal oxides (NiO, FeO, CoO) possess a well- defined (at least in the bulk phase) antiferromagnetic structure with the relatively high Néel temperatures. All of them are insulators, which rules out the indirect exchange interactions related to the conduction electrons and make them applicable in the tunneling devices. The ferromagnetic metal with the best crystallographic surface match to the rock salt oxides is bcc-Fe. Fe is widely used as a constituent of the bimetallic multilayers, with Cr [2] or Au [7], but most important, Fe with MgO forms a prototypical epitaxial MTJ [8]. The highly spin- polarized Bloch states from Fe effectively couple into the MgO leading to a huge TMR effect [9].

2. Aim of the study

This thesis aims at finding and describing the relationship between the structure and the magnetic properties of the ultrathin layered metal-oxide materials. The importance of this goal lies equally in the field of the basic, curiosity-driven science and in the field of the applied science, as the acquired knowledge might help to design useful structures of the desired properties. To realize this goal, the simplest building blocks of the layered structures, i.e. the model bilayers, composed of Fe and an oxide of the rock salt structure (MgO, NiO, CoO) were chosen as subjects of the study. The combination of the precise characterization of the chemical and crystalline structure of the bilayers, with the magnetic measurements aimed at the identifying the structure-function interplay. A distinguishing feature of the applied approach is the special attention paid to the structure of the metal/oxide interface, examined using the conversion electron Mössbauer spectroscopy (CEMS), one of the few experimental methods suitable for the analysis of the buried interfaces.

3. Experimental methods

All the samples were prepared in the ultra high vacuum (UHV) using molecular beam epitaxy (MBE). Two UHV systems were used during this study, one located in the Jerzy Haber Institute of Catalysis and Surface Chemistry PAS in Krakow and the other in the National Center on nanoStructures and bioSystems at Surfaces (S3) CNR-INFM in Modena. The photographs that show the preparation chambers of both UHV systems are presented in Fig. 1.

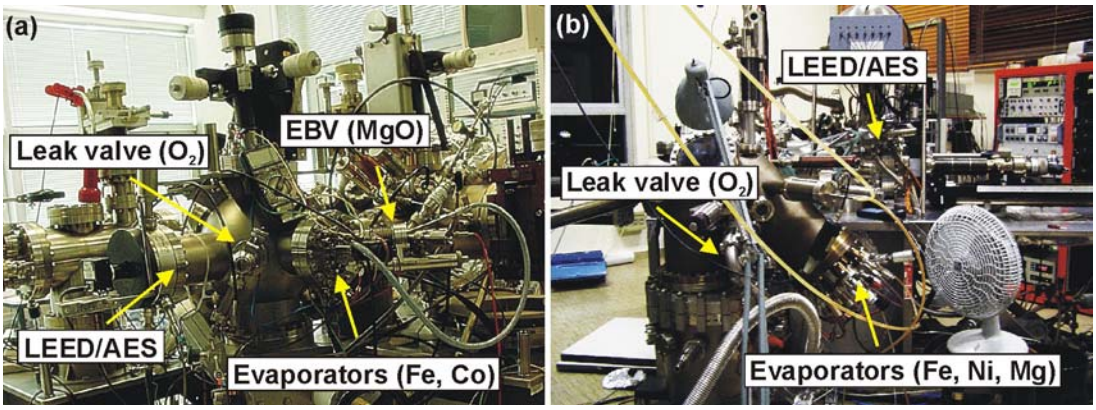

Fig. 1 UHV systems in Kraków (a) and in Modena (b)

All the samples were grown on the polished MgO single crystal substrates, which assured good epitaxial match with the bilayers and allowed *ex- situ* magnetic measurements. After introduction to the vacuum systems, the substrates were prepared using a standard method, which includes degassing by the resistive heating and annealing at the temperature of 600 °C for 30 minutes. The thickness of the deposited layers was monitored *in-situ* using a quartz microbalance. The Fe layers were deposited from the crucibles heated resistively. The oxide layers preparation method was suited to each oxide to assure the best quality of the deposited layers. MgO layers were deposited from the MgO piece wrapped in the tantalum foil, which was heated by the electron bombardment (electron beam evaporator, EBV). NiO was deposited reactively, i.e. metallic nickel was evaporated in the presence of oxygen, which pressure was carefully adjusted. CoO and FeO were prepared using post-deposition oxidation of the single metallic layers (layer-by-layer method). To apply CEMS for the study of the structure of the interfaces, the probe layers of the

Mössbauer-active ^{57}Fe were placed at the interfaces with the oxide layers, while the remaining part of the Fe films was completed with the ^{56}Fe isotope, which does not exhibit a Mössbauer effect. The schematic representation of the samples is presented in Fig. 2. The studied systems were either in the metal/oxide (CoO) or oxide/metal (NiO) configuration (Fig. 2 (a) and (b), respectively) or both (MgO). Besides the MBE evaporators, the UHV systems were equipped with the apparatus for the low energy electron diffraction (LEED) and Auger electron spectroscopy (AES). Both methods were used during sample preparation to examine the chemical composition (AES) and crystalline structure (LEED) of the substrates and the deposited ultrathin films. In Modena, X- ray photoelectron spectroscopy (XPS) was applied *in- situ* for the additional chemical characterization of the layers. In Krakow, XPS was performed in a separate UHV apparatus, accessible using a vacuum suitcase. For the study of the FeO(111) films grown on MgO(111), the entire FeO film was composed of ^{57}Fe and *in-situ* CEMS was applied (Fig. 3 (a)). All the samples were capped with the MgO protective layer, approximately 30 Å thick, to allow the *ex- situ* measurements.

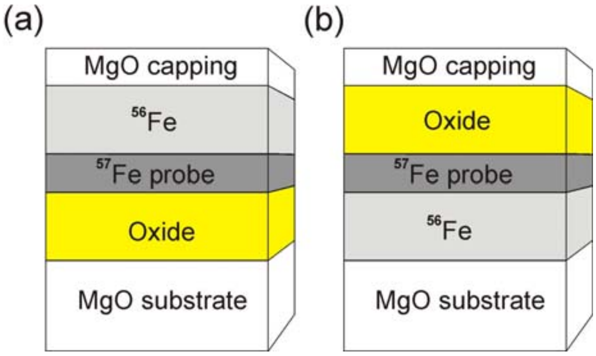

Fig. 2 Schematic representation of the samples showing the localization of the ^{57}Fe probe layer for a metal/oxide (a) and an oxide/metal interface structure (b)

For all the studied systems, *ex- situ* CEMS was used to reveal the chemical and magnetic structure of the metal-oxide interfaces. CEMS is a unique tool, which gives information on the hyperfine interactions within the probe layers. In course of the numerical analysis, the CEMS spectra were decomposed into components, each of which is characteristic for a given group of atoms. These groups of atoms are distinguished based on the combination of the hyperfine parameters: magnetic hyperfine field (B_{hf}), which brings information on the local magnetic properties, quadrupole splitting (QS), which depend on the electric field gradient at the nucleus and reflects the symmetry of the valence charge distribution and the chemically sensitive isomer shift (IS), which is related to the density of the *s* electrons in the nucleus.

The main components of the *in- situ* CEMS spectrometer are presented in Fig. 3 (a). The source of the gamma quanta is ^{57}Co, which decays to the excited state of ^{57}Fe by the electron capture with the half life time of 270 days. More than 90% of the excited ^{57}Fe atoms decay to the ground state through the 14.4 keV state with the mean lifetime of 141 ns. The moving ^{57}Co radioactive source is placed outside the vacuum system and illuminate the sample through a beryllium window. The most effective way to perform the Mossbauer spectroscopy for ultrathin films and surfaces is the detection of the conversion electrons [10], which is done by a channeltron. Thus, the experiment is performed in the scattering geometry, in contrast to the typical transmission Mössbauer measurements, where the gamma quanta are counted. The *ex- situ* CEMS measurements were accomplished using a standard spectrometer and He/CH$_4$ flow gas detector. Both experimental setups assured the ^{57}Fe-monolayer CEMS detection limit.

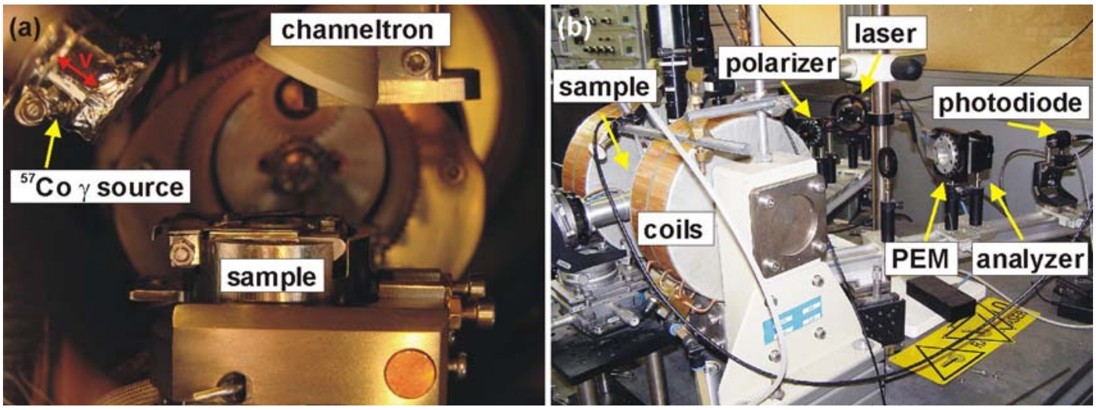

Fig. 3 (a) CEMS setup for the *in- situ* measurements (b) MOKE setup in Modena

The *ex- situ* magnetic measurements were performed using magnetooptic Kerr effect (MOKE). All the measurements were done in the longitudinal geometry. In the study of the NiO samples, a special variation of the MOKE technique based on the vector MOKE scheme [11] was applied (Fig. 3 (b)). In order to derive all three magnetization components (longitudinal - M_L, transversal - M_T and polar - M_P) it is necessary to perform MOKE using four different light polarizations: *s*, *p*, *sp* and *ps*. The light, *s*- and *p*- polarized, have the electric field component perpendicular and parallel, respectively, to the plane of incidence. The polarizations referred to as *sp* and *ps* are intermediate, with the electric field oriented +45° and -45° relative to the incidence plane, respectively. The hysteresis loops collected using these four light polarizations were further used to determine the magnetization components by calculating their linear combinations, where the proportionality coefficients had to be properly adjusted, i.e. $M_L \propto (I_S + I_P)$, $M_P \propto (I_S - I_P)$, $M_P \propto (I_{SP} + I_{PS})$, and $M_T \propto (I_{SP} - I_{PS})$.

4. Results

The investigated structures showed diverse levels of complexity, related to the oxide type and its preparation method. The proper choice of the oxide preparation method was especially important for the oxide/metal structures, for which oxygen might easily react with the exposed Fe surface in the first stages of oxide growth. On the other hand, the interface structure in the metal/oxide configuration was expected to reflect the intrinsic chemical interactions between the two constituents. In the case of the Fe-MgO bilayers, which represent the prototypical metal-oxide system, the early theoretical study predicted lack of the electronic interactions between Fe and MgO [12]. In contrast, for the structures composed of the transition metal oxides (CoO, NiO), thermodynamic considerations predict that Fe competes with the corresponding metals in terms of the oxygen affinity, which may result in the oxidation- reduction reactions experimentally observable at the metal/oxide interfaces [13].

To obtain Fe/MgO and MgO/Fe structures in their purest form, MgO layers were deposited from an MgO piece, without oxygen being present in the chamber. Such a preparation method assures that the interface between the two materials is not additionally modified. After the investigation of the theoretically inert Fe-MgO bilayers, the next step towards the increased complexity of the system was the study of the bilayers composed of Fe (top layer) and CoO (bottom layer). For this configuration the effect of the Fe oxide formation as a result of the reactive deposition could be avoided but, on the other hand, CoO was predicted to interact chemically with Fe [13]. Finally, the bilayer in the oxide/metal configuration was studied, with NiO as an oxide layer. Due to the reactive deposition, the Fe layers were exposed to the oxygen flux at the very beginning of the oxide layer deposition resulting in the formation of the extended interfacial iron oxide layers.

In each of the studies reported here, the main objectives were chosen as to cover the widest spectrum of the factors that affect the structure and consequently, magnetism of the bilayers. Therefore, the effects of the deposition order (Fe-MgO), crystal orientation (Fe-CoO) and thickness of the individual layers (Fe-NiO) were investigated.

Paper I

'*Epitaxial MgO/Fe(001) and Fe/MgO(001): structures of the interfaces*' E. Młyńczak, K. Freindl, N. Spiridis, J. Korecki, J. Appl. Phys. 113, 024320 (2013)

In contrast to the theoretical expectations of the sharp interface between Fe and MgO [12], the CEMS study reported here showed that structure of this interface is complex, both for Fe grown on MgO and for MgO grown on Fe. Despite the lack of additional oxygen in the preparation chamber, both interfaces were found to be partially oxidized. The use of the ^{57}Fe probe layer as thin as a single monolayer enabled identification of the amount of the interfacial Fe atoms that formed bonds with the oxygen, which equaled to 63% and 86%, for MgO grown on Fe and Fe grown on MgO, respectively. However, no well-defined stoichiometric iron oxide phases were detected, which is not surprising, taking into account their 2-dimesional character. What is more, for the MgO grown on Fe, 14% of the oxidized Fe sites were found to be defective (located at steps, corners or kinks). This finding is attributed to the imperfections of the Fe probe layer onto which MgO was deposited. In contrast, the reversed interface was found to be almost defect-free, which proves the crystalline perfection of the MgO film. The magnetic hyperfine field of the Fe atoms located away from the MgO/Fe interface was found to be modulated similarly to the Fe subsurface atoms at the vacuum/Fe interface, while no such modulation was observed for Fe/MgO.

Therefore, even the bilayer, which was considered to have the simplest structure was found to be complex. The proposed models of both interfaces may be applied to perform the more realistic calculations of the TMR effect in the Fe/MgO/Fe magnetic tunnel junctions.

Papers II and III

'*Layer-by-layer epitaxial growth of polar FeO(111) thin films on MgO(111)*'. J. Gurgul, E. Młyńczak, N. Spiridis, J. Korecki, Surf. Sci. 606, 711 (2012)

'*Fe/CoO(001) and Fe/CoO(111) bilayers: the effect of crystal orientation on the exchange bias*', E. Młyńczak, B. Matlak, A. Kozioł-Rachwał, J. Gurgul, N. Spiridis and J. Korecki, Phys. Rev. B, submitted.

The importance of the crystal orientation on the properties of the bilayers that show the exchange bias emerges from different, orientation related, arrangements of the interfacial magnetic moments. The most interesting cases for the oxides of the rock salt structure are the magnetically compensated (001) surface and the magnetically uncompensated (111) surface. However, the studies dealing with the (111) oriented rocksalt oxides are sparse, due to the instability of the (111) rocksalt oxides crystals related to their polarity [14]. In order to deal with this problem, a highly controllable method of the layer-by-layer (LBL) deposition of the polar oxide thin films was applied to grow FeO(111). FeO was chosen as a subject of this introductory study in view of the Mössbauer spectroscopy, which allowed precise characterization of the growing films.

The LBL method resulted in the stabilization of the polar FeO(111) films, as thick as 16 monolayers (ML) onto the MgO(111) substrate. Before evaporation of the FeO films, MgO was carefully cleaned and covered with the homoepitaxial MgO layer to trap some intrinsic MgO contaminants (carbon, calcium). The LBL method included evaporation of a single metallic Fe layer, its oxidation by a carefully adjusted dosis of the molecular oxygen, and subsequent UHV annealing. This procedure resulted in the formation of a single atomic layer of FeO and had to be repeated until the desired thickness was reached. The resulting film was unreconstructed, as showed by LEED. CEMS performed *in-situ* proved that the FeO(111) film had the hyperfine pattern of wüstite, which showed that its electronic and magnetic structure was similar to the bulk structure. The low temperature (80 K) CEMS measurements indicated the magnetic order, as expected for FeO below Néel temperature (198 K for the bulk). The acquired knowledge of the preparation of the polar ultrathin films was subsequently used to grow (111)-oriented CoO layers. To allow the direct comparison, CoO(001) was also prepared using the same LBL method. CoO(001) and CoO(111) were the base for the growth of the Fe/CoO bilayers, for which the effect of crystal orientation on the exchange bias was investigated.

The resulting CoO bilayers of both orientations were carefully characterized in terms of their crystalline structure and stoichiometry. LEED showed that the CoO layers were highly ordered and unreconstructed. For both orientations, XPS measurements revealed the spectra characteristic for CoO, with the slightly reduced surfaces. The surface reduction was deemed to be the sufficient factor stabilizing the CoO(111) polar surface. The ^{57}Fe Mössbauer probe layers, 2ML thick, were deposited onto CoO films. The structures were completed with ^{56}Fe up to 50 Å. The two bilayers were similar also in terms of the chemical structure of the Fe/CoO interface, where a fraction of the monolayer of Fe was found to be oxidized and approximately 4 Å of Fe was found to be mixed with metallic Co. Fe layers grew epitaxially onto CoO, as shown by LEED. While for the CoO(001) Fe was (001) oriented, in the case of CoO(111) Fe was exposing the Fe(110) plane, which due to the symmetry reasons formed grains of the three equivalent directions, rotated by 120°. The intrinsic magnetic anisotropy of the Fe films was related to the growth mode. While for Fe/CoO(001) the anisotropy showed a four-fold symmetry, with the anisotropy constant very close to bulk Fe, for Fe/CoO(111) a weak uniaxial growth-induced magnetic anisotropy was found, which points to a weak or even lacking magnetocrystalline anisotropy for that case.

Field cooling was applied to investigate the exchange bias in the Fe/CoO bilayers. Despite the fact that the crystalline structure and stoichiometry of the CoO films was comparable for Fe/CoO(001) and Fe/CoO(111), and the two systems contained the interfaces very similar in terms of the chemical structure, their exchange bias performance was drastically different. For Fe/CoO(111), the structure containing the magnetically uncompensated antiferromagnet and the ferromagnet of the low magnetocrystalline anisotropy, the loop shift was found to be ten times larger (354 Oe) than for the magnetically compensated Fe/CoO(001) (37 Oe). Therefore, the decisive role of the crystal orientation on the exchange bias phenomenon was proven.

Paper IV

'*NiO/Fe(001): magnetic anisotropy, exchange bias and interface structure*' E. Młyńczak, P. Luches, S. Valeri, and J. Korecki, J. Appl. Phys. 113, 234315 (2013)

The most complex of the structures studied in the framework of this thesis was the NiO/Fe system. Similarly to Fe/CoO, NiO/Fe also exhibits the exchange bias effect, however as for every exchange bias system, certain structural conditions must be fulfilled to observe the loop shift. The antiferromagnetic layer must be thick enough to have sufficiently large magnetocrystalline anisotropy and on the other hand, the ferromagnetic layer must be thin enough to response to the exchange coupling with the antiferromagnet. Therefore, it was possible to chose the combinations of the thicknesses of both layers such that the exchange bias was ('EB+' systems) or was not observed ('EB-' systems), which were 100ML NiO/24ML Fe and 50ML NiO/50ML Fe, respectively. The structural model of the NiO/Fe interface was created based on the CEMS measurements. The nominal bilayer structures were found to contain the magnetically frustrated interfacial iron oxide layer, at least 30 Å thick, of the stoichiometry close to magnetite. The resulting structures could be thus described as $NiO/Fe^{3+}_4Fe^{2+}_1O_7/Fe$. What is more, because the bilayers were prepared in the preparation chamber equipped with the evaporators that are oriented at 45 ° relative to the sample surface, a growth- induced uniaxial anisotropy was superimposed on the magnetocrystalline anisotropy of the Fe layers. All these factors made the studied system very complex in terms of the magnetic properties and a special approach was needed to examine the magnetic anisotropies properly. The magnetooptic Kerr effect based on the vector- MOKE scheme of Vavassori [11] (Fig. 3) was applied. As a result, all three magnetization components were obtained and the mechanisms of the magnetization reversal were revealed.

The magnetic anisotropies were found to be uniaxial, induced by the oblique deposition. The magnetization reversal was found to proceed via simple in-plane rotation for the 'EB-' system. For the field cooled 'EB+' system, the reversal was incoherent, affected by the strong unidirectional coupling with the NiO layer, and the non-zero out-of plane magnetization component. The EB+ sample showed the training effect, i.e. a decrease of the loop shift for the subsequent field sweeps, which was related to the magnetically disordered interfacial iron oxide layer.

5. Concluding remarks

The main findings of the reported study originate from the precise characterization of the metal/oxide bilayers, especially in terms of their interfacial structure.

The two interfaces of the Fe/MgO/Fe structure, i.e. Fe/MgO and MgO/Fe were found to be non equivalent. The interface formed when MgO was deposited onto Fe layer was much more defected in terms of the number of the low coordinated Fe atoms (edges of the terraces, kink sites) as compared to the reversed, Fe/MgO interface, which point to the structural perfection of the MgO layer and the atomic- level imperfections of the Fe film. For both, only a fraction of the interface Fe atoms formed bonds with the oxygen atoms, 63% for MgO/Fe and 86% for Fe/MgO. All these differences, together with the absence of the magnetic hyperfine field modulation near the Fe/MgO interface are growth-related and are likely to be observed in other metal/oxide systems. When MgO is deposited onto the stable and relaxed Fe layer, formation of the MgO/Fe interface brings only a chemical modification of the Fe surface. Therefore, because the electronic interaction between Fe and MgO is weak [12], the near surface magnetic hyperfine fields remain unaffected. On the other hand, to form the reversed interface, Fe is grown on the MgO film, experiencing misfit- related strain and being dependent on the quality of the oxide surface. All these findings might help to understand the magnetotransport properties of the Fe/MgO/Fe MTJ. They can be also applied in the studies of the multilayer structures where due to the large number of the interfaces, their role is decisive.

As far as the studied exchange- bias systems are concerned, the great sensitivity of this phenomena on the structural aspects of the bilayers should be stressed. The critical role of the uncompensated spins on the magnitude of exchange- bias was proven for the Fe/CoO epitaxial bilayers. This observation may be used to prepare the systems for which the magnitude of the exchange bias could be altered by the modification of the number of the uncompensated spins, for example using the vicinal substrates. Furthermore, the exchange- bias magnitude might be also enhanced by the preparation of the multilayer structures, with the increased number of the uncompensated interfaces.

The study of the NiO/Fe bilayers showed that the interfacial region formed when an oxide is deposited reactively onto Fe layer have distinct magnetic properties, which strongly affects the bilayers characteristics. Therefore, it should be possible to modify the composition of the interfacial layer, e.g. by changing the oxide preparation conditions or introducing ultrathin layer of a given metal (here: nickel) to prevent Fe oxidation, and in this way to alter the bilayer magnetic properties, like the magnetization reversal pathways or the occurrence of the training effect. The crucial role of the thicknesses of the bilayer constituents was also shown, which indicates the need of future systematic studies of the thickness- related magnetic properties that might be performed on the wedged, or preferably double- wedged, samples.

References

[1] M. Haruta, Gold Bull. 37, 27 (2004)

[2] M. N. Baibich, J. M. Broto, A. Fert, F. Nguyen Van Dau, and F. Petroff, Phys. Rev. Lett. 61, 2472 (1988); G. Binasch, P. Grünberg, F. Saurenbach, and W. Zinn, Phys. Rev. B 39, 4828 (1989)

[3] C. Liu, E. R. Moog, and S. D. Bader, Phys. Rev. Lett. 60, 2422 (1988)

[4] '*Oxide ultrathin films*', ed. G. Pacchioni and S. Valeri, Wiley- VCH, Weinheim 2012

[5] '*Surface and Interface Science*', ed. K. Wandelt, Wiley- VCH, Weinheim 2012

[6] J.F. Lawler, R. Schad, S. Jordan and H. van Kempen, J. Magn. Magn. Mat. 165, 224 (1997)

[7] K. Takanashi, S. Mitani, M. Sano, H. Fujimori, H. Nakajima and A. Osawa, Appl. Phys. Lett. 67, 1016 (1995)

[8] S. Yuasa, T. Nagahama, A. Fukushima, Y. Suzuki and K. Ando, Nature Mater. 3, 868 (2004)

[9] J. Mathon, and A. Umerski, Phys. Rev. B 63, 220403(R) (2001)

[10] K. Nomura, Y. Ujihira, and A. Vértes, J. Radioanal. Nucl. Ch. 202, 103 (1996)

[11] P. Vavassori, Appl. Phys. Lett. 77, 1605 (2000)

[12] Ch. Li and A.J. Freeman, Phys. Rev. B 43, 780 (1991)

[13] T. Regan, H. Ohldag, C. Stamm, F. Nolting, J. Lüning, J. Stöhr, and R. White, Physical Review B 64, 214422 (2001)

[14] J. Goniakowski, F. Finocchi and C. Noguera, Rep. Prog. Phys. 71, 016501 (2008)

Original Publications

Journal of
Applied Physics

Epitaxial MgO/Fe(001) and Fe/MgO(001): Structures of the interfaces

E. Młyńczak, K. Freindl, N. Spiridis, and J. Korecki

Citation: J. Appl. Phys. **113**, 024320 (2013); doi: 10.1063/1.4775707

View online: http://dx.doi.org/10.1063/1.4775707

View Table of Contents: http://jap.aip.org/resource/1/JAPIAU/v113/i2

Published by the American Institute of Physics.

Related Articles

Feedback-controlled electromigration for the fabrication of point contacts
Appl. Phys. Lett. 102, 023105 (2013)

Tunable conductivity at LaAlO3/SrxCa1−xTiO3 (0≤x≤1) heterointerfaces
Appl. Phys. Lett. 102, 012903 (2013)

Electrical characterization of inorganic-organic hybrid photovoltaic devices based on silicon-poly(3,4-ethylenedioxythiophene):poly(styrenesulfonate)
Appl. Phys. Lett. 102, 013501 (2013)

Interface relaxation and band gap shift in epitaxial layers
AIP Advances 2, 042185 (2012)

Methodological aspects of the quantum-chemical description of interface dipoles at tetrathiafulvalene/tetracyanoquinodimethane interfaces
J. Chem. Phys. 137, 174708 (2012)

Additional information on J. Appl. Phys.

Journal Homepage: http://jap.aip.org/

Journal Information: http://jap.aip.org/about/about_the_journal

Top downloads: http://jap.aip.org/features/most_downloaded

Information for Authors: http://jap.aip.org/authors

JOURNAL OF APPLIED PHYSICS **113**, 024320 (2013)

Epitaxial MgO/Fe(001) and Fe/MgO(001): Structures of the interfaces

E. Młyńczak,[1,a)] K. Freindl,[1] N. Spiridis,[1] and J. Korecki[1,2]
[1]*J. Haber Institute of Catalysis and Surface Chemistry, Polish Academy of Sciences, ul. Niezapominajek 8, 30-239 Kraków, Poland*
[2]*Faculty of Physics and Applied Computer Science, AGH University of Science and Technology, al. Mickiewicza 30, 30-059 Kraków, Poland*

(Received 20 November 2012; accepted 20 December 2012; published online 14 January 2013)

The chemical, electronic and magnetic structures of the interfaces between Fe(001) and MgO(001) thin films were studied using conversion electron Mössbauer spectroscopy (CEMS). A 1 ML thick ^{57}Fe probe located at either of the interfaces in the MgO/^{56}Fe/MgO epitaxial structure enabled precise measurements of the interfacial hyperfine interactions. Analysis of the CEMS spectra showed that both the "MgO/Fe" and "Fe/MgO" interfaces are partially oxidized (63% and 86%, respectively), although, despite good crystallinity, no well-defined iron oxide phases were detected. At the "MgO/Fe" interface, 14% of the oxidized Fe sites were found to be defective (located at steps, corners or kinks). The "Fe/MgO" interface, from which the formation of ^{57}Fe islands of at least 3 ML in height was inferred, was found to be almost defect-free. No modification of the hyperfine parameters of Fe atoms located away from the interface was detected for "Fe/MgO," in contrast with the "MgO/Fe" interface. Approximately 6% of the probe layer diffused into the MgO films at both interfaces. *© 2013 American Institute of Physics*.
[http://dx.doi.org/10.1063/1.4775707]

I. INTRODUCTION

Epitaxial metal-insulator bilayers and multilayers are the subject of intensive scientific activity due to the variety of magnetic phenomena related to their reduced dimensionality, which is important from the viewpoint of basic research and applications.[1] Epitaxial Fe/MgO(001) is considered to be a model system in this class of materials.[2] In the (001) oriented Fe/MgO/Fe epitaxial trilayers, a tunneling magnetoresistance (TMR) effect occurs that originates from the coherent tunneling of fully spin-polarized electrons across the MgO barrier.[3] The TMR is theoretically expected to reach 1000% for junctions having a crystalline barrier thickness of $t_{MgO} \approx 40$ Å.[3,4] Quantum tunneling of spin-polarized electrons is also responsible for interlayer exchange coupling (IEC), which is observed in the Fe/MgO/Fe trilayers when $t_{MgO} < 15$ Å.[5,6] The IEC changes from antiferromagnetic for the thinnest barriers ($t_{MgO} < 8$ Å) to ferromagnetic. Both the TMR and IEC depend crucially on the crystalline and chemical quality of the layers and interfaces that form the trilayer structure. The TMR values measured for epitaxial Fe/MgO/Fe reach 180% at room temperature[7,8] and approximately 300% at 10 K.[8] These low experimental values of the TMR relative to the theoretical predictions may be attributed to the nature of the trilayer growth, which is marked by lattice mismatch, by structural defects, by intermixing and hybridization effects at the interfaces and especially by the formation of Fe-O bonds. First-principles calculations showed that a single atomic layer of FeO present at the interface causes a reduction in the tunneling magnetoconductance of the Fe/MgO/FeO/Fe magnetic tunnel junction of one order of magnitude.[9] Interfacial oxidation is also known to give rise to perpendicular coupling of Fe magnetizations for barriers with $t_{MgO} < 5$ Å.[10]

The occurrence of FeO_x at the MgO/Fe interface (MgO is deposited on Fe, deemed the "bottom" interface in the Fe/MgO/Fe trilayer) was shown by several groups,[11–14] while others did not find any evidence of this occurrence.[15–17] Similarly, there is no consensus concerning the reversed, Fe/MgO, "top" interface. Some experimental results support the lack of interactions between Fe and MgO,[18,19] as found theoretically,[20] and the formation of Fe-O bonds at that interface.[21–23] These differences could be due to different experimental conditions,[24] but a clear explanation is still lacking. The atomic arrangements at both interfaces were studied experimentally and theoretically, leading to the widely accepted model of the Fe atoms sitting on top of the O atoms (Fe/MgO configuration) and the O atoms sitting on top of the Fe atoms (MgO/Fe configuration).[4,11,12,20–22,24,25] Calculations show that the formation of Fe-O chemical bonds between the interface iron and the oxygen in MgO is unlikely,[9,20] while the Mg-Fe covalent bond, at the second-nearest neighbor distance, predominantly determines the interfacial bond strength.[25] These type of interfaces, with no oxygen incorporated into the Fe atomic layers, will be referred to as the "metallic top" interface (Fe/MgO) and the "metallic bottom" interface (MgO/Fe). In contrast, a recent contribution of Beltrán *et al.*[26] presents a first-principles analysis where the most stable configuration of the first MgO layer grown on Fe without Fe-O layer formation is Mg sitting on top of Fe, while O on top of Fe is preferred only when an iron oxide layer is formed. For the MgO/Fe configuration, where the formation of an FeO layer was shown using surface x-ray diffraction, the following geometrical model of the oxidized interface was found: oxygen atoms are placed in the fourfold hollow sites of the Fe interfacial layer with a small

---

[a)] Electronic mail: ncmlyncz@cyf-kr.edu.pl.

(0.2 Å) shift above the Fe surface[12], which coincides with the *ab initio* calculations.[24] This type of interfacial structure will be referred to as the "oxidized" bottom interface. For the Fe/MgO interface grown in ultra-high vacuum (UHV) conditions, Tusche *et al.*[22] found that some Fe atoms substitute for the Mg ones in the interfacial MgO layer, forming a 2-dimensional iron oxide. We term such Fe sites the "oxidized top" interface.

In the context of the serious discrepancies among the many experimental and theoretical works on this subject, we undertook experimental verification of the local atomic structure at both Fe-MgO interfaces using a unique tool, conversion electron Mössbauer spectroscopy (CEMS). The analysis of the interfaces between thin films of Fe and MgO was performed for two configurations: with the Fe epitaxial film (i) as a buffer layer ("MgO/Fe") and (ii) as a capping layer ("Fe/MgO"), which simulated the "bottom" and the "top" interfaces, respectively. Ultrathin ^{57}Fe probe layers were placed alternatively at one or the other of the interfaces in an epitaxial MgO(001)/^{56}Fe(001)/MgO(001) structure grown on a cleaved MgO single crystal by molecular beam epitaxy (MBE). CEMS is a well-adapted tool for local studies of structural and magnetic properties at surfaces and interfaces.[27] Placing the Mössbauer isotope ultrathin probes at the region of interest in a thin film sample enables measurements with monoatomic layer precision. CEMS directly measures the nuclear hyperfine parameters: the hyperfine magnetic field (B_{hf}) that is a measure of the local magnetization, the isomer shift (IS) that is determined by the valence state and the quadrupole interaction (ε) that indicates the lowering of the local charge distribution symmetry from cubic or hexagonal. These parameters are the fingerprints of the electronic and chemical states of the Mössbauer atoms present in the bulk samples. However, ultrathin films are complex, and the bulk Mössbauer reference data are not representative of them. The modification of the hyperfine parameters due to reduced dimensionality does not always allow an unambiguous interpretation of the CEMS spectra. Nevertheless, it is often possible to distinguish atoms in different oxidation and magnetic states, which allows us to analyze the interactions between adjacent layers of Fe and MgO and to reveal the real atomic arrangements at the interfaces. CEMS is sensitive enough to detect the atomic sites with lowered coordination (atomic steps, kink sites, vacancies and adatoms), which gives additional motivation for using this technique to characterize interfaces. In the discussion of the CEMS results, "defected" interface structures will be introduced to complete the picture of the interfacial sites that are present at the real interface.

II. EXPERIMENT

The samples were prepared in a multi-chamber ultra-high vacuum (UHV) system with a base pressure of 1×10^{-10} mbar. MgO(001) substrates were cleaved *ex-situ* before introducing them into the preparation chamber. The substrates were then degassed and annealed under UHV at 600 °C for 30 min, leading to a clear, background-free (1×1) low energy electron diffraction (LEED) pattern. Thin films were prepared using MBE. Magnesium oxide was evaporated from an MgO piece using an electron beam evaporator, while Fe was evaporated from a BeO crucible heated by a wrap-around tungsten coil and embedded in a water-cooled shroud. Using electron beam evaporation under UHV conditions drastically reduces the amount of oxygen present in the preparation chamber compared with reactive evaporation. Due to this effect, we are able to investigate intrinsic MgO/Fe interfacial properties, which are not affected by massive Fe oxidation. The thicknesses of the films were determined with an accuracy of approximately 0.2 ML using a quartz microbalance previously calibrated with x-ray reflectivity data.

The sharpness of the studied interfaces is determined mainly by the flatness of the substrate layer, and, therefore, the preparation conditions of "MgO/Fe" and "Fe/MgO" were different. The first step in the "MgO/Fe" preparation procedure was the deposition of 200 Å of ^{56}Fe onto MgO(001) at room temperature, which was subsequently annealed at 550 °C to obtain an atomically flat surface. LEED showed sharp diffraction spots, indicating good crystalline quality (Fig. 1(a)). However, as observed in a pattern at an energy of 70 eV, additional spots from the $(\sqrt{2} \times \sqrt{2})$R45° reconstruction were present. This reconstruction type for Fe/MgO(001) is not precisely interpreted, though it is usually assumed to be induced by carbon, which segregates from the MgO(001) substrate towards the Fe surface.[28] A 1 ML ^{57}Fe probe layer [1 ML Fe(001) = 1.43 Å] was deposited at an elevated temperature (380 °C) to promote ^{57}Fe surface diffusion. Possible interdiffusion between the atoms of the ^{57}Fe probe and the ^{56}Fe layer was taken into account in the analysis of the CEMS spectra. The Fe layer was then covered with 50 Å of MgO, which completed the bilayer structure and served as a capping layer.

To ensure that the "Fe/MgO" interface simulates the one present in Fe/MgO/Fe thin film structures accurately, instead

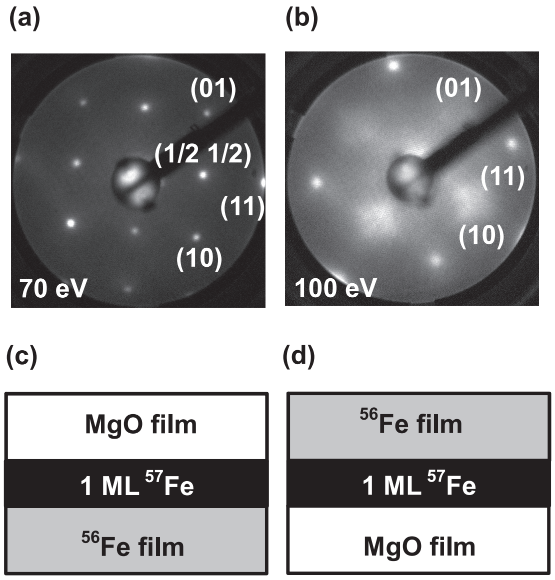

FIG. 1. LEED patterns for Fe layers: Fe as a buffer layer in "MgO/Fe" (a) and Fe as a capping layer in "Fe/MgO" (b) with the schematic representation of the samples for Mössbauer studies of the MgO/Fe (c) and Fe/MgO (d) interfaces.

of using a bare MgO substrate we used a homoepitaxial MgO film as a buffer for Fe deposition. 30 Å of MgO was deposited at 600 °C to enhance the surface diffusion. Because iron on top of MgO shows a strong tendency for cluster growth, the 1 ML ^{57}Fe probe and the following 50 Å of ^{56}Fe were deposited at room temperature. The Fe layer was not annealed to avoid promotion of interfacial oxidation-reduction reactions. The LEED pattern presented in Fig. 1(b) was selected to show the diffuse character of the spots, which is best visualized at an electron energy of 100 eV. The pattern shows (1 × 1) symmetry, proving the absence of surface reconstruction. The blurry diffraction spots indicate an increased roughness, which is caused by the room temperature deposition. The sample was capped with a 50 Å MgO protective layer for *ex-situ* CEMS measurements. The obtained "MgO/Fe" and "Fe/MgO" structures are presented schematically in Figs. 1(c) and 1(d).

CEMS measurements were carried out *ex-situ* at room temperature using a standard Mössbauer spectrometer equipped with a CEMS He/CH$_4$ flow proportional detector and a 100 mCi ^{57}Co/Rh source. The CEMS spectra were collected in the normal incidence geometry. Commercial software[29] was used to fit the spectra using a Voigt-line-based method, thus approximating the distribution of the hyperfine magnetic field B$_{hf}$ at a given site using a sum of Gaussian components.

III. CEMS RESULTS AND DISCUSSION

The CEMS spectra obtained for both interfaces, together with the corresponding fits are presented in Fig. 2. The spectra were fitted with the smallest possible number of components giving statistically good fit ($\chi^2 \approx 1$). Each component reflects the group of atoms characterized by different set of the hyperfine parameters, which depend on the coordination and chemical state of atoms. Relative weights of the components are directly related to the fraction of atoms in the given state. Knowing the thickness of the probe layer used, it is possible to calculate the amount of atoms corresponding to each component.

A. "MgO/Fe" interface

The "MgO/Fe" (bottom interface) spectrum was fitted with eight components, as shown in Fig. 2(a) and listed in Table I using Arabic numerals. Four of the components (components "1"–"4") have an IS value close to zero (relative to α-Fe), which indicates that the corresponding atoms form bulk Fe-like metallic bonds. These four "metallic" components have different values of B$_{hf}$ and ε. Taking into account the theoretical prediction of a lack of electronic interactions between Fe and MgO, we compare the values of the hyperfine fields found in our experiment with theoretical ones calculated for Fe atoms adjacent to vacuum (a "vacuum/Fe" interface). We use the calculations of the hyperfine magnetic field for Fe(001) surface (S) and subsurface (S-1) nuclei from Ohnishi *et al.*[30] The theoretical value of the total B$_{hf}$ for Fe(001) surface atoms (25.2 T) is significantly lower than the experimental value for the bulk (in the ground state, approximately 34 T[31]) as a result of the more

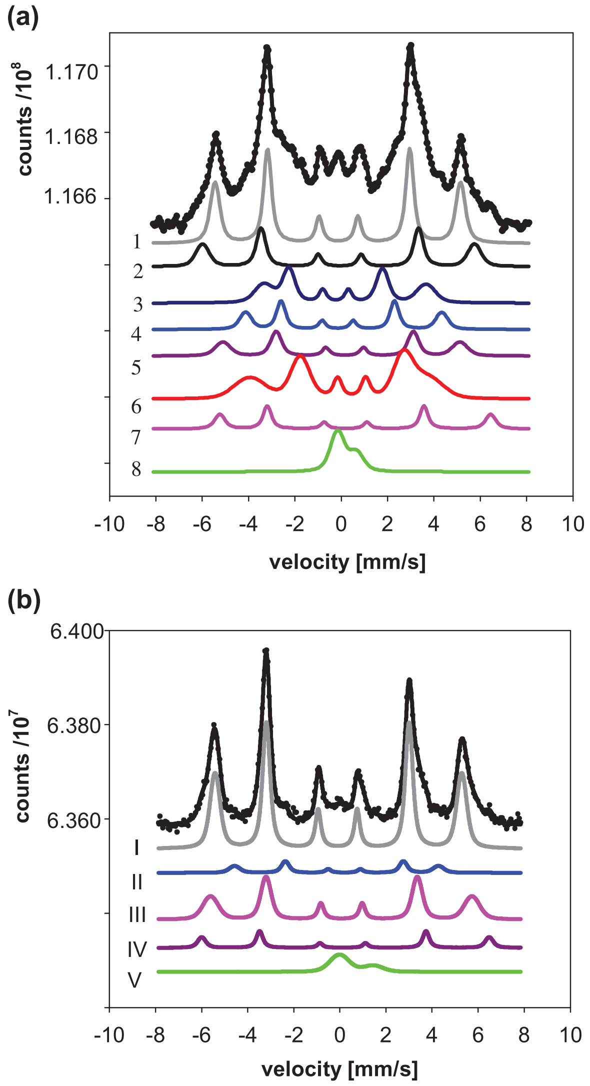

FIG. 2. CEMS spectra (dots) measured for (a) "MgO/Fe" (MgO/1 ML^{57}Fe/^{56}Fe) and for (b) "Fe/MgO" (^{56}Fe/1 ML^{57}Fe/MgO) with the results of the best fits and the deconvolution into spectral components (solid lines). The components are shifted for clarity. Numbers identifying each component correspond to Table I.

atomic-like character of the *4s* electrons. Atoms in the S-1 layer sense B$_{hf}$ fields of 39.5 T, which are higher than the Fe bulk value. The non-monotonic change in the hyperfine field with depth is related to Friedel-like oscillations of the valence electron density. In our "MgO/Fe" spectrum, we easily identify the metallic components having B$_{hf}$ values that follow the theoretical tendency, arising from the first, "S$_I$," layer (adjacent to MgO, components "3" and "4") and the second, "S$_I$-1," layer (component "2"), as well as of bulk character (component "1"). The appearance of these components corresponding to at least three interface-close layers, where a probe layer of 1 ML nominal thickness was used, could be interpreted as the formation of 3 ML thick ^{57}Fe islands on top of the ^{56}Fe substrate. However, the preparation conditions used in our study ensure the flatness of the ^{57}Fe probe, as the increased temperature promotes two dimensional growth over the nucleation of islands for Fe homoepitaxy.[32] Our explanation for the existence of "S$_I$-1" and bulk-like ^{57}Fe atoms is related to the diffusion of ^{57}Fe atoms

TABLE I. Hyperfine parameters derived from the numerical fits for "MgO/Fe" (MgO/1 ML^{57}Fe/^{56}Fe) and "Fe/MgO" (^{56}Fe/1 ML^{57}Fe/MgO) spectra. Numbers in parentheses indicate the last digit uncertainty resulting from the least squares fit analysis.

Interface	Component	IS[a] (mm/s)	ε or QS[b] (mm/s)	B_{hf}[c] (T)	RW[d] (%)	F_{ML}[e] (%)
"MgO/Fe"	1	−0.03(1)	−0.02(1)	32.9(1)	25(4)	—
	2	0.01(3)	−0.03(2)	36.4(4)	12(4)	—
	3	0.06(9)	0.20(9)	21.7(6)	13(3)	23
	4	0.08(4)	0.13(4)	26.3(3)	8(3)	14
	5	0.18(9)	−0.07(7)	31.7(5)	8(3)	14
	6	0.27(7)	−0.29(8)	23.8(3)	22(3)	39
	7	0.50(5)	0.21(4)	36.3(4)	6(2)	10
	8	0.35(5)	0.83(9)	—	6(0)	—
"Fe/MgO"	I	0.02(1)	0.01(5)	33.2(7)	57(7)	—
	II	0.12(6)	−0.17(6)	27.5(5)	5(1)	14
	III	0.17(3)	−0.01(2)	35.2(5)	25(7)	67
	IV	0.28(4)	0.06(4)	38.7(4)	7(3)	19
	V	0.8(1)	1.5(2)	—	6(1)	—

[a] IS is the average isomer shift with respect to α-Fe.

[b] Average quadrupole interaction (ε) (sextets) or quadrupole splitting (QS) (doublets).

[c] B_{hf} is the average hyperfine magnetic field.

[d] RW is the relative weight of the components.

[e] F_{ML} denotes the corresponding fraction of monolayer interface atoms calculated excluding the ^{57}Fe probe atoms located away from the interface.

from the probe layer into the ^{56}Fe film. The surface diffusion coefficient for single Fe atoms on an Fe(001) surface at the ^{57}Fe probe deposition temperature (380 °C) is approximately 2×10^{-7} cm^2 s^{-1}, which is four orders of magnitude larger than the coefficient at room temperature.[32] Therefore, we have strong evidence that interdiffusion between ^{57}Fe and ^{56}Fe is significant in our system.

As a consequence of diffusion, the component with a hyperfine magnetic field of $B_{hf} = 32.9$ T (component "1") could be interpreted as originating from the Fe atoms that diffused deeper than the "S_I-1" layer and attained bulk-like coordination, while the component with a hyperfine field of $B_{hf} = 36.4$ T (component "2") could be interpreted as originating from the sub-interface "S_I-1" atoms. Based on the relative weights of these two components, we can estimate the amount of ^{57}Fe atoms that penetrated into the ^{56}Fe film to be approximately 0.37 ML. To correctly assess the amount of interfacial atoms, we have to exclude from the calculation the ^{57}Fe atoms that diffused into the MgO layer. These atoms are revealed in the "MgO/Fe" spectrum by a doublet with IS = 0.35 mm/s (component "8"). The non-ferromagnetic character of this component proves that the corresponding Fe atoms are magnetically decoupled from the Fe film. The isomer shift value indicates that the Fe atoms are in a defected MgO matrix where ferric ions exist in complexes with cationic vacancies.[33] The amount of these isolated Fe atoms equals 0.06 ML. Knowing that 0.43 ML of ^{57}Fe atoms are located away from the interface, we can recalculate the fraction of interfacial atoms in the various chemical and coordination states as a percentage of the interfacial Fe monolayer (F_{ML} values in Table I). This calculation uses the assumption that the preference for a given site is not isotope-specific.

The dominant interfacial components are in the group characterized by distinctly positive values of the IS (components "5"–"7," 63% of the "MgO/Fe" interface in total). The isomer shift is a measure of the *s* electron density at the nucleus, which in the simplest case becomes smaller when the 4*s* electrons are shifted towards oxygen to form a covalent bond. This notion is valid if the bonds are formed only by 4*s* electrons, i.e., for lower oxidation states. For higher iron oxides, when the oxide formation requires transfer of an electron from the 3*d* shell, the indirect change in the 3*s* electron density induced by the modification of the Coulomb interaction with *d*-electrons must be considered. Within the reasonable assumption that the oxidation state of iron at the MgO/Fe interface does not exceed Fe^{2+} (the 3*d* electron does not take part in the bond formation), the increase in the IS parameter relative to Fe reveals a more oxidic character for the corresponding Fe atoms understood as the lowering of 4*s* electron density. The absence of higher iron oxides at the MgO/Fe interface is supported by the values of the hyperfine field measured for the oxidic components "5"–"7," which are lower than expected for Fe_3O_4 or for Fe_2O_3 (approximately 50 T).[31] However, the oxide phase formed at this interface cannot be identified as FeO because an isomer shift of approximately 0.9 mm/s is expected for a wüstite-type oxide.[31] The fact that the hyperfine parameters describing the oxidic components could not be interpreted as arising from any of the known stoichiometric oxide phases can be understood by taking into account the interfacial coordination of the iron atoms involved. Following the accepted models of interfacial oxidation, we can conclude that the oxygen atoms are located in approximately 60% of the fourfold hollow sites in the interfacial Fe layer.[12,24] It is worth noting that this result is in perfect agreement with the surface x-ray diffraction studies conducted by Meyerheim *et al.*,[11] where a $FeO_{0.6}$ stoichiometry was found for the iron oxide layer. Two of the oxidic components ("6" and "7") have significantly positive IS values (0.27 mm/s and 0.50 mm/s, respectively), which imply a strong shift in the Fe valence electrons towards the oxygen atoms with the possible formation of in-plane Fe-O bonds. These two components are also characterized by an increase in the ε value (−0.29 mm/s and 0.21 mm/s). The quadrupole interaction is a measure of the electric field gradient (EFG) at a nucleus that has an electric quadrupole moment. Generally, there are two sources of the EFG: (i) the valence (local) electron contribution and (ii) the lattice (non-local) contribution arising from the charges of all ions in the lattice.[34] Because the long-range interatomic contribution is usually one or two orders of magnitude smaller than the local contribution,[35] the quadrupole splitting observed in CEMS should be interpreted as the result of changes in the local charge symmetry. Possible mechanisms responsible for the aspherical character of the valence charge include charge transfer, changes in the directional bonding and shifts in the near neighbor nuclear positions. As a nonzero quadrupole interaction was observed for the interfacial Fe atoms, one could explain the aspherical valence charge solely as a result of the broken symmetry. However, as will be shown later, an increase in ε is not exhibited in the major part (86%) of the reversed "Fe/MgO" top interface and also in some parts (14%) of the discussed "MgO/Fe" bottom interface. In this context, this property cannot be understood as an intrinsic feature of all site types in the interfacial layers. It seems more appropriate to explain this effect as a result of the local changes in the symmetry of the 3*d* orbitals. These changes are associated with asymmetry in bond formation and/or with the expansion of the S_I-S_{I-1} interlayer distance (relaxation), which can reach 20% of the bulk value of 1.43 Å for the oxidized MgO/Fe interface.[12,24] Thus, the non-zero ε suggests that the corresponding atoms are located at perfect (not-defected) interfacial sites, where lattice relaxation is the most probable mechanism for the energy minimization.

A special comment is needed to account for the decreased hyperfine field ($B_{hf} = 23.8$ T) of component "6," which reflects the most abundant interfacial atoms (39%). Such a low B_{hf} is atypical not only for higher Fe oxides, as mentioned above, but also for the FeO-wüstite phase, where $B_{hf} = 38$ T was found for the antiferromagnetic state at low temperatures.[36] This result means that, similarly to the metallic sites (components "1"–"4"), the modification of the B_{hf} relative to the bulk is related not only to the formation of Fe-O bonds but also to the disturbance of the *4s* electron density arising from the broken symmetry at the interface. Using such an interpretation of the spectral component, we find that 49% of the interfacial atoms (components "6" and "7") are located at the "oxidized" MgO/Fe interface (Fig. 3(a)), with the oxygen atoms at the fourfold hollow sites of the Fe(001) surface. However, the local stoichiometry of the interfacial oxide layer does not need to be uniform along the entire interface, i.e., a planar oxide could be formed by iron atoms having one to four oxygen nearest neighbors. This non-uniformity is reflected in the differences in the hyperfine parameters for components "6" and "7". A higher oxidation state should be attributed to component "7" (10% of the "MgO/Fe" interface), where the formation of Fe-O bonds enhances the B_{hf} to 36.6 T. However, the determination of the actual number of oxygen nearest neighbors for these two components is not possible based only on the CEMS results. Calculations of the hyperfine field could elucidate this issue. The third oxidic component, (component "5," 14% of the "MgO/Fe" interface) is characterized by an IS value of 0.18 mm/s and by a hyperfine field of $B_{hf} = 31.7$ T, a value between those measured for components "6" and "7." This component is interpreted as originating from atoms which are located at the steps of terraces or at kink sites and experience a relatively strong chemical interaction with oxygen (the "defected oxidized" interface, Fig. 3(c)). The basis for this interpretation is the negligible quadrupole interaction, $\varepsilon = -0.07(7)$, observed for this component. This interpretation suggests that the ε value is averaged out due to the different orientations of the V_{zz} principal axis with respect to the hyperfine magnetic field, which is expected to occur at sites with a low Fe-Fe coordination within the steps that have a different orientation relative to the main crystallographic directions. Summarizing, we can conclude that 63% of Fe at the "MgO/Fe" interface has an oxidic character but does not form any distinct oxide phases in terms of typical 3-dimensional coordinations.

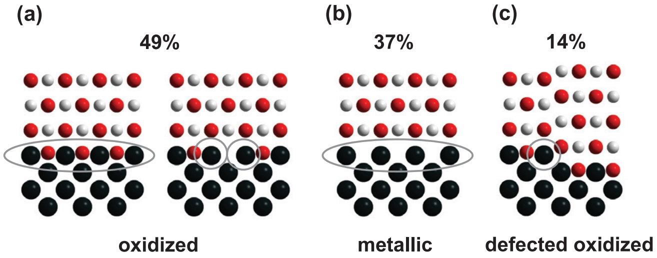

FIG. 3. Model of the "MgO/Fe" interface (MgO/1 ML^{57}Fe/^{56}Fe) showing the percentage of interface atoms located at the specific interfacial sites as identified using components of the CEMS spectrum: (a) "oxidized" sites (components "6" and "7"), (b) "metallic" sites (components "3" and "4") and (c) "defected oxidized" sites (component "5"). The ellipses encircle the corresponding Fe atoms. Large (black) balls—Fe, medium (red) balls—O, small (white) balls—Mg.

The remaining two components (components "3" and "4") reflect the population of ^{57}Fe atoms that retained their metallic character even though they are situated at the interface with MgO (location S_I, the "metallic" interface in Fig. 3(b)), which is reflected in the low hyperfine field values (as discussed above) and in the non-zero ε values. The total amount of these atoms equals 37%. This type of interface was shown to be formed under the Mg-rich conditions by *ab initio* calculations.[24] The difference between the atomic sites contributing to components "3" and "4" is insignificant, as both are characterized by very similar sets of hyperfine parameters. The strong quadrupole interaction ($\varepsilon = 0.20$ mm/s and $\varepsilon = 0.13$ mm/s), similar to components "6" and "7," indicates a lowered charge distribution symmetry. While ε was interpreted in terms of the expansion of the interlayer distance between the interfacial Fe layer and the "S_I-1" layer (relative to the bulk) for the oxidized part of the interface, the abrupt "metallic" MgO/Fe interface is characterized by the interlayer distance compression reaching 6%,[12,24] resulting in a similar value for ε. A slight increase in the isomer shift for components "3" and "4" (if any, taking into account experimental uncertainty) correlates well with the properties of Fe/vacuum and Fe/metal interfaces.[37]

B. "Fe/MgO" interface

The CEMS spectrum measured for "Fe/MgO" (top interface) (Fig. 2(b)) comprises five components, labeled with Roman numerals. The dominant one (RW = 57%) is a metallic component with a bulk character (component "I"). To interpret the high intensity of the signal coming from the bulk coordinated ^{57}Fe atoms for a nominally 1 ML thick ^{57}Fe probe, one has to recall the island growth mode of iron on MgO(001).[38] Due to the differences in the surface free energies of MgO(001) and Fe(001) (1.1 J/m^2 and 2.9 J/m^2, respectively[39]), formation of Fe islands is thermodynamically favored. Consequently, the ^{57}Fe probe formed three dimensional islands on MgO(001), and, in the next preparation step, the ^{57}Fe islands were covered with 50 Å of ^{56}Fe that completely buried the probe layer. As a result, only a fraction of the ^{57}Fe atoms were located at the Fe/MgO interface, while most of them gained bulk-like coordinations by being surrounded by other ^{56}Fe and ^{57}Fe atoms. The Fe layer was deposited at room temperature, so interdiffusion of ^{56}Fe and ^{57}Fe atoms can be neglected.[32] Hence, the relative weight of component "I," amounting to 57%, indicates that the ^{57}Fe islands formed on MgO were at least 3 ML high. The analysis of the "Fe/MgO" spectrum did not allow us to distinguish the Fe atoms located in the second Fe interfacial layer (S_I-1) from the Fe atoms with bulk coordination. The absence of hyperfine field modulation near this interface is surprising and differentiates it both from the "MgO/Fe" bottom interface measured directly in the present study and from the "vacuum/Fe" interface observed theoretically.[30] This difference must have its origin in the atomic structure of the interface formed by the reverse deposition order of its constituents. Similar to the "MgO/Fe" case, we could identify isolated Fe atoms that diffused into MgO and formed complexes with vacancies (the doublet with an $IS = 0.8$ mm/s).[33] Therefore, in total, only 37% of the ^{57}Fe probe layer atoms are located at the interface with MgO, and, analogous to the "MgO/Fe" case, this value will be used to recalculate the relative amount of given interfacial atoms.

The majority of the "Fe/MgO" top interface atoms (86%) contribute to components "III" and "IV." The ε values of these two components are close to zero, which suggests that the atoms retained the high symmetry of the valence electrons distribution. The interpretation of ε presented for component "5" of the reverse interface (the averaging out of the V_{zz} at differently oriented sites with low Fe-Fe coordination) is not relevant in this case as it is hardly possible that 86% of interfacial sites are low-coordinated. Therefore, the absence of the quadrupole interaction could be interpreted in terms of the bulk-like distance between the S_I and S_{I-1} layers. This conclusion is consistent with the S_I–S_{I-1} interlayer spacing of 1.5 Å, measured for 8 ML of Fe deposited on MgO(001).[22] The increased values in the isomer shifts (0.17 mm/s and 0.28 mm/s) and the hyperfine fields (35.2 T and 38.7 T) imply that interactions between iron and oxygen atoms at this interface are not negligible. A strong modification of the electronic state of Fe took place due to the incorporation of oxygen atoms in the interfacial Fe layer and the formation of the "oxidized top" interface structure (Fig. 4(a)). Because components "III" and "IV" are characterized by different IS and B_{hf} values, they must correspond to Fe atoms in slightly different chemical environments, possibly having different numbers of oxygen in-plane nearest neighbors. However, similarly to the "MgO/Fe" interface, we cannot identify any of the known stoichiometric bulk-like oxides.

The hyperfine parameters of component "II" suggest that it reflects the ^{57}Fe atoms that are located at metallic interfacial sites (the "metallic top" interface, Fig. 4(b)). The hyperfine field of this component is lower than that of the bulk ($B_{hf} = 27.5$ T), revealing a more atomic-like character for the valence electrons, similar to components "3," "4," and "6" of the "MgO/Fe" bottom interface spectrum. The isomer shift value of component "II" is slightly higher relative to α-Fe (0.12 mm/s) and is equal to, within the uncertainty limits, the IS values of components "3" and "4" (for the "MgO/Fe" interface). The value of the ε is non-zero (−0.17 mm/s), which we interpret as the result of interlayer distance relaxation. The amount of Fe atoms occupying these metallic (not oxidized) interfacial sites at the "Fe/MgO" interface is relatively low, equal to 14%.

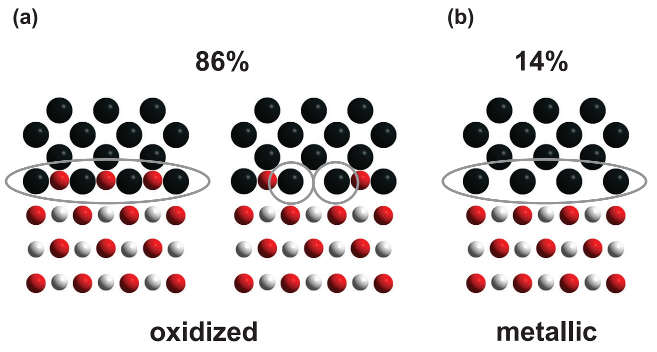

FIG. 4. Model of the "Fe/MgO" interface (^{56}Fe/1 ML^{57}Fe/MgO) showing the percentage of interface atoms located at the specific interfacial sites as identified using components of the CEMS spectrum: (a) "oxidized" sites (components "III" and "IV") and (b) "metallic" sites (component "II"). The ellipses encircle the corresponding Fe atoms. Large (black) balls—Fe, medium (red) balls—O, small (white) balls—Mg.

IV. SUMMARY

Both interfaces characteristic for Fe/MgO/Fe structures were studied. Using CEMS and ^{57}Fe probe atoms, we were able to identify iron sites directly neighboring the MgO barrier. For "MgO/Fe" bottom interface, 63% of interfacial Fe atoms were found to have an oxidic character. The interface was determined to be a mixture of diverse sites, where 14% of the oxidized Fe atoms were located at defected sites with lowered coordination (steps, corners, kinks), which refines the picture of the often-assumed homogenous interfacial structure.[9,12,24] Our measurements also support the findings[12,24] of an expanded S_I-S_{I-1} interlayer distance for the oxidized parts of the interface and a compressed distance for the unoxidized parts. Only 37% of interfacial atoms were identified to be located at metallic sites (with four in-plane Fe nearest neighbors, no Fe-O bonds), which were assumed to form the entire interface in the pioneer calculations of the TMR for the epitaxial Fe/MgO/Fe structure.[3,4] The hyperfine magnetic fields near the "MgO/Fe" interface were found to be similar to those at the "vacuum/Fe" interface, displaying Friedel-type oscillations. For "Fe/MgO", where Fe layer was placed on top of MgO, 86% of the Fe atoms located at the interface were found to have direct bonds with oxygen, while 14% formed a metallic interface. Our measurements suggest the absence of relaxation in the oxidized part of the Fe capping layer deposited on MgO barrier.

The striking difference between the two interfaces is that no components were detected for the "Fe/MgO" one, which could be unambiguously attributed to defected sites. This result proves the perfection of the MgO layer beneath the capping Fe. Moreover, no modification of the hyperfine parameters of Fe atoms located further from the interface was measured, in contrast with both the "MgO/Fe" bottom interface and "vacuum/Fe" interface. The observed difference must be related to the growth sequence. For the "MgO/Fe" case, the ^{57}Fe probe morphology is not affected by the MgO layer because it is completely developed before the deposition of MgO. It is also worth noting that the ^{57}Fe probe layer at the "MgO/Fe" interface is grown on a thick and relaxed Fe film and, therefore, is not subjected to significant strains. MgO acts only as a modifier of the chemical state of the Fe atoms. In this case, one could expect the characteristics of the ^{57}Fe probe layer to be similar to the properties of the Fe surface, which was shown above. Conversely, for the "Fe/MgO" top interface, the positions and coordinations of the Fe atoms, including a Fe lattice expansion of -3.6%, are governed by the structure of the oxide film beneath them.

ACKNOWLEDGMENTS

This work was supported in part by the National Science Center (Grant No. 2011/02/A/ST3/00150) and by the MPD and Team Programs of the Foundation for Polish Science cofinanced by the EU Regional Development Fund.

[1] A. M. Bratkovsky, Rep. Prog. Phys. **71**, 026502 (2008).
[2] C. Martínez Boubeta, J. L. Costa-Krämer, and A. Cebollada, J. Phys.: Condens. Matter **15**, R1123 (2003).
[3] J. Mathon, and A. Umerski, Phys. Rev. B **63**, 220403(R) (2001).
[4] W. H. Butler, X.-G. Zhang, T. C. Schulthess, and J. M. MacLaren, Phys. Rev. B **63**, 054416 (2001).
[5] J. Faure-Vincent, C. Tiusan, C. Bellouard, E. Popova, M. Hehn, F. Montaigne, and A. Schuhl, Phys. Rev. Lett. **89**, 107206 (2002).
[6] T. Katayama, S. Yuasa, J. Velev, M. Ye. Zhuravlev, S. S. Jaswal, and E. Y. Tsymbal Appl. Phys. Lett. **89**, 112503 (2006).
[7] S. Yuasa, T. Nagahama, A. Fukushima, Y. Suzuki, and K. Ando, Nature Mater. **3**, 868 (2004).
[8] S. G. Wang, R. C. C. Ward, G. X. Du, X. F. Han, C. Wang, and A. Kohn, Phys. Rev B **78**, 180411(R) (2008).
[9] X.-G. Zhang, W. H. Butler, and A. Bandyopadhyay, Phys. Rev. B **68**, 092402 (2003).
[10] Y. F. Chiang, J. J. I. Wong, X. Tan, Y. Li, K. Pi, W. H. Wang, H. W. K. Tom, and R. K. Kawakami, Phys. Rev. B **79**, 184410 (2009).
[11] H. L. Meyerheim, R. Popescu, J. Kirschner, N. Jedrecy, M. Sauvage-Simkin, B. Heinrich, and R. Pinchaux, Phys. Rev. Lett. **87**, 076102 (2001).
[12] H. L. Meyerheim, R. Popescu, N. Jedrecy, M. Vedpathak, M. Sauvage-Simkin, R. Pinchaux, B. Heinrich, and J. Kirschner, Phys. Rev. B **65**, 144433 (2002).
[13] H. Oh, S. B. Lee, J. Seo, H. G. Min, and J.-S. Kim, Appl. Phys. Lett. **82**, 361 (2003).
[14] D. Telesca, B. Sinkovic, See - Hun Yang, and S. S. P. Parkin, J. Electron Spectroscop. **185**, 133 (2012).
[15] M. Sicot, S. Andrieu, P. Turban, Y. Fagot-Revurat, H. Cercellier, A. Tagliaferri, C. De Nadai, N. B. Brookes, F. Bertran, and F. Fortuna, Phys. Rev. B **68**, 184406 (2003).
[16] C. Wang, S. Wang, A. Kohn, R. C. C. Ward, and A. K. Petford-Long, IEEE Trans. Magn. **43**, 2779 (2007).
[17] L. Plucinski, Y. Zhao, and B. Sinkovic, Phys. Rev. B **75**, 214411 (2007).
[18] P. Luches, S. Benedetti, M. Liberati, F. Boscherini, I. I. Pronin, and S. Valeri, Surf. Sci. **583**, 191 (2005).
[19] S. Colonna, A. Cricenti, P. Luches, S. Valeri, F. Boscherini, J. Qi, Y. Xu, and N. Tolk, Superlattices Microstruct. **46**, 107 (2009).
[20] Ch. Li and A.J. Freeman, Phys. Rev. B **43**, 780 (1991).
[21] C. Tusche, H. L. Meyerheim, N. Jedrecy, G. Renaud, A. Ernst, J. Henk, P. Bruno, and J. Kirschner, Phys. Rev. Lett. **95**, 176101 (2005).
[22] C. Tusche, H.L. Meyerheim, N. Jedrecy, G. Renaud, and J. Kirschner, Phys. Rev. B **74**, 195422 (2006).
[23] V. Serin, S. Andrieu, R. Serra, F. Bonell, C. Tiusan, L. Calmels, M. Varela, S. J. Pennycook, E. Snoeck, M. Walls, and C. Colliex, Phys. Rev. B **79**, 144413 (2009).
[24] B. D. Yu and J.-S. Kim, Phys. Rev. B **73**, 125408 (2006).
[25] I. Tanaka, M. Mizuno, S. Nakajyo, and H. Adachi, Acta mater. **46**, 6511 (1998).
[26] J. I. Beltrán, L. Balcells, and C. Martínez-Boubeta, Phys. Rev. B **85**, 064417 (2012).
[27] T. Shinjo and W. Keune, J. Magn. Magn. Mater. **200**, 598 (1999).
[28] V. Blum, A. Schmidt, W. Meier, L. Hammer, and K. Heinz, J. Phys. Condens. Matter **15**, 3517 (2003).
[29] Recoil 1.05 Mössbauer Analysis Software for Windows, © 1998, 2002, Ken Lagarec.
[30] S. Ohnishi, A. J. Freeman, and M. Weinert, Phys. Rev. B **28**, 6741 (1983).
[31] N. N. Greenwood and T. C. Gibb, *Mössbauer Spectroscopy* (Chapman and Hall LTD, London, 1971).
[32] J. A. Stroscio, D. T. Pierce, and R. A. Dragoset, Phys. Rev. Lett. **70**, 3615 (1993).
[33] A. Perez, G. Marest, B. D. Sawicka, J. A. Sawicki, and T. Tyliszczak, Phys. Rev. B **28**, 1227 (1983).
[34] R. Ingalls, Phys. Rev. **133**, A787 (1964).
[35] R. E. Watson, R. M. Sternheimer, and L. H. Bennett, Phys. Rev. B **30**, 5209 (1984).
[36] C. Wilkinson, A. K. Cheetham, G. J. Long, P. D. Battle, and D. A. O. Hope, Inorg. Chem. **23**, 3136 (1984).
[37] J. Korecki and U. Gradmann, Phys. Rev. Lett. **55**, 2491 (1985).
[38] J. F. Lawler, R. Schad, S. Jordan, and H. van Kempen, J. Magn. Magn. Mater. **165**, 224–226 (1997).
[39] G. Fahsold, A. Pucci, and K.-H. Rieder, Phys. Rev. B **61**, 8475 (2000).

Volume 606, issues 7–8 April 2012 ISSN 0039-6028

ELSEVIER

surface science

A journal devoted to the physics and chemistry of all interfaces

http://www.elsevier.com/locate/susc

Surface Science 606 (2012) 711–714

Contents lists available at SciVerse ScienceDirect

Surface Science

journal homepage: www.elsevier.com/locate/susc

Layer-by-layer epitaxial growth of polar FeO(111) thin films on MgO(111)

Jacek Gurgul [a,*], Ewa Młyńczak [a], Nika Spiridis [a], Józef Korecki [a,b]

[a] Jerzy Haber Institute of Catalysis and Surface Chemistry, Polish Academy of Sciences, Niezapominajek 8, 30-239 Kraków, Poland
[b] Faculty of Physics and Applied Computer Science, AGH University of Science and Technology, al. Mickiewicza 30, 30-059 Kraków, Poland

ARTICLE INFO

Article history:
Received 18 October 2011
Accepted 16 December 2011
Available online 28 December 2011

Keywords:
Iron oxide
Wüstite
FeO
Epitaxial films
Polar surface
CEMS

ABSTRACT

We report on the structural properties of epitaxial FeO layers grown by molecular beam epitaxy on MgO(111). The successful stabilization of polar FeO films as thick as 16 monolayers (ML), obtained by deposition and subsequent oxidation of single Fe layers, is presented. FeO/MgO(111) thin films were chemically and structurally characterized using low-energy electron diffraction, Auger electron spectroscopy and conversion electron Mössbauer spectroscopy (CEMS). Detailed *in situ* CEMS measurements as a function of the film thickness demonstrated a size-effect-induced evolution of the hyperfine parameters, with the thickest film exhibiting the bulk-wüstite hyperfine pattern. *Ex situ* CEMS investigation confirmed existence of magnetic ordering of the wüstite thin film phase at liquid nitrogen temperature.

1. Introduction

The latest advances in the description of polar oxide surfaces have shed light on the physical properties of the surfaces and interfaces of ionic materials [1]. However, our understanding of low-dimensionality effects in such materials is still very poor. Theoretical predictions and experimental results have shown that bulk-terminated polar surfaces are not stable because alternating layers of oppositely charged ions produce a large dipole moment perpendicular to the surface, which results in a diverging electrostatic potential. Two mechanisms provide solutions to this infinite energy problem: the surface could facet into neutral planes or it could reconstruct to balance its surface charge [1,2]. In contrast to the surfaces of single crystals, non-reconstructed polar surfaces can be produced in thin films below a critical thickness [1 and references therein]. From this perspective, the preparation and study of stable non-reconstructed polar surfaces are of great interest. On the other hand, the stabilization of orientations, which do not occur naturally when cleaving a bulk material, opens the way to the fabrication of artificial structures for controlled catalysis or nanostructures for electronic and magnetic applications.

The simple cubic rock-salt structure is one of the most stable structures for highly ionic solids, such as metal monoxides (*e.g.*, MgO, CoO, FeO, *etc.*). It consists of two interpenetrating fcc lattices of anions and cations. While the {001} faces are neutral and can be easily stabilized by epitaxial growth [3], obtaining the polar plane orientation of the lowest index {111} is challenging. A crystal cut along (111) presents alternating layers of metal and oxygen ions. Because of charge compensation, the surface tends to reconstruct or facet. The most common stable surface configuration is found to be the octopolar (2×2) reconstruction [4 and references therein]. This reconstruction is obtained by removing 75% of the atoms in the outermost layer and 25% in the layer beneath, which produces {100} facets. Polar surface stabilization mechanisms may be altered in ultrathin polar films and nanostructures because of their reduced dimensionality [5]. Additionally, in these systems, surface relaxation, diffusion of atoms, filling of surface states or covalency modifications are possible stabilizing processes. However, these mechanisms have not yet been quantitatively assessed, and there is a need for experimental work in these fields.

We have chosen to study FeO because of its importance in basic research, as well as in technological applications. Iron monoxide (FeO) adopts the rock salt structure above its Néel temperature ($T_N \approx 198$ K). However, it is well known that FeO is nonstoichiometric, accommodating a cation deficiency by the formation of octahedral iron vacancies and a small number of tetrahedral iron(III) interstitials. These defects tend to aggregate and form tetrahedral units that have been identified by neutron diffraction and Mössbauer spectroscopy [6,7]. The bulk magnetic properties of wüstite Fe_yO are complex; it is an antiferromagnet with an exact Néel temperature that depends on the value of y [6,8]. Below the magnetic ordering temperature, it undergoes a rhombohedral distortion, and its iron spins align along the [111] direction of the unit cell, forming antiferromagnetically coupled alternate (111) iron ferromagnetic sheets [9].

---

[*] Corresponding author at: Jerzy Haber Institute of Catalysis and Surface Chemistry, Polish Academy of Sciences, Niezapominajek 8, 30-239 Kraków, Poland. Tel.: +48 126395116; Fax: +48 124251923.

E-mail addresses: ncgurgul@cyf-kr.edu.pl (J. Gurgul), ncmlyncz@cyf-kr.edu.pl (E. Młyńczak), ncspirid@cyf-kr.edu.pl (N. Spiridis), korecki@agh.edu.pl (J. Korecki).

0039-6028/$ – see front matter © 2011 Elsevier B.V. All rights reserved.
doi:10.1016/j.susc.2011.12.012

Although iron oxide thin films prepared by different methods, ranging from the direct oxidation of metallic Fe(110) and (001) surfaces to the deposition and oxidation of Fe layers on many substrates, are widely investigated (for a review, see [10]), the literature on polar FeO(111) films is scarce. Most studies consider ultrathin FeO(111) films prepared on Pt(111) [11]. There are several experiments showing that FeO(111) can be obtained by oxidation of the Fe(110) surface [12 and references therein], and to our knowledge, there has been only one example of the growth of FeO(111) monolayers on oxide surfaces [13]. In particular, there are no published papers related to FeO/MgO(111) systems.

In this paper, we report the successful preparation of polar FeO thin films on MgO(111). Because of the layer-by-layer technique, we were able to stabilize an epitaxial FeO film as thick as 16 ML. Every step of the preparation sequences was accompanied by detailed structural studies with low electron energy diffraction (LEED), Auger electron spectroscopy (AES) and conversion electron Mössbauer spectroscopy (CEMS). Compared to standard surface sensitive characterization methods, CEMS has the advantage of probing deeper layers (down to 100 nm) with a monolayer resolution, as well as their local structure and symmetry [3,14].

2. Material and methods

The experiments were performed in a multi-chamber ultrahigh vacuum (UHV) system (base pressure 2×10^{-10} mbar) equipped with facilities for the growth of epitaxial films, along with their structural and chemical characterizations and *in situ* CEMS measurements. The preparation chamber contains a molecular beam epitaxy (MBE) system, including an evaporator for iron that is 95% enriched with the ^{57}Fe isotope, a quartz monitor to control the deposition rate, a LEED/AES spectrometer for fast sample characterization and a MgO evaporator. A MgO(111) polished single crystal ($10\times10\times1$ mm^3) was used as the substrate. The substrate was annealed at 903 K for 3 h at UHV, and a homoepitaxial 30 Å layer of MgO was deposited at 723 K in three steps (10 Å each) and annealed at 823 K (30 min) in oxygen atmosphere (5×10^{-9} mbar) to improve the quality of the surface. Single monolayers of FeO were grown by the deposition of an ^{57}Fe monolayer at normal incidence at RT and subsequent oxidation in O_2 (5×10^{-8} mbar, 10 L) at 543 K, followed by UHV annealing at 873 K for 30 min. The FeO monolayer deposition procedure was repeated 16 times, which resulted in the 16 ML FeO film. After every monolayer preparation cycle, the surface structure and composition of the thin films were monitored by LEED and AES.

The *in situ* CEMS measurements were performed at selected preparation stages at room temperature using an UHV spectrometer, similar to that described previously [15] and a standard 100 mCi Mössbauer ^{57}Co(Rh) γ-ray source. The *in situ* spectra were taken at a fixed angle of 36° between the direction of the γ-ray propagation and the sample normal. For low temperature (LT) *ex situ* CEMS measurements, the sample was capped with a 50 Å protective MgO film. The LT CEMS experiments were performed at 80 K in a separate UHV system [16] equipped with a liquid nitrogen stationary cryostat.

The Mössbauer spectra were analyzed numerically by fitting a hyperfine parameter distribution (HPD) using the Voigt-line-based method of Rancourt and Ping [17]. In this method, the HPD for a given crystal site corresponding to similar structural, chemical and magnetic properties is constructed by a sum of Gaussian components for the quadrupole splitting (QS) distributions and, if necessary, the magnetic hyperfine field B_{hf} distributions. The isomer shift (IS) can be linearly coupled to the primary hyperfine parameters (QS, B_{hf}). The isomer shift values are quoted relative to α-Fe at room temperature.

3. Results and discussion

The Auger spectrum induced by 1.7 keV electrons showed small amounts of carbon (KE = 270 eV) and calcium (KE = 291 eV) at the polished MgO(111) crystal surface (Fig. 1). To obtain a cleaner surface, homoepitaxial MgO buffer layers were deposited. The deposition of 30 Å of MgO clearly resulted in a calcium-free surface. However, small traces of carbon were still present at the surface. The oxygen KLL Auger electron peak at KE = 508 eV with respect to the Fermi level is characteristic for the uncharged surface of MgO [18].

Because of the insulating character of MgO, LEED patterns could be obtained only for high electron energies. Fig. 2 shows the LEED patterns recorded for a primary electron energy of 190 eV before and after the deposition of 30 Å of MgO. Both patterns exhibit a (1 × 1) hexagonal symmetry, confirming the homoepitaxial growth of MgO. The spots are less sharp in the case of the surface with an additional 30 Å of MgO, most likely because of stronger charging or slightly poorer structural long-range order.

The deposition of the thinnest FeO layers drastically changed the electrical state of the samples, making LEED observation possible down to the lowest energies, which demonstrates the much lower energy gap of FeO compared to MgO.

Fig. 3 compares the LEED patterns obtained from the FeO(111) films of different thicknesses. All patterns exhibit a (1 × 1) hexagonal symmetry that confirms epitaxial growth through the entire FeO film. The orientation of the FeO films is expected to be $(111)_{FeO}//(111)_{MgO}$ because of the small mismatch of the lattice parameters, and we can conclude that the FeO follows the orientation of the MgO substrate with high fidelity.

Remarkably, the metallic Fe monolayers produced very poor diffraction patterns with visible 3-fold symmetry (not shown here), and only the oxidation process caused meaningful improvement of the long range order of the surface. The brightness and sharpness of the spots are comparable for all cases, showing the good crystalline quality of the films and their uniform growth mode; however, the broadening of the diffraction spots is an indication of a grainy film structure. It is well known that the initial growth of iron on MgO is island-like [19], and this adsorbate morphology is transmitted to the oxide film. Under the above-mentioned conditions, there is no appearance of {100} facets, which can be easily understood in view of the low dimensionality of the oxide structure [5].

For discussion of the Mössbauer results that are presented below it is useful to recall the spectra for bulk compounds. Under ambient conditions, in the cubic rock-salt structure of FeO, the cations occupy octahedral positions, which have nominally perfect cubic symmetry O_h. In such a case, there are no lattice and valence electron contributions to the electric field gradient on the Fe^{2+} nuclei, and therefore quadrupole interaction should be negligible. Indeed, in stoichiometric

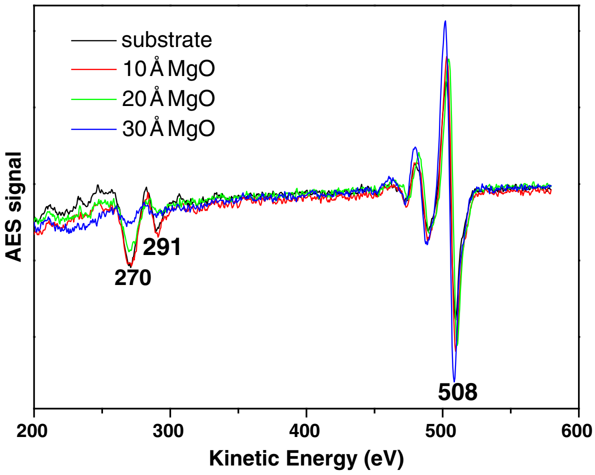

Fig. 1. The AES spectrum for annealed MgO(111) substrate before and after covering with homoepitaxial layers of varying thickness.

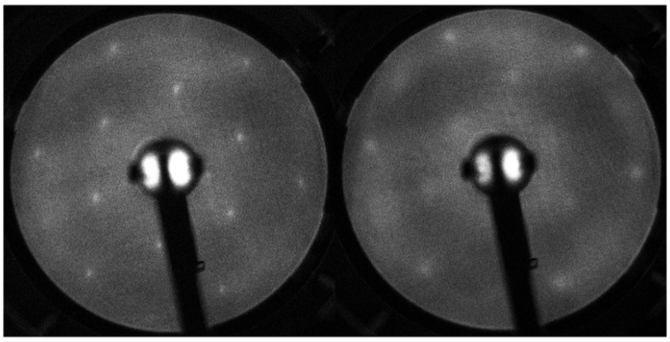

Fig. 2. The LEED patterns at the primary electron energy 190 eV for the MgO(111) substrate after annealing (left) and for 30 Å of homoepitaxial MgO layer (right).

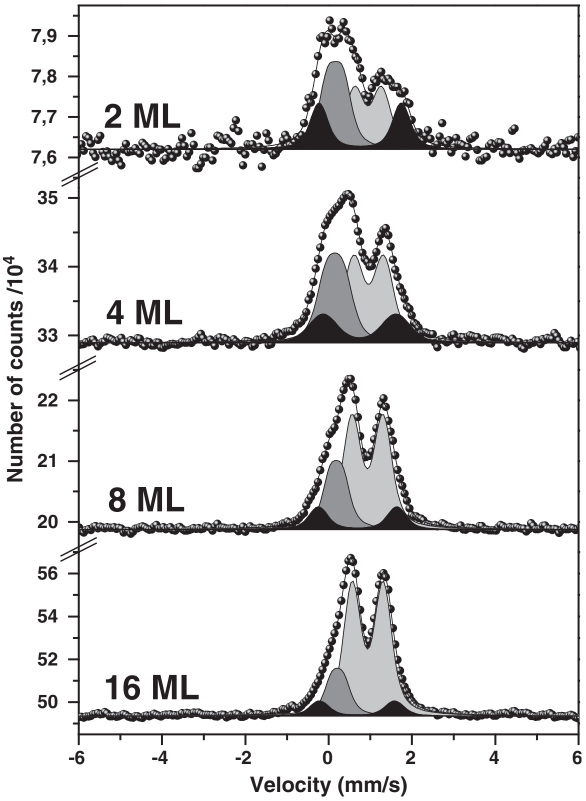

Fig. 4. *In situ* room temperature ^{57}Fe-CEMS spectra for FeO films on MgO(111) as a function of the FeO thickness.

FeO [20] or in extremely diluted (Mg, Fe)O [21] quadrupole splitting is quite small (<0.2 mm/s) coming from the valence d-shell, mainly due to the small Jahn–Teller distortion of the FeO$_6$ octahedron. In all other cases Mössbauer spectra are more complex due to some local distortions of oxygen octahedra and nonequivalent nearest neighbor coordinations, and typical interpretation involves singlets and doublets because of the presence of undistorted octahedral Fe^{2+} sites, octahedral Fe^{2+} sites associated with vacancies and complex defect clustering and also Fe^{3+} in octahedral and tetrahedral positions [22].

The room temperature *in situ* CEMS spectra of the FeO(111) films at different growth stage layers are presented in Fig. **4**. The apparent asymmetric doublets are qualitatively similar to the well-known bulk-Fe$_y$O spectra in the paramagnetic state [6,7], but detailed numerical analysis reveals quantitative differences that are not surprising when the possible deviation from oxygen stoichiometry, formation of FeO–MgO solid solution [23,24] at the substrate-film interface or low dimensionality of our samples are considered. To accurately and consistently describe our spectra, in analogy to bulk FeO, three doublets were required. The hyperfine parameters of the fitted components and their intensities are listed in Table **1**. The doublets D1 and D2 are characterized by a large isomer shift, which is typical for Fe^{2+}. The central doublet (D1) with the larger IS (~1.05 mm/s) and smaller QS (~0.75 mm/s), which is shaded light gray in Fig. **4**, is attributed to the undistorted octahedral Fe^{2+} sites. This assumption is consistent with the values of the hyperfine parameters, which are close to those of the bulk [6]; it is also consistent with the increasing peak intensity with increasing film thickness. From this trend, we make the obvious assumption that the inner layers of the films present more bulk-like behavior than the surface and interface layers. Consequently, the outer doublet (D2) with lower IS, which is shaded black in Fig. **4** and decreases in intensity with increasing film thickness, can be attributed to the octahedral Fe^{2+} sites at the FeO–MgO interface. The large QS value of this spectral component (~1.8 mm/s) can be explained by a specific local symmetry at the interface, where the Fe ions are coordinated asymmetrically to six Mg and six Fe next-nearest cation neighbors. By analogy to bulk Fe$_{1-x}$Mg$_x$O mixed compounds [25], such a configuration results in the highest value of the quadrupole splitting QS, which can be estimated as 1.65 mm/s using the model proposed by Kantor et al. [23], in a fair agreement with the observed experimental value. It must be noted that also a certain degree of the interdiffusion between the MgO substrate and the FeO film cannot be excluded. However, considering other factors, which in ultrathin films can contribute to modification of the hyperfine parameters, such as the lack of the translational symmetry, lattice distortions, high contribution of defects, the presence of the surface and interface, an ultimate interpretation of the spectral component is hardly possible. On the other hand, the LEED and Auger analysis do not indicate that a massive MgO–FeO intermixing takes place.

The doublet (D3) with a small IS and small QS, shaded dark gray in Fig. **4**, can be attributed to octahedral Fe^{3+} ions along with charge-compensating cation vacancies corresponding to the replacement $(\mathrm{Fe}^{3+}-\square-\mathrm{Fe}^{3+})=3\mathrm{Fe}^{2+}$ [23,26]. However, some of Fe^{3+} ions can occupy interstitial tetrahedral positions of the *fcc* oxygen

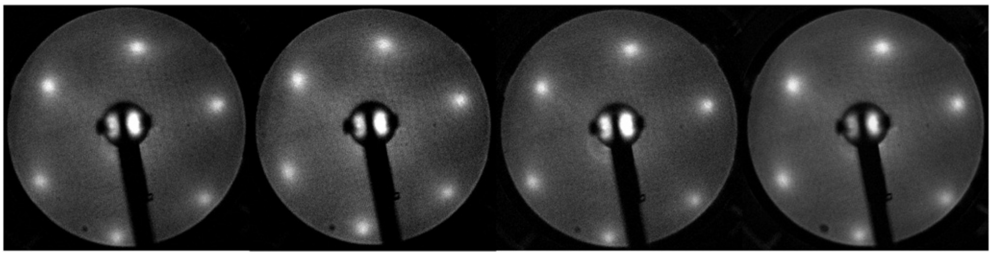

Fig. 3. LEED patterns at the primary electron energy 67 eV of 2, 4, 8 and 16 ML thick FeO, from left to right, respectively.

Table 1
Hyperfine parameters derived from the room-temperature CEMS spectra for FeO films on MgO(111) as a function of the film thickness. Isomer shift (IS) is given in mm/s relative to α-Fe foil. <QS>=$e^2qQ/2$ (in mm/s) and σ (in mm/s) are the average quadrupole splitting and the Gaussian width of the QS distribution of the given spectral component, respectively.

	Iron(II)								Iron(III)				
	Central doublet (D1)				Outer doublet (D2)				Doublet (D3)				
	IS	<QS>	σ	% A[a]	IS	<QS>	σ	% A	IS	<QS>	σ	% A	χ^2
2 ML	1.05	0.65	0.29	35.3	0.87	1.98	0.28	27.5	0.27	0.36	0.25	37.2	0.48
4 ML	1.07	0.72	0.33	44.7	0.85	1.75	0.54	20.9	0.26	0.39	0.33	34.4	0.55
8 ML	1.04	0.75	0.28	62.0	0.80	1.88	0.31	13.6	0.29	0.29	0.20	24.4	0.53
16 ML	1.04	0.75	0.26	73.4	0.79	1.80	0.31	9.6	0.32	0.28	0.20	17.0	0.85

[a] The percentage area of spectra components.

sublattice and contribute to this component, too. The observed value of IS = 0.3 mm/s is typical of the $3d^5$ state [6]. In our fits, we used a quadrupole doublet rather than a broadened single line, in accordance with high statistic Mössbauer spectra of non-stoichiometric wüstite and FeO–MgO solid solutions that showed Fe^{3+} spectral components with a non-zero quadrupole interaction [25].

The *ex situ* Mössbauer spectra obtained for 16 ML of FeO(111) at 300 and 80 K are shown in Fig. **5**. The spectrum at 300 K is very similar to the corresponding spectrum measured *in situ*, but the improved signal-to-noise ratio allows the detection of a small amount (approximately 9%) of a magnetically split component which comes from nano-phase magnetite (Fe_3O_4) [14,27]. The spectrum measured at 80 K becomes complex (see inset in Fig. **5**), but the spectrum quality excludes an unambiguous interpretation. However, despite some peaks belonging to magnetite (visible at high velocities), a change (broadening) of the central part of the spectrum indicating a magnetic splitting is obvious. We attribute this change to a transition to an ordered phase, probably to the antiferromagnetic one, in analogy to bulk wüstite. Additionally to the complex magnetic hyperfine pattern of wüstite at low temperature [6,28,29], superparamagnetic relaxation can contribute to the spectrum complexity.

4. Conclusions

It was shown that epitaxial growth of FeO(111) thin layers on MgO(111) is possible by deposition and subsequent oxidation of single Fe layers. In this case, special attention must be paid to the preparation of the MgO(111) substrate, and a special treatment procedure is necessary during the iron deposition and oxidation. Analysis of the CEMS spectra showed that a FeO wüstite phase is formed. The low-temperature CEMS spectrum measured at 80 K indicates transition to a magnetically ordered state.

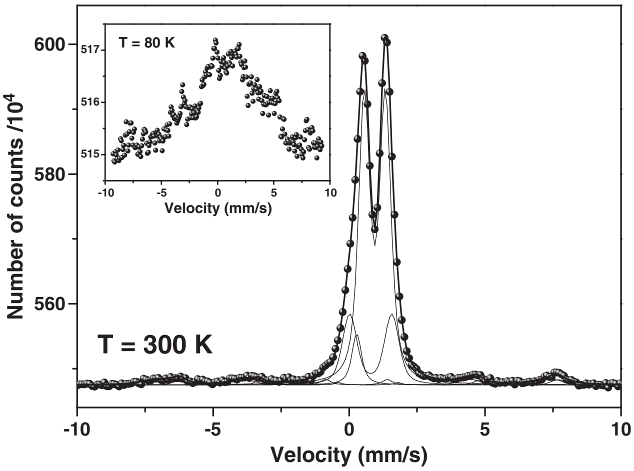

Fig. 5. *Ex situ* CEMS spectra for 16 ML of FeO(111) on MgO(111) at 300 K and 80 K (inset).

Acknowledgments

This work was supported in part by the Polish Ministry of Science and Higher Education and by the MPD and Team Programs of the Foundation for Polish Science co-financed by the EU European Regional Development Fund.

References

[1] C. Noguera, J. Phys. Condens. Matter 12 (2000) R367.
[2] G.W. Watson, E.T. Kelsey, N.H. de Leeuw, D.J. Harris, S.C. Parker, J. Chem, J. Chem. Soc., Faraday Trans. 92 (1996) 433.
[3] J. Gurgul, K. Freindl, A. Kozioł-Rachwał, K. Matlak, N. Spiridis, T. Ślęzak, D. Wilgocka-Ślęzak, J. Korecki, Surf. Interface Anal. 42 (2010) 696.
[4] A. Pojani, F. Finocchi, J. Goniakowski, C. Noguera, Surf. Sci. 387 (1997) 354.
[5] J. Goniakowski, C. Noguera, Phys. Rev. B 83 (2011) 115413.
[6] C. Wilkinson, A.K. Cheetham, G.J. Long, P.D. Battle, D.A.O. Hope, Inorg. Chem. 23 (1984) 3136.
[7] N.N. Greenwood, A.T. Howe, J. Chem, J. Chem. Soc., Dalton Trans. 1 (1972) 110.
[8] D.A.O. Hope, A.K. Cheetham, G.J. Long, Inorg. Chem. 21 (1982) 2804.
[9] G.J. Long, D.A.O. Hope, A.K. Cheetham, Inorg. Chem. 23 (1982) 3141.
[10] H.-J. Freund, H. Kuhlenbeck, V. Staemmler, Rep. Prog. Phys. 59 (1996) 283.
[11] W. Weiss, M. Ritter, Phys. Rev. B 59 (1999) 5201.
[12] K. Koike, T. Furukawa, Phys. Rev. Lett. 77 (1996) 3921.
[13] S. Gota, E. Guiot, M. Henriot, M. Gautier-Soyer, Phys. Rev. B 60 (1999) 14387.
[14] M. Zając, K. Freindl, T. Ślęzak, M. Ślęzak, N. Spiridis, D. Wilgocka-Ślęzak, J. Korecki, Thin Solid Films 519 (2011) 5588.
[15] N. Spiridis, R.P. Socha, B. Handke, J. Haber, M. Szczepanik, J. Korecki, Catal. Today 169 (2011) 24.
[16] J. Korecki, M. Kubik, N. Spiridis, T. Ślęzak, Acta Phys. Pol. A 97 (2000) 129.
[17] D.G. Rancourt, J.Y. Ping, Nucl. Instrum. Meth. Phys. Rev. B 58 (1991) 85.
[18] M.P. Seah, S.J. Spencer, J. Electron Spec. Relat. Phenom. 109 (2000) 291.
[19] M. Zając, K. Freindl, K. Matlak, M. Ślęzak, T. Ślęzak, N. Spiridis, J. Korecki, Surf. Sci. 601 (2007) 4305.
[20] L. Broussard, J. Phys. Chem. 73 (1969) 1848.
[21] H.R. Leider, D.N. Pipkorn, Phys. Rev. 165 (1968) 494.
[22] I.Yu. Kantor, C.A. McCammon, L.S. Dubrovinsky, J. Alloys Compd. 376 (2004) 5.
[23] G.A. Waychunas, W.A. Dollase, C.R. Ross II, Am. Mineral. 79 (1994) 274.
[24] I. Kantor, L. Dubrovinsky, C. McCammon, G. Steinle-Neumann, A. Kantor, N. Skorodumova, S. Pascarelli, G. Aquilanti, Phys. Rev. B 80 (2009) 014204.
[25] I.S. Lyubutin, A.G. Gavriliuk, K.V. Frolov, J.F. Lin, I.A. Troyan, JETP Lett. 90 (2009) 617.
[26] D.P. Dobson, N.S. Cohen, Q.A. Pankhurst, J.P. Brodholt, Am. Mineral. 83 (1998) 794.
[27] N. Spiridis, D. Wilgocka-Ślęzak, K. Freindl, B. Figarska, T. Giela, E. Młyńczak, B. Strzelczyk, M. Zając, J. Korecki, arXiv:1111.5938v2 [cond-mat.mtrl-sci], submitted for publication Phys. Rev. B.
[28] G.J. Long, F. Grandjean, in: C.R.A. Catlow (Ed.), Advances in Solid State Chemistry, Vol. 2, JAI Press, London, 1991, p. 187.
[29] C.A. McCammon, Q.A. Pankhurst, Hyperfine Interact. 94 (1994) 1989.

Fe/CoO(001) and Fe/CoO(111) bilayers: the effect of crystal orientation on the exchange bias

E. Młyńczak[1*], B. Matlak[2], A. Kozioł- Rachwał[2], J. Gurgul[1], N. Spiridis[1] and J. Korecki[1,2]

[1] *Jerzy Haber Institute of Catalysis and Surface Chemistry, Polish Academy of Sciences, Niezapominajek 8, 30-239 Krakow, Poland,*

[2] *Faculty of Physics and Applied Computer Science, AGH University of Science and Technology, al. Mickiewicza 30, 30-059 Krakow, Poland*

ABSTRACT

A comparative study of the structure and magnetism of Fe/CoO(111) and Fe/CoO(001) epitaxial bilayers was performed to investigate the role of uncompensated spins in the exchange bias (EB) phenomenon. Low energy electron diffraction (LEED), x-ray photoelectron spectroscopy (XPS), conversion electron Mössbauer spectroscopy (CEMS) and the magneto-optic Kerr effect (MOKE) were used to characterize the structural and magnetic properties of the bilayers. Magnetically compensated and uncompensated CoO films were prepared using molecular beam epitaxy through the evaporation of single Co atomic layers and their subsequent oxidation (layer-by-layer technique) on MgO crystals with (001) and (111) orientations. Two-monolayer (ML)-thick ^{57}Fe probes located on top of the oxide films and covered with ^{56}Fe allowed for an analysis of the interfacial chemical and magnetic structure using CEMS. For both structures, sub-monolayer oxidation of the iron detected at the Fe/CoO interface was found to be accompanied by the formation of a mixed FeCo region. The Fe layers showed fourfold magnetocrystalline anisotropy when grown on CoO(001) and weak uniaxial anisotropy when grown on CoO(111). Although the structural quality and composition of the two structures were comparable, they exhibited distinct EB properties. A hysteresis loop shift as high as 354 Oe at 80 K was obtained for the Fe/CoO(111) bilayer, compared to only 37 Oe for the magnetically compensated Fe/CoO(001).

I. INTRODUCTION

Ferromagnetic (FM)-antiferromagnetic (AFM) layered structures have been extensively studied over the last decades[1,2] due to the effect of the exchange bias (EB), which renders these structures technologically important[3,4] and interesting from the viewpoint of basic research[5]. EB occurs as a horizontal shift and broadening of the FM hysteresis loop. One of the most discussed and still controversial aspects of EB is the role of the interfacial spin structure. In the pioneering work of Meiklejohn and Bean [6], the AFM spins at the interface of the FM layer were assumed to be magnetically uncompensated. In that case, the net magnetic moment, which exists in the AFM component of the interface, pins the magnetization direction of the FM component due to a high AFM anisotropy and produces a loop shift. However, the hysteresis loop shifts calculated based on the model of Meiklejohn and Bean are a few orders of magnitude larger than those observed experimentally[5]. Furthermore, an EB was also observed for nominally compensated AFM surfaces, such as CoO(001)[7] and NiO(001)[8]. To explain this result, a different approach is needed. The model of Malozemoff[9] considered random roughness at the interface, which produced uncompensated areas for the nominally compensated AFM surface. Schulthess and Butler[10] also noted that for structures with a perfectly compensated AFM order, additional factors, e.g., interfacial defects, are necessary to produce a loop shift. Using element-specific x-ray magnetic circular dichroism, Ohldag et al. found uncompensated Ni spins at a nominally compensated Co/NiO(001) interface, localized in the interfacial $CoNiO_x$ layer, which was formed as a result of the oxidation-reduction reactions[11]. The presence of the uncompensated spins resulted in increased coercivity; however, these spins were not sufficient to produce an EB[11]. For the loop shift to be observed, some of the uncompensated spins must be pinned; however, as little as 4% of a monolayer is sufficient[12].

Epitaxial FM/AFM bilayers, with CoO as the AFM layer, are well suited for model investigations. CoO has an easily accessible Néel temperature (T_N=293K for bulk) and a high magnetocrystalline anisotropy, which enhances the EB effect[13,14]. Furthermore, CoO has a NaCl-type crystal structure to which the antiferromagnetic order is closely related, which is crucial for the present study. In bulk CoO, the magnetic moments of the Co atoms in a (111) plane are aligned parallel while the adjacent planes are coupled antiparallel[15]. As a consequence, it is possible to access two different interfacial spin configurations of CoO simply by using CoO(001)- or CoO(111)-oriented layers (Fig. **1**(a) and (b), respectively). While CoO(001) atomic layers are compensated in terms of the net magnetic moment, the CoO(111) surface is magnetically uncompensated. In parallel, in contrast to the neutral (001) surface, the (111) surface of the rocksalt oxides is polar, due to the alternatively stacked anionic and cationic layers, as shown in Fig. **1**(e) and (f). The resulting divergence of the electrostatic energy must be neutralized in such systems to stabilize the surface. Deviations from the stoichiometry, surface reconstructions or the adsorption of foreign species are possible stabilization mechanisms[16].

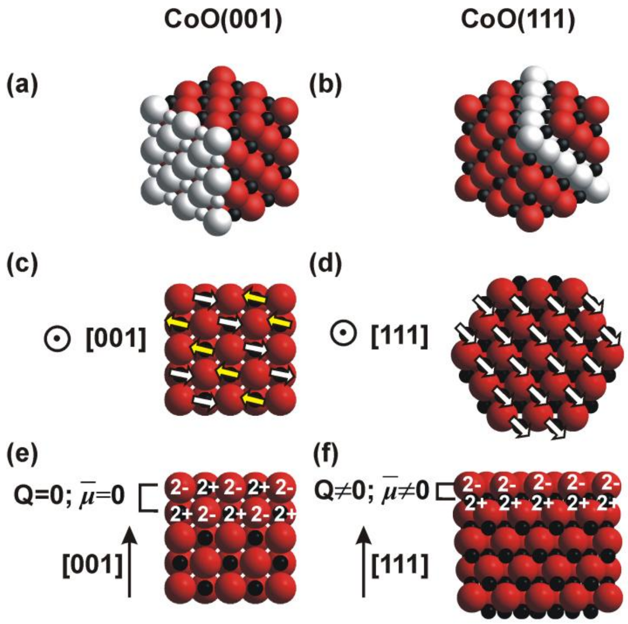

Fig. 1 CoO(001) (a) and CoO(111) (b) planes of the bulk NaCl crystal structure, marked by white balls. The red and black balls mark the oxygen and cobalt atoms, respectively. The corresponding arrangement of the magnetic moments (arrows) in the CoO(001) (c) and CoO(111) (d) planes. Charge arrangement perpendicular to the CoO(001) (e) and CoO(111) (f) planes. Along the [001] direction, each (001) bilayer is charge-compensated (Q=0) and has no dipole electric moment (μ=0), while non-zero dipole electric moments along the [111] direction lead to a diverging electrostatic potential, which destabilizes the surface.

Direct comparisons between bilayer systems with compensated and uncompensated CoO surfaces have been performed; however, contradictory results have been obtained. For CoO/Py epitaxial bilayers, Gökemeijer et al. showed that an EB occurred only for the CoO(111) orientation, in contrast to CoO(001)[17]. However, Ghadimi et al.[18] reported a larger EB effect for Co/$Co_{1-y}O$(001) in comparison to Co/$Co_{1-y}O$ (111). For Fe_3O_4/CoO epitaxial bilayers, van der Zaag et al. found no significant differences in the EB between the (001) and (111) orientations[19]. Thus, it appears that not only the orientation but also the degree of structural perfection plays a role in these systems. To firmly establish the role of the (un)compensation, care must be taken to compare systems that are similar with respect to the crystal quality, stoichiometry and chemical structure of the interfaces.

In the present work, to prepare cobalt oxide layers of both orientations, we utilized a layer-by-layer method that was previously shown to result in stable polar thin films of FeO grown on MgO(111)[20]. By growing bilayer CoO-Fe structures based on magnetically compensated CoO(001) and magnetically uncompensated CoO(111) under precisely controlled conditions and by performing a thorough analysis of the chemical structure of the CoO layers and the Fe/CoO interfaces, we can investigate the relation between the occurrence and magnitude of the EB and the (un)compensation of the antiferromagnetic interface.

II. EXPERIMENTAL PROCEDURE

Fe/CoO bilayers were prepared in an ultra high vacuum (UHV) system equipped with a molecular beam epitaxy facility, following standard surface characterization techniques. Polished MgO(001) and MgO(111) single crystals were used as the substrates. MgO has the same rocksalt crystalline structure as CoO, and the mismatch between the two materials is approximately 1%[21]. Metals (Co and Fe) were evaporated from thermally heated BeO crucibles, and MgO layers, used as buffer and capping layers, were evaporated from an MgO piece using an electron beam evaporator. The thickness was controlled by a precisely calibrated quartz crystal monitor.

The substrates were degassed under UHV conditions and annealed at 600 °C for 30 minutes. Auger electron spectroscopy (AES) was performed on the annealed substrates and showed significant carbon contamination; therefore, a homoepitaxial MgO layer (30 Å thick) was deposited onto the substrates at 450 °C to obtain clean surfaces. The homoepitaxial buffer layers were subsequently annealed at 600 °C for 30 minutes at an oxygen background pressure of

$5\text{x}10^{-9}$ mbar. CoO films were prepared via a layer-by-layer oxidation process of metallic Co monolayers. Single layers of metallic Co were deposited at room temperature (RT). The thicknesses of the Co layers corresponded to the Co amount in a single monolayer (ML) of CoO, i.e., 1.19 Å and 1.39 Å for the (001) and (111) orientation, respectively. The single metallic Co layers were oxidized by exposure to 20 L of molecular oxygen at a partial pressure of p_{O2}= $5\text{x}10^{-8}$ mbar at 270 °C, followed by UHV annealing at 550 °C for 30 minutes. This procedure ensured a precise control of the oxygen dose for a single metal layer. The crystalline structure of the growing CoO layers was monitored using low energy electron diffraction (LEED) after each metallic layer deposition and each UHV annealing step. The procedure was repeated ten times for the (001) orientation and nine times for the (111) orientation, resulting in 20-Å-thick CoO films.

After preparation, the CoO layers were transferred to another UHV system using a vacuum suitcase for x-ray photoelectron spectroscopy (XPS) measurements. The XPS spectra were measured using an Al Kα (1486.6 eV) x-ray source and an SES R4000 hemispherical analyzer (Gammadata Scienta). The spectra were calibrated using the carbon C 1s line at a binding energy of 285 eV. The spectral analysis was conducted with commercial software[22].

Next, 50-Å-thick Fe layers were deposited onto the CoO films at RT. To characterize the chemical and magnetic structure of the Fe/CoO interface using conversion electron Mössbauer spectroscopy (CEMS), first, an ultrathin (2 ML=2.86 Å) ^{57}Fe layer was evaporated on the CoO, followed by 33 ML (47 Å) of ^{56}Fe. The samples were capped with approximately 70 Å of MgO. A schematic representation of the samples is shown in **Fig. 2**.

Magnetic characterization of the samples was performed *ex situ* using the longitudinal magneto-optic Kerr effect (MOKE). Measurements as a function of the azimuthal angle φ between the magnetic field and the characteristic in-plane crystallographic directions were acquired at RT, enabling an identification of the intrinsic magnetic anisotropies in the Fe film. The Fe-CoO magnetic exchange coupling was investigated using the field cooling (FC) procedure. During FC, the samples were placed in a cryostat, where they were cooled from RT passing through the Néel temperature of bulk CoO (291 K) and reaching 80 K in the presence of a static magnetic field of 4000 Oe oriented along the easiest magnetization direction. Then, the hysteresis loops were measured as a function of temperature, up to 300 K. The exchange coupling was described using the EB field $H_{EB}=(|H_{C1}|-|H_{C2}|)/2$ and the coercive field $H_C=(|H_{C1}|+|H_{C2}|)/2$, where H_{C1} and H_{C2} are the coercive fields of the ascending and descending branches of the hysteresis loop, respectively.

To examine the chemical structure of the Fe/CoO interfaces, CEMS measurements were performed *ex situ* using a standard Mössbauer spectrometer equipped with a He/CH_4 flow proportional detector and a 100-mCi ^{57}Co/Rh source. The CEMS spectra were collected under a normal incidence geometry. Commercial software[23] was used to fit the spectra using a Voigt-line-based least-squares method, thus approximating the distribution of the hyperfine magnetic field B_{hf} at a given site with a sum of Gaussian components.

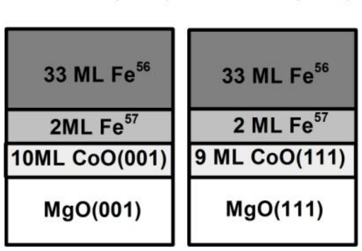

Fig. 2 Schematic representation of the samples.

III. RESULTS AND DISCUSSION

A. Chemical and structural characterization

The AES results for the MgO(001) and MgO(111) substrates revealed significant contamination (Fig. **3**), including carbon and calcium. To reduce surface contamination, homoepitaxial MgO buffer layers were deposited onto the substrates prior to the preparation of the CoO films. The decreased intensity of the AES C KLL (270eV) and Ca KLL (291 eV) lines with respect to the O KLL signal (503 eV) indicate that the intrinsic MgO contaminants were covered by the buffer layers.

The LEED patterns observed for the substrates and buffers of both orientations verified epitaxial growth of the buffer layers (Fig. **4**). As expected, the crystalline symmetry was fourfold for MgO(001) and threefold for MgO(111). For MgO(111), the LEED pattern for E_P=375 eV is shown; for the lower primary beam energies, the spots were faint and the background was high due to charging effects.

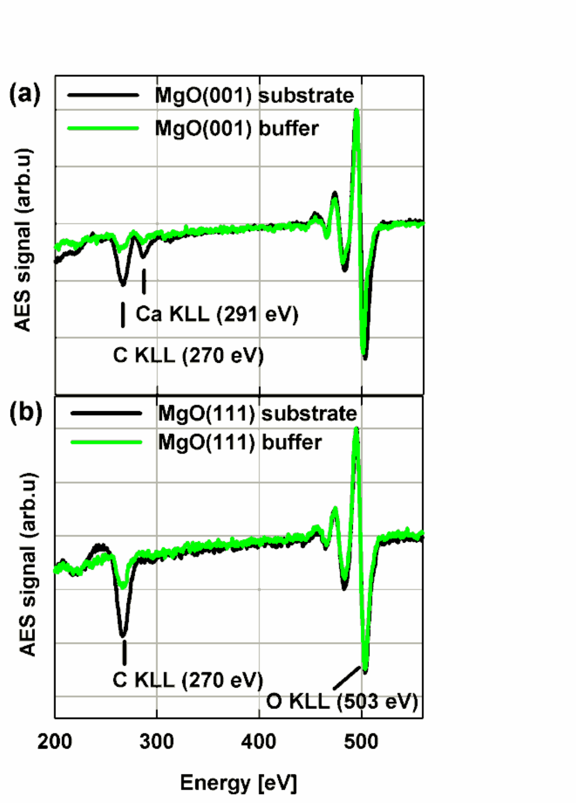

Fig. 3. AES spectra of the MgO(001) (a) and MgO(111) (b) substrates and the homoepitaxial buffer layers. The spectra are normalized to the oxygen peak.

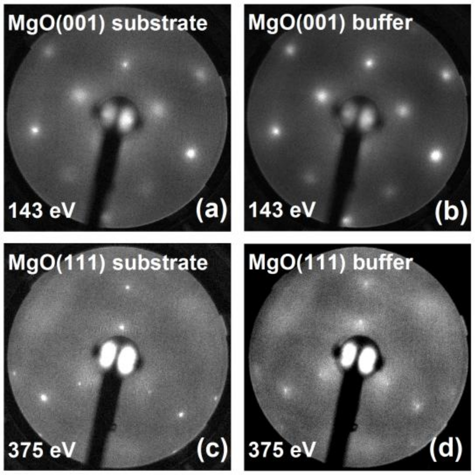

Fig. 4. LEED patterns of the MgO(001) and MgO(111) substrates ((a) and (c), respectively) and of the corresponding homoepitaxial buffer layers deposited onto the substrates ((b) and (d), respectively).

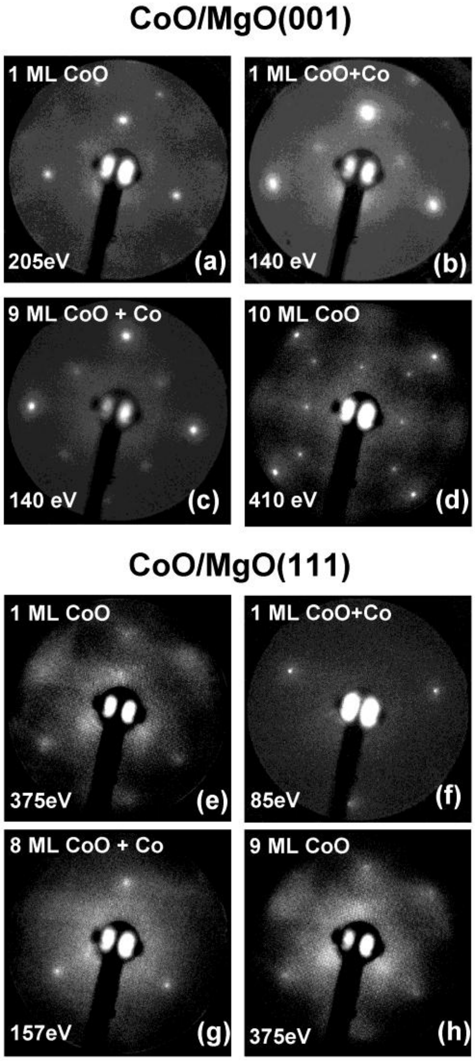

Fig. 5. LEED patterns recorded during CoO layer preparation onto MgO(001) and MgO(111) ((a)-(d) and (e)-(h), respectively).

LEED was also used to monitor the crystalline quality of the CoO films grown on MgO(001) and MgO(111). The LEED patterns were recorded after each preparation step. Selected patterns are shown in Fig. 5. For both crystal orientations, LEED observations were difficult due to charging effects. The minimum primary beam energy (E_{min}) for which the diffraction pattern was experimentally observable increased with increasing CoO thickness, from 205 eV for 1 ML to 410 eV for 10 ML for CoO grown on MgO(001) (Fig. 5(a) and (d)) and from 120 eV for 1 ML to approximately 370 eV for 9 ML for CoO grown on MgO(111) (Fig. 5(e) and (h)). The enhanced charging might be related to the different band gaps of MgO and CoO, which equal 7.8 eV[24] and approximately 3 eV[25], respectively. The patterns observed throughout the entire growth of the CoO films reflect the symmetry of the MgO substrates, and hence, the CoO films that resulted from the layer-by-layer deposition onto the MgO(001) and MgO(111) substrates were unambiguously identified as CoO(001) and CoO(111), respectively.

The diffraction spots observed for CoO(111) were more diffused than those for CoO(001). However, in contrast to CoO(001), where the spots were equally sharp for the metallic and oxidic layers, the differences between the qualities of the images were significant for the CoO(111) case. Due to the enhanced conductivity of the metal surface, the background was suppressed and the diffraction spots became sharper and brighter after deposition of the metallic Co layer. This finding indicates that the wider and more diffused spots observed for the oxidized layers are related to charging effects rather than being caused by a lower structural quality. For both cases, after each deposition of metallic Co, a LEED pattern was obtained for an E_{min} of approximately 100 eV.

Charging of the samples influenced the LEED patterns of the Fe films deposited onto CoO(001) and CoO(111). Although the patterns were very weak, with the diffused spots appearing only at high primary beam energies (larger than 300 eV) (Fig. 6), the known epitaxial relation with CoO(001), i.e., Fe(001)[110]||CoO(001)[100][26], is evident (Fig. 6(a)). Fe grown on CoO(111) showed a diffused diffraction pattern, in which a sixfold symmetry is clearly visible (Fig. 6b), corresponding to the expected epitaxial growth[27]. When Fe is grown on CoO(111), (110)-oriented grains are formed, which, due to their twofold symmetry, have different in-plane orientations rotated by 120°(Ref. 27). The incoherent superposition of the diffraction patterns from different epitaxial grains leads to the observed pattern of the threefold symmetry, which may be further blurred by charging effects.

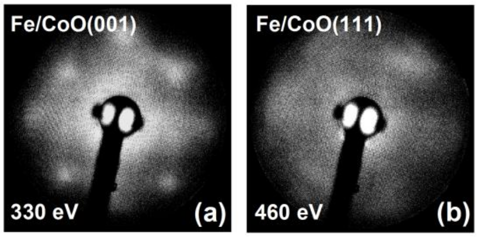

Fig. 6 LEED patterns recorded at the surfaces of Fe grown on CoO(001) (a) and CoO(111) (b).

XPS was employed to characterize the chemical structure of the CoO films. The spectra recorded at the electron exit angle θ=0° (along the surface normal) and at θ=60° are presented in Fig. 7. The Co 2p lines showed a distinct satellite structure, characteristic of CoO[28-30]. The spectra measured for both CoO(001) and CoO(111) were fitted with two doublets (A and B) and two satellite lines (S). The main parameters of the fitted components are presented in Table 1.

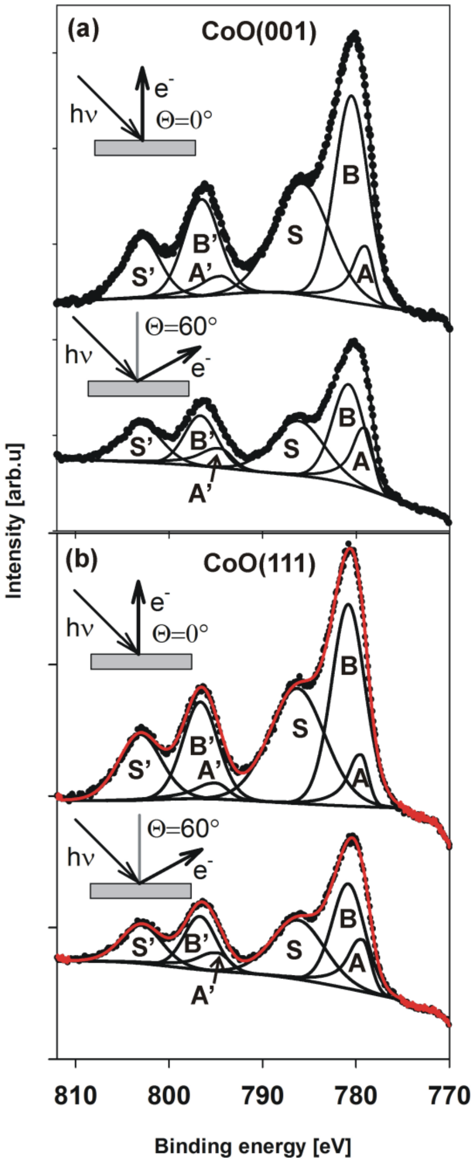

Fig. 7 Co 2p XPS lines measured for CoO(001) (a) and CoO(111) (b) with θ=0° and θ=60°.

Table 1 The main parameters of the XPS components derived from the Co 2p spectra. The binding energy of the Co $2p_{3/2}$ line and the corresponding FWHM are listed in columns 3 and 4. Δ represents the spin-orbit splitting. The percent of the spectral area of a given line is listed in column 6.

Sample	Cp	E_B Co $2p_{3/2}$ (eV)	FWHM (eV)	Δ (eV)	Area(%)
CoO(001)	A	778.9	1.9	15.5	17
θ=0°	B	780.5	4.2	16.0	83
	S	785.7	7.0	17.2	
CoO(001)	A	779.0	1.9	15.5	31
θ=60°	B	780.8	4.1	15.8	69
	S	786.1	6.5	16.8	
CoO(111)	A	779.5	1.9	15.4	15
θ=0°	B	780.8	4.2	15.8	85
	S	786.3	7.0	16.8	
CoO(111)	A	779.2	2.0	15.5	26
θ=60°	B	780.8	3.9	15.9	74
	S	786.1	6.5	16.9	

A deconvolution of the Co 2p spectra showed dominating components at similar binding energies of 780.5 eV and 780.8 eV for CoO(001) and CoO(111), respectively. The value of 780.5 eV is typical for CoO[29,31,32]. Other parameters, such as spin-orbit splitting, equal to 15.7 eV and 15.8 eV for CoO(001) and CoO(111), respectively, and the separation between the $2p_{3/2}$ main line (B) and the satellite (S) (5.2 eV and 5.5 eV for CoO(001) and CoO(111), respectively), agree with the values reported for CoO powder and differ significantly from the values reported for Co_3O_4[31]. In addition, the width of component B, which equals 4.2 eV in both cases, is only slightly larger than the FWHM reported for CoO powder (3.7 eV). This slight broadening can be easily understood by considering that the binding energy of the cobalt core electrons may be slightly different at the MgO/CoO interface, the CoO surface and the center of the film. In addition to the main doublet B, additional components at the lower binding energy were fitted (doublet A). Their binding energies, equal to 778.9 eV and 779.4 eV for CoO(001) and

CoO(111), respectively, lie between the values expected for metallic Co (778.2 eV) and Co_3O_4 (779.6-779.8 eV)[32,33]. The relative intensity of doublet A increases with the angle θ, suggesting that the species responsible for this component are located in the surface region. We identified this component as reduced cobalt oxide, based on the result that the best fit was obtained using an asymmetric peak shape and without additional satellite lines, both characteristic traits of metallic species. In addition, the preparation conditions in our experiment were reducing (each oxidation was followed by annealing); thus, an oxygen deficiency in the surface region is not surprising. In summary, the two CoO films were found to have very similar chemical structures, with the stoichiometry close to Co_1O_1, and slightly reduced surface regions.

Having characterized the composition and crystalline structure of the CoO films, possible stabilization mechanisms of the polar CoO(111) film should be discussed. One possible mechanisms is p(2x2) octopolar reconstruction, which leads to the formation of {100} nanofacets[16]. This mechanism cannot be excluded due to the vague LEED patterns. The CoO(111) surface might be also stabilized by adsorbed OH^- groups; in that case, the surface is not reconstructed[34]. However, we propose that the CoO(111) film is sufficiently stable due to the metallization of the CoO surface region, and in this case, no additional stabilization mechanisms are needed.

To investigate the chemical structure of the Fe/CoO interfaces, CEMS spectra were recorded (**Fig. 8**). The hyperfine parameters, which characterize each spectral component, are given in Table **2**. Each of the components corresponds to a different atomic site occupied by the ^{57}Fe atoms. Hyperfine parameters are used to identify the chemical state and atomic surroundings of given groups of atoms. The isomer shift (IS), which changes with the density of *s* electrons at the nucleus, provides information on the oxidation state of the ^{57}Fe atoms, the hyperfine magnetic field (B_{hf}) is related to the magnetic moment of the ^{57}Fe probe atoms and its nearest neighbors, and the quadrupole interaction (ε) is sensitive to the electric field gradient and reflects the local symmetry of the valence electron charge distribution[35]. The spectra measured for Fe/CoO(001) and Fe/CoO(111) are characterized by a similar set of the components. Therefore, the interfacial model proposed here applies to the bilayers of both orientations, with small differences, which are highlighted below.

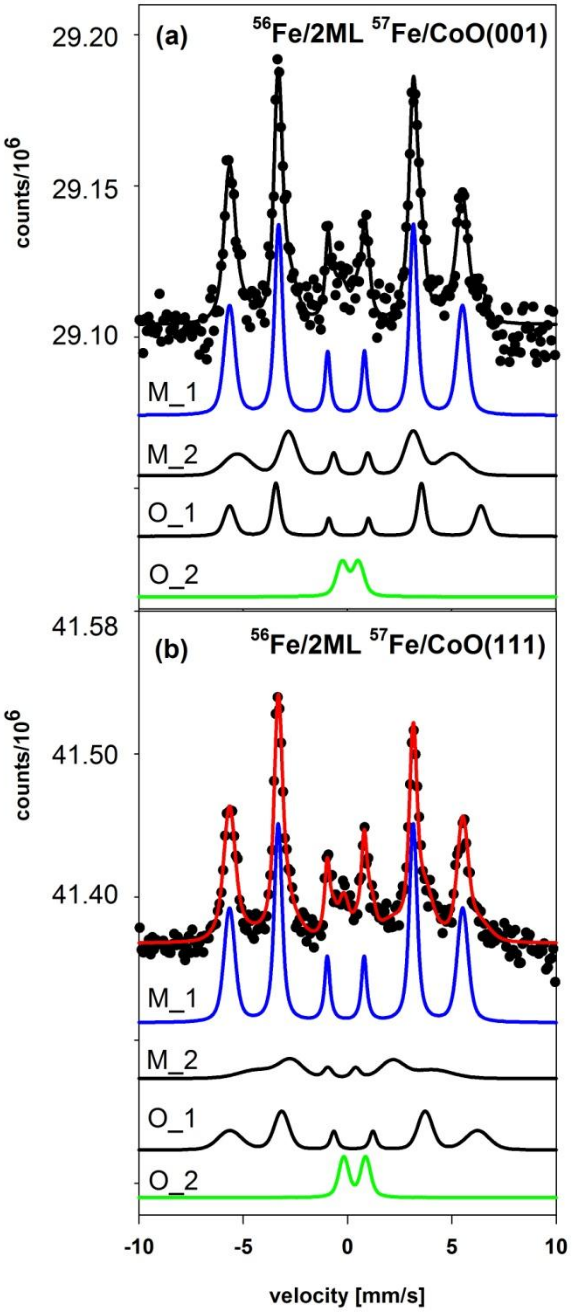

Fig. 8 CEMS spectra (dotted line) measured for ^{56}Fe/2ML ^{57}Fe/CoO(001) (a) and ^{56}Fe/2ML ^{57}Fe/CoO(111) (b) together with the best fit (solid line), deconvoluted into components, which are shifted along the y axis for clarity.

Table 2 Hyperfine parameters derived from numerical fits of the CEMS spectra for the Fe/CoO(001) and Fe/CoO(111) interfaces. IS is the average value of the isomer shift with respect to α-Fe. Average quadrupole interaction (ε) (sextets) or quadrupole splitting (QS) (doublets) are listed in column 4. B_{hf} is the average hyperfine magnetic field and ΔB_{hf} is the Gaussian width of the B_{hf} distribution for a given component. RW is the relative weight of the component. The asterisks mark the parameters fixed during the fitting process.

Sample	Site	IS (mm/s)	ε/QS (mm/s)	B_{hf} (T)	ΔB_{hf} (T)	RW (%)
Fe/CoO(001)	M_1	0.04(4)	0.00(2)	34.6(3)	1.2*	55(7)
	M_2	0.1(2)	-0.1(2)	32(2)	3(1)	24(10)
	O_1	0.3(1)	0.1(1)	37(1)	1.2(9)	15(8)
	O_2	0.2(2)	0.8(3)	-	-	6(2)
Fe/CoO(111)	M_1	0.02(1)	0.00(1)	34.6(1)	1.2*	61(4)
	M_2	0.0(4)	0.0(4)	26(3)	5(4)	13(7)
	O_1	0.4(1)	0.0(1)	36.8(8)	3(1)	19(4)
	O_2	0.44(7)	1.0(1)	-	-	7(2)

Knowing the thickness of the ^{57}Fe probe, it is possible to calculate the amount of ^{57}Fe atoms corresponding to each component using its relative weight RW. An easily distinguishable component is a doublet (component O_2), which in both spectra comes from a small amount of ^{57}Fe atoms (6-7% of the probe) that diffused into the CoO[36] and which are magnetically decoupled from the rest of the Fe film. The most intense component in both spectra (M_1) is characterized by an IS, indicating its metallic character (IS≈0). However, the hyperfine magnetic field, equal to 34.6 T in both spectra, is larger than the typical value for α-Fe (B_{hf}=33 T at RT[35]). Such an increased B_{hf} is a result of the proximity of Co atoms to Fe atoms at the Fe-CoO interface. Because the XPS measurements indicated that the surfaces of the CoO films were reduced, we interpret component M_1 as originating from the metallic intermixed Fe-Co interfacial region. In iron-rich FeCo alloys, the hyperfine magnetic field at the Fe nucleus increases almost linearly with the Co content, reaching 35 T for 10 at. % of Co, i.e., $Fe_{0.9}Co_{0.1}$[37].

Additional CEMS measurements conducted with a thicker probe layer (not shown) revealed that approximately 4 Å of iron is mixed with cobalt at the Fe/CoO interface.

Among the two remaining components in the spectra, one has a metallic (M_2) and one has an (O_1) oxidic character. The O_1 component, with a hyperfine magnetic field of B_{hf}=37 T, is characterized by an isomer shift IS=0.3-0.4 mm/s, which is typical for bulk iron in the Fe^{3+} oxidation state[35]. The oxidation of Fe atoms is a result of the CoO proximity and often accompanies the formation of a metallic alloy at the metal/oxide interface[38]. The hyperfine magnetic field of the O_1 component is significantly lower than expected for different Fe_2O_3 phases (approximately 50T[35]), but is close to the value of 38.4 T reported for α-FeOOH[39]. However, the identification of the O_1 component in terms of stoichiometric bulk phases may not be relevant due to the low-dimensional nature of the interfacial iron oxide. Hence, we interpret the interfacial oxidation in the Fe/CoO bilayers as the formation of iron-oxygen bonds, most likely due to the incorporation of oxygen atoms in the hollow sites of the bcc Fe structure, analogous to Fe/MgO[40]. The metallic component M_2, identified by an IS close to zero, exhibited a markedly different hyperfine magnetic field for the (001) and (111) orientations: B_{hf}=32 T and B_{hf}=26 T, respectively. In combination with the large width of the B_{hf} distribution, this finding indicates an interfacial origin of this component. Apparently, at the Fe/CoO(001) interface, the coordination of the Fe atoms to their metallic neighbors is different than at the more defective Fe/CoO(111) interface. A similar high sensitivity of the hyperfine magnetic field to the local atomic coordination was recently demonstrated for the Fe/MgO interface[40]. The amount of iron oxide formed at the Fe/CoO interface corresponds to only a fraction of the monolayer.

If we assume that only components O_1 and M_2 come from the interface, while the FeCo mixed region links this interfacial layer with the interior of the Fe film, the quantitative considerations lead to the conclusion that the ^{57}Fe grown on CoO formed islands, which is in line with recent experimental findings[41]. Consequently, the amount of iron oxide was recalculated to 40% of the interfacial Fe monolayer for Fe/CoO(001) and to 60% for Fe/CoO(111). This result is similar to the finding of 0.3 ML of FeO based on x-ray absorption spectroscopy at the interface with CoO in an Fe/CoO/Ag(001) structure[42]. The small difference in the amount of the interfacial iron oxide for Fe/CoO(001) and Fe/CoO(111) may be related to different terminations of the CoO surfaces and thus different oxidation conditions.

In summary, the Fe/CoO(001) and Fe/CoO(111) bilayers were very similar in terms of the crystalline quality and stoichiometry of the CoO films, as well as in the chemical structure of the Fe/CoO interface.

B. Magnetic properties

The MOKE measured at RT for different azimuthal angles φ revealed the intrinsic magnetic anisotropies of the two structures. The angle φ was measured with respect to MgO[100] and MgO[-110] for Fe/CoO/MgO(001) and Fe/CoO/MgO(111), respectively. Representative hysteresis loops are shown in Fig. **9**(a), while Fig. **9**(b) presents polar plots of the reduced remanence. For both orientations, the coercivity measured along the easiest anisotropy direction was equal to 12 Oe. Significant differences appeared in the saturation field (H_S) along the hardest anisotropy directions, which indicates differences in the effective magnetic anisotropies. For Fe/CoO(001), H_S equals 500 Oe. Using the bulk magnetization for the Fe layer, this value corresponds to an effective anisotropy of $4.2\text{x}10^5$ erg/cm^3, which is very close to the magnetocrystalline anisotropy of bulk Fe (4.8×10^5 erg/cm^3 (Ref. 43)). Meanwhile, for Fe/CoO(111), H_S=100 Oe, which reflects a much smaller value for the effective anisotropy, i.e., 0.84×10^5 erg/cm^3.

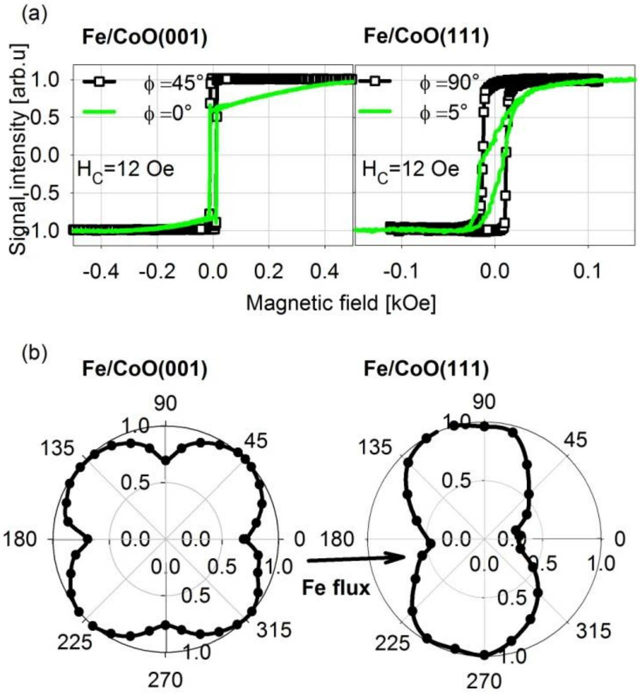

Fig. 9 (a) Hysteresis loops measured at RT along the easiest and hardest anisotropy directions, corresponding to φ=45° and φ=0° for Fe/CoO(001) and φ=90° and φ=5° for Fe/CoO(111). The azimuthal angle is measured relative to the MgO[100] and MgO[-110] directions for Fe/CoO(001) and Fe/CoO(111), respectively. (b) Polar plots of the reduced remanence showing the fourfold anisotropy of Fe/CoO(001) and the uniaxial anisotropy of Fe/CoO(111).

Fe grown on CoO(001) exhibited two orthogonal in-plane easy axes, along the Fe[100] and Fe[010] directions, as expected for Fe(001) films. In contrast, the magnetic anisotropy of the Fe film grown on CoO(111) was uniaxial. Indeed, the Fe(110) surface contains only one easy magnetocrystalline anisotropy axis (Fe[100]), but the uniaxial magnetic anisotropy (UMA) presently observed for Fe/CoO(111) cannot be of magnetocrystalline origin because the Fe film is composed of grains rotated by 120°. The uniaxial anisotropy contributions may have diverse origins: interface anisotropy, as in Fe/GaAs(100)[44], shape anisotropy[45] or growth-induced anisotropy, which originates from the shadowing effect[46,47]. Although the evaporator used in this study produced an Fe flux at only 12° from the substrate normal, growth-induced anisotropy[46] was responsible for the UMA in the Fe/CoO(111) sample. The easy magnetization direction was oriented perpendicular to the projection of the Fe flux direction onto the sample surface, which was also verified in analogous samples prepared on substrates rotated relative to the evaporator. The UMA contribution is not apparent for the Fe/CoO(001) sample; for that case, the total magnetic anisotropy is dominated by the magnetocrystalline term.

To investigate the AFM-FM magnetic exchange couplings that are characteristic of Fe/CoO(001) and Fe/CoO(111), the samples were field cooled to 80 K. The cooling magnetic field was applied along the easiest magnetization directions because the hysteresis loops before FC were very similar in this case. At 80 K, both systems showed a large coercivity, which increased by factors of 60 (up to H_C=740 Oe) and 100 (up to H_C=1280 Oe) relative to RT for Fe/CoO(001) and Fe/CoO(111), respectively (Fig. **10**).

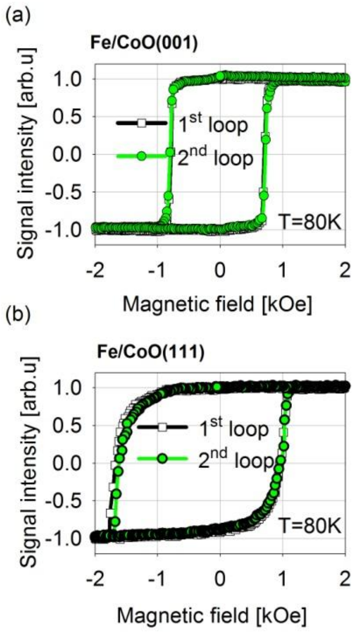

Fig. 10 First and second hysteresis loops measured at 80 K after FC for Fe/CoO(001) (a) and Fe/CoO(111) (b).

The coercivity in AFM-FM systems is known to follow the number of uncompensated AFM interfacial spins[11], the majority of which are rotatable[12]. However, Radu et al. argued that the spins belonging to the AFM layer might be rotatable only when the interfacial region has a lowered AFM anisotropy[48]. An interfacial region supplying AFM spins that can rotate together with the FM might exist also for nominally compensated systems as a result of roughness or other structural defects[48]. In our samples, the FM/AFM interface contains mixed FeCo regions, which, for both orientations, may be a source of magnetic moments that increase the coercivity. However, the much larger coercivity enhancement observed for the Fe/CoO(111) system suggests a more complex phenomenon, which is also reflected in the differences in the EB fields, which are clearly shown in Fig. **10**. For both configurations, the first hysteresis loop measured at 80 K ('1st loop') was shifted by H_{EB}=37 Oe and H_{EB}=354 Oe for Fe/CoO(001) and Fe/CoO(111), respectively, in the direction opposite to the magnetic field applied during FC. The value of H_{EB}=354 Oe measured at 80 K is much larger than previously reported values for other bilayer systems based on CoO(111) and a metallic ferromagnetic layer[17,18,49,50]. The occurrence of the training effect was verified through a subsequent measurement of another hysteresis loop ('2nd loop'), which was identical to the '1st loop' for Fe/CoO(001) and which indicated a slightly (7%) decreased EB field (H_{EB}=328 Oe) for Fe/CoO(111). This weak training effect is related to the high structural quality of the bilayers, as this effect is usually observed for polycrystalline samples[51,52].

The EB effect in the Fe/CoO bilayers was studied as a function of temperature. Hysteresis loops were measured for temperatures ranging from 80 K to 300 K after FC to 80 K (procedure A). To account for the slight training effect observed for the Fe/CoO(111) system, measurements were also performed in which the FC was performed to each temperature separately (procedure B). The temperature dependence of H_C and H_{EB} is presented in Fig. **11**. Measurement procedures A and B led to very similar results, as expected based on the very small training effect observed for the Fe/CoO(111) sample. For both samples, H_{EB} and H_C decreased with temperature. However, the temperature dependences of H_{EB} and H_C for Fe/CoO(001) and Fe/CoO(111) are different. For Fe/CoO(111), both quantities show a linear temperature dependence; however, a plateau for intermediate temperatures is observed for Fe/CoO(001). For both samples, the coercivity is larger at lower temperatures due to the increased magnetocrystalline anisotropies of both Fe and CoO. The coercivity enhancement is observed below T=265 K, which is slightly lower than the Néel temperature of bulk CoO, as expected.

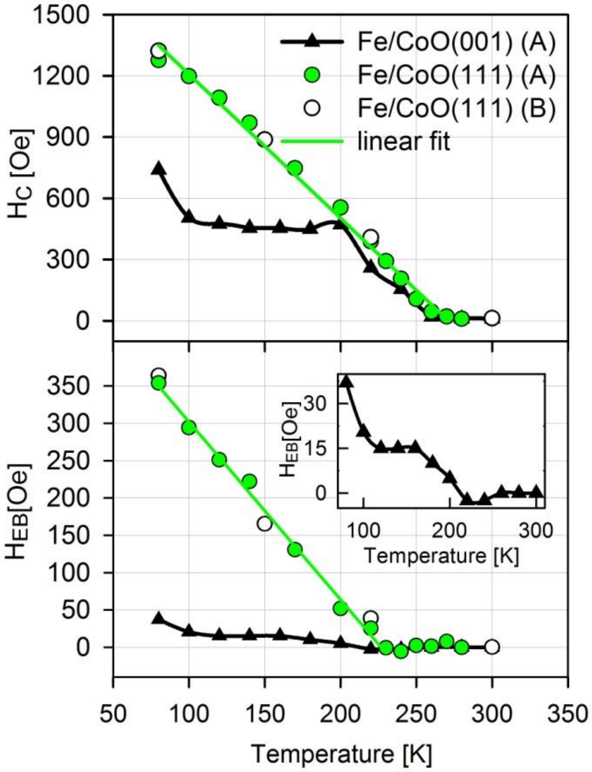

Fig. 11 Temperature dependence of the coercive field (H_C) and EB field (H_{EB}) for Fe/CoO(001) and Fe/CoO(111) measured after a single FC procedure (procedure A, full symbols) and measured after FC was performed for Fe/CoO(111) separately at each temperature (procedure B, empty symbols). The inset presents a rescaled H_{EB} temperature dependence for the Fe/CoO(001) sample. For the Fe/CoO(111) sample, both parameters were fitted with a linear temperature dependence. For Fe/CoO(001), the solid lines are guides to the eye.

The linear temperature dependence of H_{EB} found for Fe/CoO(111) has been observed in many EB systems[53,54,14]. According to the Malozemoff EB model[9], H_{EB} is proportional to the energy stored in the domain wall (σ_{AF}), which is formed in the antiferromagnet. Because $\sigma_{AF} \propto (A_{AFM} K_{AFM})^{1/2}$, where A_{AFM} represents the exchange stiffness and K_{AFM} indicates the anisotropy constant of the AFM component, the temperature dependence of H_{EB} is governed by changes in K_{AFM}, assuming that A_{AFM} is temperature-independent. For a cubic AFM anisotropy, the linear temperature dependence of $H_{EB}(T)$ within the Malozzemoff model follows from the temperature dependence of the anisotropy constant: $K_{AFM}(T)= K_{AFM}(0)(1-T/T_N)^2$ (Ref. 9,53). Consequently, the temperature dependence of H_{EB} for Fe/CoO(111) was fitted with $H_{EB}(T)\propto(1-T/T_B)$, where T_N was replaced by the blocking temperature T_B=227 K. T_B is the temperature above which the AFM domains become stable against the exchange interactions with the FM layer[50], and H_{EB} vanishes. The blocking temperature found for the Fe/CoO(111) bilayer is lower than the Néel temperature of bulk CoO. Such a significant lowering of T_B with respect to T_N could be attributed to the deviation from the Co_1O_1 stoichiometry towards Co_3O_4 ($T_N(Co_3O_4)$=34 K)[49]. However, because the CoO films prepared in the present study were reduced rather than over-oxidized (Section IIIA), we propose that the lowered T_B is due to the small thickness of the CoO films (20 Å). Similarly reduced values of T_B have been observed for diverse systems, such as CoNiO/NiFe, NiO/NiFe[55] and Fe_3O_4/CoO[54] bilayers with AFM layers thinner than approximately 50 Å. This effect is related to the weakening of exchange interactions with decreasing AFM layer thickness rather than a finite size effect of the T_N reduction[54,56].

The EB field measured for Fe/CoO(001) was much smaller compared to Fe/CoO(111) and presented a more complex temperature dependence. Below 210 K, the hysteresis loop was shifted in the direction opposite to the magnetic field used for FC, which is a typical negative EB effect[5]. After the rapid low temperature decrease, a plateau region occurred between 120 K and 160 K, followed by a linear decrease to 210 K. A similar temperature dependence was reported for the EB in polycrystalline Py/CoO layers, in which the EB followed the thermoremanent magnetization of the CoO interfacial uncompensated spins[57]. The measurements between 220 K and 240 K exhibited hysteresis loops slightly shifted along the FC direction, indicating a small positive EB effect. Similar effects near the blocking temperature have been previously reported for polycrystalline Co/CoO[58] and textured CoO/Co(111)[59] bilayers. However, for our sample, this positive H_{EB} equals only 3 Oe, which is on the order of the experimental uncertainty; hence, we find this value negligible. Thus, for the Fe/CoO(001) sample, we consider T_B=210 K as the temperature below which a negative EB occurs. This value is similar to that of Fe/CoO(111), which supports the interpretation of its relation to the reduced thickness of the CoO films.

IV. SUMMARY AND CONCLUSIONS

In conclusion, we have investigated Fe/CoO(001) and Fe/CoO(111) epitaxial bilayers with nominally compensated and uncompensated FM-AFM interfaces through structural and magnetic characterization. The layer-by-layer deposition method employed in this work resulted in nearly stoichiometric CoO films with reduced surfaces. A fraction of a monolayer of Fe oxide was identified at the Fe/CoO interfaces for both orientations. The Fe oxidation was accompanied by the formation of a mixed metallic $Fe_{0.9}Co_{0.1}$ region. The Fe films grown on CoO(001) exhibited the expected fourfold magnetic anisotropy, while the Fe films deposited on CoO(111) were uniaxial. Field cooling resulted in a strong coercivity enhancement for both samples, while the exchange bias was drastically larger for Fe/CoO(111) compared to Fe/CoO(001). The temperature dependences of H_{EB} and H_C were similar within each system, yet different for the two crystal orientations.

We attribute the exchange bias and coercivity enhancement in the Fe/CoO bilayers to the uncompensated pinned and rotatable spins, respectively, present at the Fe/CoO interface. The number of uncompensated spins is much larger for CoO(111) than for nominally compensated CoO(001), where their only source is the atomic level roughness. Furthermore, the intrinsic magnetic anisotropy of the Fe film grown on CoO(111) is much weaker than in the Fe/CoO(001) configuration; thus, the total anisotropy of the system is much more sensitive to the unidirectional anisotropy introduced during field cooling. The origin of the remarkably strong exchange bias observed for Fe/CoO(111) should be attributed to the combination of the uncompensated spin structure of CoO(111) and the low intrinsic magnetic anisotropy of the Fe film. Therefore, we provide direct evidence of the dominant role of crystalline orientation in the magnetic behavior of epitaxial systems.

ACKNOWLEDGMENTS

This work was supported in part by the National Science Center (NCN), Poland (Grant No. 2011/02/A/ST3/00150), and by the MPD and TEAM Programs of the Foundation for Polish Science co-financed by the EU European Regional Development Fund.

* Author to whom correspondence should be addressed: Ewa Młyńczak, Jerzy Haber Institute of Catalysis and Surface Chemistry, Polish Academy of Sciences, ul. Niezapominajek 8, 30-239 Krakow, Poland; Electronic mail: ncmlyncz@cyf-kr.edu.pl

[1] M. Finazzi, L. Duò, F. Ciccacci, Surf. Sci. Rep. 64, 139 (2009)
[2] K. O’Grady, L. E. Fernandez-Outon and G. Vallejo-Fernandez, J. Magn. Magn. Mat. 322, 883 (2010)
[3] C. Tsang, R. E. Fontana, T. Lin, D. E. Heim, V. S. Speriosu, B. A. Gurney, and M. L. Williams, IEEE Trans. Magn. 30, 3801 (1994)
[4] S. S. P. Parkin, K. P. Roche, M. G. Samant, P. M. Rice, R. B. Beyers, R. E. Scheuerlein, E. J. O’Sullivan, S. L. Brown, J. Bucchigano, D. W. Abraham, Yu Lu, M. Rooks, P. L. Trouilloud, R. A. Wanner, and W. J. Gallagher, J. Appl. Phys. 85, 5828 (1999)
[5] J. Nogués, I. K. Schuller, J. Magn. Magn. Mat. 192, 203 (1999)
[6] W. H. Meiklejohn and C. P. Bean, Phys. Rev. 102, 1413 (1956)
[7] J. Gurgul, K. Freindl, A. Kozioł- Rachwał, K. Matlak, N. Spiridis, T. Ślęzak, D. Wilgocka- Ślęzak, and J. Korecki, Surf. Interface Anal. 42, 696 (2010).
[8] P. Luches, S. Benedetti, A. di Bona and S. Valeri, Phys. Rev. B 81, 054431 (2010)
[9] A. P. Malozemoff, Phys. Rev. B. 35, 3679 (1987)
[10] C. Schulthess and W.H. Butler, Phys. Rev. Lett. 20, 4516 (1998)
[11] H. Ohldag, T. J. Regan, J. Stöhr, A. Scholl, F. Nolting, J. Lüning, C. Stamm, S. Anders, and R. L. White, Phys. Rev. Lett. 87, 247201 (2001)
[12] H. Ohldag, A. Scholl, F. Nolting, E. Arenholz, S. Maat, A.T. Young, M. Carey, and J. Stöhr, Phys. Rev. Lett. 91, 017203 (2003)
[13] A. E. Berkowitz, K. Takano, J. Magn. Magn. Mat. 200, 552 (1999)

[14] M. Gruyters, J. Magn. Magn. Mat. 248, 248 (2002)
[15] W. L. Roth, Phys. Rev. 110, 1333 (1958)
[16] J. Goniakowski, F. Finocchi and C. Noguera, Rep. Prog. Phys. 71, 016501 (2008)
[17] N. J. Gökemeijer, R. L. Penn, D. R. Veblen and C. L. Chien, Phys. Rev. B 63, 174422 (2001)
[18] M.R. Ghadimi, B. Beschoten, and G. Güntherodt, Appl. Phys. Lett. 87, 261903 (2005)
[19] P.J. van der Zaag, A. R. Ball, L.F. Feiner, R.M. Wolf, and P. A. A. van der Heijden, J. Appl. Phys. **79**, 5103 (1996)
[20] J. Gurgul, E. Młyńczak, N. Spiridis and J. Korecki, Surf. Sci. 606, 711 (2012)
[21] S. A. Chambers, Surf. Sci. Rep 39, 105 (2000)
[22] CasaXPS 2.3.15, © 1999-2009, Casa Software Ltd
[23] Recoil 1.05 Mössbauer Analysis Software for Windows, © 1998, 2002, Ken Lagarec.
[24] D. M. Roessler and W. C. Walker, Phys. Rev. 159, 733 (1967)
[25] V. I. Anisimov, M. A. Korotin and E. Z. Kurmaev, J. Phys.: Condens. Matter 2**,** 3973 (1990)
[26] A. Brambilla, P. Sessi, M. Cantoni, L. Duò, M. Finazzi, and F. Ciccacci, Thin Solid Films 516, 7519 (2008).
[27] G. Nowak, A. Remhof, F. Radu, A. Nefedov, H.-W. Becker and H. Zabel, Phys. Rev. B. 75, 174405 (2007)
[28] K.S. Kim, Phys. Rev. B. 11, 2177 (1975)
[29] G. A. Carson, M. H. Nassir, and M.A. Langell, J. Vac. Sci. Technol. A 14, 1637 (1996)
[30] S. Valeri, A. Borghi, G.C. Gazzadi, and A. di Bona, Surf. Sci. 423, 346 (1999)
[31] T.J. Chuang, C.R. Brundle and D. W. Rice, Surf. Sci. 59, 413 (1976)
[32] S. C. Petitto and M. A. Langell, J. Vac. Sci. Technol. A, 22, 1690 (2004)
[33] C. R. Brundle, T. J. Chuang and D. W. Rice, Surf. Sci. 60, 286 (1976)
[34] D. Cappus, M. Haßel, E. Neuhaus, M. Heber, F. Rohr, H.-J. Freund, Surf. Sci. 337, 268 (1995)
[35] N.N. Greenwood and T. C Gibb *Mössbauer Spectroscopy*, (Chapman and Hall LTD, London 1971)
[36] V. G. Bhide and G. K. Shenoy, Phys. Rev. 147, 306 (1966)
[37] E. Jartych, J. K. Zurawicz and M. Budzyński, J. Phys.: Condens. Matter 5, 927 (1993)
[38] T. J. Regan, H. Ohldag, C. Stamm, F. Nolting, J. Lüning, J. Stöhr and R. L. White, Phys. Rev. B 64, 214422 (2001)
[39] J. B. Forsyth, I.G. Hedley, and C.E. Johnson, J. Phys. C. 1, 179 (1968)
[40] E. Młyńczak, K. Freindl, N. Spiridis and J. Korecki, J. Appl. Phys. 113, 024320 (2013)
[41] A. Brambilla, A. Picone, M. Finazzi, L. Duò, and F. Ciccacci, Surf. Sci. 605, 95 (2011).
[42] R. Abrudan, J. Miguel, M. Bernien, C. Tieg, M. Piantek, J. Kirschner and W. Kuch, Phys. Rev. B 77, 014411 (2008)
[43] C.D. Graham, Jr. Phys. Rev. 112, 1117 (1958)
[44] O. Thomas, Q. Shen, P. Schieffer, N. Tournerie, and B. Lépine, Phys. Rev. Lett. 90, 017205 (2003)
[45] Q. Zhan, S. Vandezande, C. Van Haesendonck, and K. Temst, Appl. Phys. Lett. 91, 122510 (2007)
[46] Q. Zhan, C. Van Haesendonck, S. Vandezande, and K. Temst, Appl. Phys. Lett. 94**,** 042504 (2009)

[47] S. van Dijken, L. C. Jorritsma, and B. Poelsema, Phys. Rev. Let.. 82, 4038 (1999)

[48] F. Radu, A. Westphalen, K. Theis-Bröhl and H. Zabel, J. Phys.: Condens. Matter 18, L29 (2006)

[49] G. Nowak, A. Remhof, F. Radu, A. Nefedov, H.-W. Becker, and H. Zabel, Phys. Rev. B 75, 174405 (2007)

[50] F. Radu, S. K. Mishra, I. Zizak, A. I. Erko, H. A. Durr, W. Eberhardt, G. Nowak, S. Buschhorn, H. Zabel, K. Zhernenkov, M. Wolff, D. Schmitz, E. Schierle, E. Dudzik, and R. Feyerherm, Phys. Rev. B 79, 184425 (2009)

[51] A. Hochstrat, Ch. Binek, and W. Kleemann, Phys. Rev. B. 66, 092409 (2002)

[52] C. Fleischmann, F. Almeida, J. Demeter, K. Paredis, A. Teichert, R. Steitz, S. Brems, B. Opperdoes, C. Van Haesendonck, A. Vantomme, and K. Temst, J. Appl. Phys. 107, 113907 (2010)

[53] Z.Y. Liu and S. Adenwalla, J. Appl. Phys. 94, 1105 (2003).

[54] P. J. van der Zaag, Y. Ijiri, J. A. Borchers, L. F. Feiner, R. M. Wolf, J. M. Gaines, R.W. Erwin, and M. A. Verheijen, Phys. Rev. Lett. 26, 6102 (2000)

[55] A. J. Devasahayam and M. H. Kryder, J. Appl. Phys. 85, 5519 (1999)

[56] X. Y. Lang, W. T. Zheng and Q. Jiang, Nanotechnology 18, 155701 (2007)

[57] K. Takano, R. H. Kodama, and A. E. Berkowitz, Phys. Rev. Lett. 79, 1130 (1997)

[58] T. Gredig, I. N. Krivorotov, P. Eames, and E. D. Dahlberg, Appl. Phys. Lett. 81, 1270 (2002)

[59] F. Radu, M. Etzkorn, R. Siebrecht, T. Schmitte, K. Westerholt, and H. Zabel, Phys. Rev. B 67, 134409 (2003)

AIP | Journal of Applied Physics

NiO/Fe(001): Magnetic anisotropy, exchange bias, and interface structure

E. Młyńczak, P. Luches, S. Valeri, and J. Korecki

Citation: J. Appl. Phys. **113**, 234315 (2013); doi: 10.1063/1.4811528

JOURNAL OF APPLIED PHYSICS **113**, 234315 (2013)

NiO/Fe(001): Magnetic anisotropy, exchange bias, and interface structure

E. Młyńczak,[1,a)] P. Luches,[2] S. Valeri,[2,3] and J. Korecki[1,4]
[1]*Jerzy Haber Institute of Catalysis and Surface Chemistry, Polish Academy of Sciences, Niezapominajek 8, 30-239 Krakow, Poland*
[2]*S3, Istituto Nanoscienze—CNR, Via G. Campi 213/a, I-41125 Modena, Italy*
[3]*Dipartimento di Scienze Fisiche, Matematiche e Informatiche, Università di Modena e Reggio Emilia, Via G. Campi 213/a, 41100 Modena, Italy*
[4]*Faculty of Physics and Applied Computer Science, AGH University of Science and Technology, al.Mickiewicza 30, 30-059 Krakow, Poland*

(Received 25 April 2013; accepted 4 June 2013; published online 21 June 2013)

The magnetic and structural properties of NiO/Fe epitaxial bilayers grown on MgO(001) were studied using magnetooptic Kerr effect (MOKE) and conversion electron Mössbauer spectroscopy (CEMS). The bilayers were prepared under ultra high vacuum conditions using molecular beam epitaxy with oblique deposition. Two systems were compared: one showing the exchange bias (100ML-NiO/24ML-Fe), ML stands for a monolayer, and another where the exchange bias was not observed (50ML-NiO/50ML-Fe). For both, the magnetic anisotropy was found to be complex, yet dominated by the growth-induced uniaxial anisotropy. The training effect was observed for the 100ML-NiO/24ML-Fe system and quantitatively described using the *spin glass* model. The composition and magnetic state of the interfacial Fe layers were studied using ^{57}Fe-CEMS. An iron oxide phase ($Fe^{3+}{}_4Fe^{2+}{}_1O_7$), as thick as 31 Å, was identified at the NiO/Fe interface in the as-deposited samples. The ferrimagnetic nature of the interfacial iron oxide film explains the complex magnetic anisotropy observed in the samples. *© 2013 AIP Publishing LLC.*
[http://dx.doi.org/10.1063/1.4811528]

I. INTRODUCTION

The exchange bias (EB) phenomenon, occurring in the systems composed of a ferromagnet (FM) and antiferromagnet (AFM), finds wide technological applications in the read heads of recording devices[1] and in magnetoresistive random access memories (MRAM).[2] Since its discovery in 1956 by Meiklejohn and Bean[3] several theoretical models explaining EB have been proposed but a satisfactory quantitative explanation of this phenomenon is still lacking.[4,5] A lot of experimental effort has already been put to describe and understand EB using model layered FM/AFM systems composed of well crystallographically and magnetically defined structures.[6] Epitaxial Fe/NiO bilayers have been extensively studied in the last years, however, most of the attention was directed towards the systems where iron is grown on top of nickel oxide.[7–11] Much fewer works dealt with the reversed bilayer, hereafter referred to as NiO/Fe.[12,13] The reason for that is the much more complicated interface structure formed when oxide is deposited onto a metal surface.[14] These interfacial properties are not easy to be characterized experimentally, as the methods suited for the analysis of buried interfaces are scarce. What is more, the geometrical and chemical structure of the interface between FM and AFM is known to significantly affect the exchange coupling of the magnetic layers.[6] Hence, the characterization of the interface structure in correlation with the magnetic behavior of the layered systems is a prerequisite for the understanding of the physics involved, and it is necessary to design multilayer structures with tailored properties. In the present study, we report on the results of a combined structural and magnetic characterization of the epitaxial NiO/Fe system grown on MgO(001). The characterization of the AFM/FM interface structure was performed using conversion electron Mössbauer spectroscopy (CEMS). Based on the CEMS results, a model of the interface structure is proposed, which explains the magnetic properties characterized using magnetooptic Kerr effect (MOKE) measurements.

The detailed purpose of the reported study is the comparison of the magnetic behavior of the NiO/Fe epitaxial system in two cases: when the exchange bias could not be established and when the field cooling procedure led to an hysteresis loop shift. Generally, the exchange bias can be introduced in a FM-AFM system under certain circumstances that emerge already from the simplest intuitive models of the effect.[4] First, the product of the antiferromagnetic anisotropy and the antiferromagnetic layer thickness must be larger than the interface coupling constant ($K_{AFM}t_{AFM} > J_{INT}$) in order to pin the magnetic moment of the ferromagnet and to produce a loop shift. As a consequence, the EB is observed only above a certain critical thickness of the AFM layer. For example, for the Fe/NiO epitaxial system, a critical thickness of 25 monolayers (ML) was found.[15] Next, the loop shift is inversely proportional to the thickness of the ferromagnetic layer ($H_{EB} \sim 1/t_{FM}$),[4] indicating that the exchange bias is an interfacial effect. Therefore, two systems were designed to differ only in the thicknesses of the layers. Using this approach, it was possible to get insight into the nature of the EB by examination of two NiO/Fe bilayers, one showing the EB and the other where EB could not be established, prepared, and treated identically, where the only differences are

---

[a)]Author to whom correspondence should be addressed. Electronic mail: ncmlyncz@cyf-kr.edu.pl

the thicknesses of the layers. The exchange coupling and the magnetization reversal pathways were observed to be related to the systems' ability to set EB, rather than to result simply from the given combination of the materials in the bilayer.

The paper is organized as follows: the details of the preparation and measurements procedures are presented in Sec. II. Section III contains the experimental results. The magnetic anisotropies in the as-grown samples and the results of the field cooling procedure which establishes EB are described in Sec. III A. Section III B contains a detailed study of the magnetization reversal for the field cooled samples. The interface structure revealed in Sec. III C was used to interpret the magnetic behavior of the NiO/Fe bilayers, which is discussed in Sec. III D.

II. EXPERIMENTAL

All the studied NiO/Fe samples were prepared in a multichamber UHV apparatus on MgO(001) substrates using molecular beam epitaxy (MBE). Prior to the thin films deposition, the MgO(001) polished substrates were annealed up to 500 °C for 1 h under an oxygen pressure of 1.3×10^{-7} mbar. Two kinds of samples were prepared, differing only in the thicknesses of the ferromagnetic and antiferromagnetic layers: the first one, for which the combination of the Fe and NiO gave no exchange bias ("EB−") and the other, where the exchange bias was observed ("EB+"). The "EB−" sample was made of 50 monolayers (ML) of natural iron ($\mathrm{Fe}_{\mathrm{nat}}$) evaporated onto the MgO(001) substrates at room temperature (RT). 1ML of Fe is equivalent to the thickness of 1.43 Å. The resulting Fe layer was annealed at 200 °C for 30 min. The NiO film, 50ML thick (1ML of NiO = 2.08 Å), was deposited onto the Fe layer reactively, i.e., by evaporation of metallic Ni in an oxygen pressure of 1.3×10^{-7} mbar at RT to minimize interfacial reactions. Both iron and nickel were evaporated from Knudsen cells. The evaporation rate of each material was determined using a quartz microbalance. In addition, x- ray photoelectron spectroscopy (XPS) was used to assess the thickness of the deposited Fe layers. To enable CEMS investigations of the chemical state of the as- grown NiO/Fe interface two additional samples were prepared: one with a thick ^{57}Fe probe layer (actual thickness of 11.2ML) located on top of a 43 ML $\mathrm{Fe}_{\mathrm{nat}}$ film ("1_EB−") and the other one, with a thin ^{57}Fe probe of 3.2 ML on top of a 48 ML $\mathrm{Fe}_{\mathrm{nat}}$ ("2_EB−"), both covered with 50 ML of NiO. For the "EB+" samples, the Fe thickness was set to a lower value, equal to 24 ML, while the NiO thickness was increased to 100 ML. The entire 24ML Fe film was composed of the ^{57}Fe isotope to avoid interpretation ambiguity related to $\mathrm{Fe}_{\mathrm{nat}}$-^{57}Fe intermixing, which may take place at the temperatures of around 200 °C[16] used to establish the exchange bias. For all the samples, the LEED patterns of the NiO surface proved the epitaxial growth of the bilayers as exemplarily shown in Fig. 1(a) for a typical 50ML NiO film deposited onto Fe(001). Finally, the samples were capped with a 50 Å MgO protective layer. The epitaxial relations are: MgO(001)[100]||Fe(001)[110]||NiO(001)[100]. The schematic representation of the prepared samples is shown in Fig. 1(b).

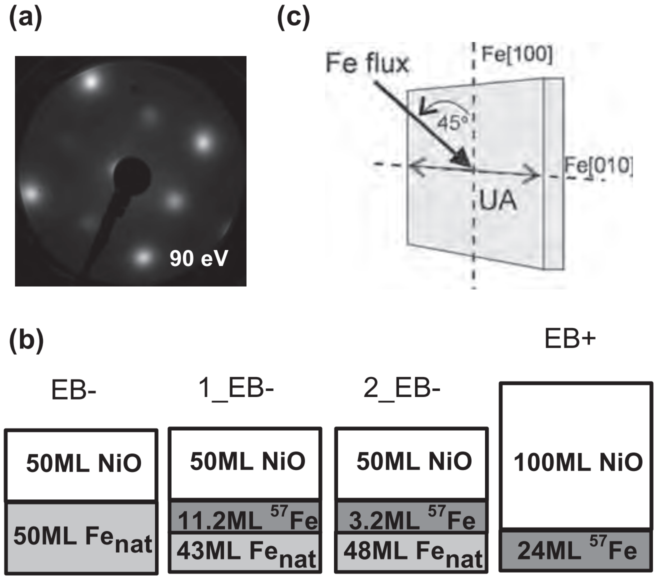

FIG. 1. (a) A typical LEED pattern for the 50ML NiO/Fe(001). Primary beam energy is equal to 90 eV. (b) Schematic representation of the samples. (c) Direction of the uniaxial magnetic anisotropy (UA) induced by the oblique deposition is marked by a double-sided arrow.

In the MBE system used in this study, the evaporator cells make an angle of 45° with the sample surface. Such an oblique deposition is known to introduce the uniaxial magnetic anisotropy (UA) into the Fe films, (Fig. 1(c)), along the direction perpendicular to the projection of the flux onto the sample surface.[17,18] The discussed samples were fabricated with the projection of the Fe flux oriented along Fe[100] (hereafter called the growth direction).

The magnetic properties of the "EB−" and "EB+" bilayers were studied using MOKE. The measurements were conducted *ex-situ* in the longitudinal geometry based on the vector-MOKE scheme by Vavassori.[19] On the as-grown samples, MOKE was measured using the *s* polarized light, which gives information on the longitudinal component of the magnetization vector.[19] Variation of the azimuthal angle (φ) with respect to the magnetic field direction enabled identification of the easy magnetization direction. The field cooling (FC) procedure was applied to introduce the biased state that was characterized by the exchange bias field H_{EB} and the coercive field H_C ($H_{EB} = (|H_{C1}| - |H_{C2}|)/2$, while $H_C = (|H_{C1}| + |H_{C2}|)/2$, where H_{C1} and H_{C2} are the coercive fields of the ascending and descending branches of the hysteresis loop, respectively). The FC procedure was performed on both "EB−" and "EB+" systems, with the field applied along the easiest magnetization directions. The procedure included heating the sample up in a low-vacuum (6.5×10^{-3} mbar) resistive heating furnace and cooling to RT in an external static magnetic field of 3000 Oe. The details of the FC procedure used for each system are described in Sec. III A.

The detailed study of the magnetization reversal was performed for the field cooled samples. Linear combinations of signals measured for different polarizations of the incident light were used to derive the hysteresis loops of three magnetization components: longitudinal (M_L), transverse (M_T), and polar (M_P), as a function of the azimuthal angle (φ). Specifically, the following relations hold: $M_L \propto (I_S + I_P)$, $M_P \propto (I_S - I_P)$, $M_P \propto (I_{SP} + I_{PS})$, and $M_T \propto (I_{SP} - I_{PS})$, where I_S, I_P, I_{SP}, and I_{PS} correspond to the signals measured for the polarization of the incident light oriented perpendicular, parallel, at +45° and at −45° relative to the incidence plane, respectively.[15,19] The magnetic anisotropies of the field cooled samples were analyzed using the polar plots of the reduced remanence of the longitudinal magnetization components.

The Mössbauer measurements were carried out *ex situ* at RT in the backscattering geometry with the detection of the conversion electrons. A standard Mössbauer spectrometer equipped with a CEMS He/CH_4 flow proportional detector and a 100 mCi ^{57}Co/Rh source was used. The CEMS spectra were collected in the normal incidence geometry. A commercial software[20] was used for fitting the spectra using a Voigt- line based method, thus approximating the distribution of the hyperfine magnetic field B_{hf} at a given site with a sum of Gaussians.

III. RESULTS

A. Exchange bias

As a starting point, the MOKE measurements were performed on the as-grown "EB−" and "EB+" samples, using *s* polarized light. The magnetic hysteresis loops measured with the magnetic field oriented along the main in-plane crystallographic directions of Fe are presented in Fig. 2. The azimuthal angle $\varphi = 0°$ corresponds to the Fe[110] crystallographic direction for both samples.

Both systems exhibited single easy anisotropy direction, along $\varphi = 135°$, i.e., perpendicular to the growth direction, which coincided with the Fe[100] direction. However, the loop shapes were markedly different for the "EB−" and "EB+". For the "EB−," hysteresis loops observed for $\varphi = 0°$ and $\varphi = 90°$ point to the reversal proceeding by coherent rotation. The magnetization reversal of "EB+" shows the elongated hysteresis loops, characteristic for more complex reversals (e.g., combination of rotation and domain wall motion). The magnetization reversal mechanism will be analyzed in detail in Sec. III B. For both systems, coercivities larger than 100 Oe were observed, which is much more than the coercivities of single Fe epitaxial films grown on MgO(001) (around 10 Oe).[21] Some of the loops have an asymmetrical shape, especially evident for $\varphi = 45°$ of the 'EB−' and for $\varphi = 135°$ of the "EB+" sample. Related with the asymmetry is the difference between the coercive fields of the ascending and descending branches of the hysteresis loop. This intrinsic shift of the hysteresis loop will be referred to as H_{shift} ($H_{shift} = (|H_{C1}| - |H_{C1}|)/2$) to differentiate from the FC-induced exchange bias shift (H_{EB}). H_{shift} and H_C are presented in Fig. 3. as a function of the azimuthal angle for both systems. For "EB−" a sizable loop shift was

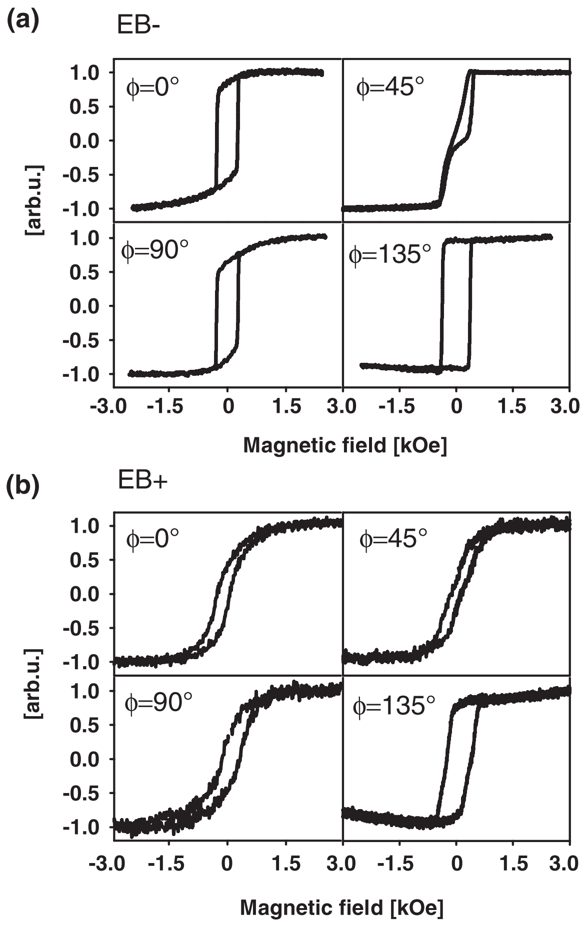

FIG. 2. Hysteresis loops measured for the main crystallographic directions for the as- deposited samples using *s* polarized light (a) "EB−" system, (b) "EB+" system.

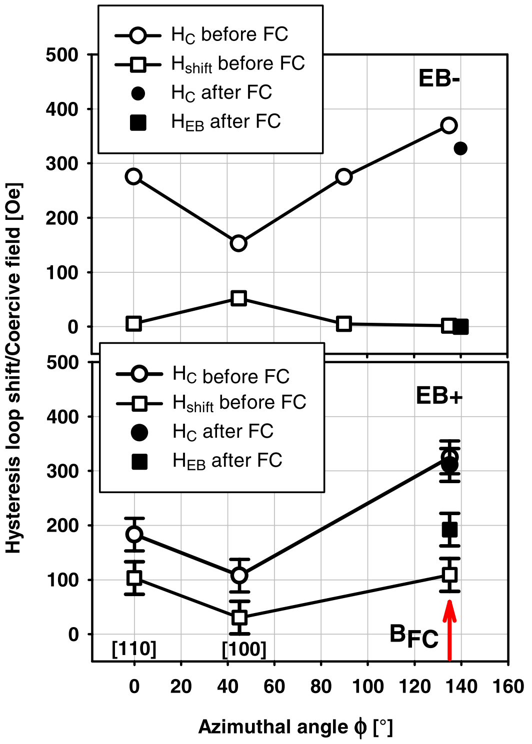

FIG. 3. Azimuthal dependence of the coercive field and the hysteresis loop shift measured before (open circles and open squares, respectively) and after field cooling (filled circles and filled squares, respectively). The error bars reflect the noise level during the measurements. The error bars for the "EB−" case are smaller than the data points. The direction of the magnetic field applied during FC is marked by an arrow.

recorded only for the most asymmetrical hysteresis loop measured along $\varphi = 45^\circ$. For the "EB+" system, the hysteresis loop shift was detected in the whole range of the azimuthal directions. Loop shifts reaching 100 Oe were observed for $\varphi = 0^\circ$ and $\varphi = 135\,^\circ$C.

FC was performed with the external magnetic field along the easiest anisotropy direction, i.e., along $\varphi = 135^\circ$ for both "EB−" and "EB+" systems. For effective field cooling, the temperature T_S, from which the field cooling begins, must be higher than the Néel temperature (T_N) of the antiferromagnet. However, it is known that T_N for thin films is a function of the layer thickness.[22] For the NiO films grown on MgO(001), T_N changes from 247 °C for the bulk, down to 197 °C for the 20ML film.[22] FC was performed on the "EB+" system with $T_S = 230\,^\circ$C. This temperature was high enough to establish the exchange bias effect and in the same time low enough (comparable to the annealing temperature used during Fe deposition) not to introduce drastic changes in the sample structure, as verified on the reverse interface.[15,23] The change of the loop shift measured along the FC direction is presented in Fig. 3 by a filled square data mark. The most significant shift was observed for the first loop measured after FC ($H_{EB} = 192$ Oe). The shift occurred in the direction opposite to the static magnetic field used during FC, which is a typical negative exchange bias effect.[4] Simultaneously, the coercive field remained almost unchanged ($H_C = 320$ Oe and 310 Oe before and after FC, respectively). The hysteresis loop measured with the magnetic field along the FC direction was repeated 4 times and all measurements for the "EB+" sample are collected in Fig. 4(a). Obviously, the FC procedure induced some irreversible changes in the system that are reflected in a more rectangular shape of the loop after FC.

Furthermore, each of the subsequent field sweeps yielded smaller loop displacements in such a way that the coercive field of the ascending branch was decreasing, while the coercive field of the descending branch was constant, the behavior observed before in the Fe(110)/NiO(100) system.[11] Consequently, the coercivity after the fourth field sweep decreased to $H_C = 260$ Oe, which is less than the value observed before FC. The lowering of H_{EB} with the number of field cycles (*n*), shown in Fig. 4(b), is referred to as the training effect and represents changes in the antiferromagnetic spin structure towards equilibrium.[4] The experimental data in Fig. 4(b) (filled circles) were fitted with a simple power- law: $H_{EB} \sim (n)^{-1/2}$ (solid line), which holds for $n > 1$, as often observed experimentally.[11] Radu and Zabel[5] proposed a formula, which relates the training effect to the interfacial spin disorder. The spin disorder formula has a form: $H_{EB}^n = H_{EB}^\infty + A_f \exp(-n/P_f) + A_i \exp(-n/P_i)$, where H_{EB}^n stands for the exchange bias field after the n^{th} field cycle, A_f and P_f are related to the frozen spin evolution, while A_i and P_i are parameters of the interfacial disorder. According to the spin disorder model, H_{EB} decreased with n, approaching the limit of H_{EB}^∞ for the infinite number of field cycles. From our experimental data for the NiO/Fe system the following values were obtained: $H_{EB}^\infty = 92.3$ Oe, $A_f = 81.75$ Oe, $P_f = 5.04$, $A_i = 1566$ Oe, $P_i = 0.26$. As expected within the model,[5] the obtained relation is composed of the fast decaying component related to the interfacial spin structure (indicated by the P_i value) and the slowly decaying contribution from the frozen uncompensated spins belonging to the AFM domains. After multiple field sweeps performed during the magnetization reversal experiments (Section III B) H_{EB} decreased to 100 Oe, which agrees well with the value of H_{EB}^∞ predicted by the model. The effect of training is usually absent in single-crystalline systems,[15,24] and significant for less ordered polycrystalline samples.[4,11,25] The occurrence of training in our epitaxial NiO(001)/Fe(001) system, related to the spin disorder at the interface, suggests that the chemical and magnetic structure of the interface is complex.

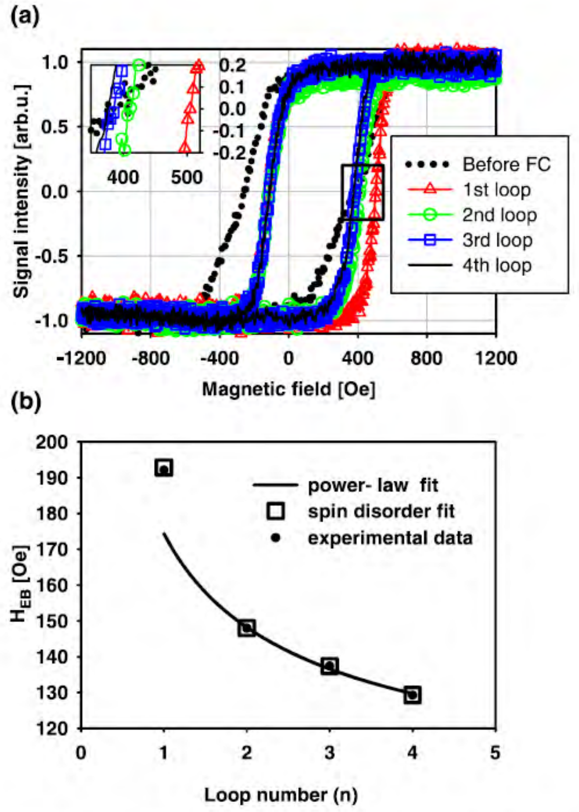

FIG. 4. (a) Hysteresis loops for the sample EB+ measured with the s polarized light along the easiest anisotropy direction before (dotted line) and after field cooling performed at 230 °C, showing the exchange bias and training effects. The inset shows a magnification of the region marked by a rectangle (b) Decrease of the exchange bias field for the consecutive hysteresis loops measured after field cooling.

The field cooling procedure yielded no additional loop shift for the "EB−" sample, as can be seen in Fig. 3, top, where the data points derived from the loop measured after FC performed with $T_S = 180\,^\circ$C are shown. The only observed effect was a decrease of the coercivity. The effect was further studied varying T_S up to 255 °C, i.e., above the Néel temperature of bulk NiO. The hysteresis loops measured along the field cooling direction after each FC are presented in Fig. 5. The symmetrical and gradual decrease of the coercivity with T_S was observed. Because the coercivity in our samples is governed by the exchange coupling at the NiO/Fe interface, changes in the loops' width should be attributed to some temperature- induced changes of the interface chemical structure.

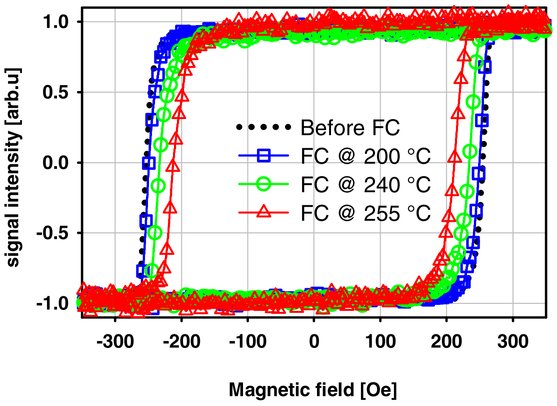

FIG. 5. Hysteresis loops for the sample "EB−" measured with the s polarized light along the easiest anisotropy direction before (dotted line) and after field cooling performed at 200 °C, 240 °C, and 255 °C showing the absence of exchange bias and gradual decrease of the coercivity.

The interface structure both for the as-deposited "EB−" samples and for the "EB+" sample after thermal treatment will be analyzed in detail in Sec. III C.

B. Magnetization reversal

The magnetization components derived from the measurements performed on the "EB−" sample at different azimuthal angles are presented in Fig. 6. The measurements were performed after the sample was field cooled along the $\varphi = 135°$ azimuth, after which no loop shift was detected (Sec. III A). Comparison of the longitudinal magnetization components (M_L) with the ones measured for the as-deposited sample (Fig. 2(a)) suggest that the reversal mechanism did not change after field cooling. Based on the loops measured as a function of the angle φ, the polar plot of the remanence normalized to the saturation magnetization (M_R/M_S) was constructed, as shown in Fig. 7. The plot shows a uniaxial anisotropy that dominates the four-fold magnetocrystalline anisotropy that is expected for the epitaxial Fe(001).

The magnetization reversal for the "EB−" system proceeds within the sample plane, which is reflected in the negligible polar magnetization components (not shown). The rectangular hysteresis loop in the longitudinal direction (M_L) and the absence of the transversal component observed for $\varphi = 140°$ (and correspondingly for $\varphi' = \varphi + 180°$, i.e., for 320°) indicates the uniaxial anisotropy direction. When the saturating magnetic field applied at the angles $\varphi = 90°$ or $\varphi = 0°$ is reduced to zero, the magnetization rotates towards the easy axis direction ($\varphi = 140°$ or $\varphi = 320°$, respectively), which is reflected in the rounded shapes of the M_L loops and the M_T loops showing the opposite reversal sense (counterclockwise and clockwise, respectively). The longitudinal hysteresis loops with a near-zero remanence, characteristic for the hard magnetization direction, is observed for $\varphi = 50°$, i.e., perpendicularly to the easy direction. It was accompanied by an atypical unidirectional behavior of the transversal component. A slight deviation of the angle φ (±5°) from the hard direction results in slightly asymmetric longitudinal loops and oval transversal ones. After saturation along $\varphi = 45°$ or $\varphi = 55°$ and reducing the field to zero the magnetization rotates to an easy direction in the opposite sense, because for both cases the magnetization rotates towards the closest easy direction, which is $\varphi = 320°$ or $\varphi = 135°$. A similar behavior around the hardest magnetization direction for a system with uniaxial anisotropy was reported before for Fe/GaAs(110).[26] However, the shape of the transversal magnetization component for the hardest anisotropy direction reported in Ref. 26 was oval, indicating a 360° rotation when the field was swept from the positive saturation to the negative saturation and *vice versa*. Such a behavior is consistent with the expectations of the Stoner–Wohlfarth model of the coherent magnetization rotation for the case of the uniaxial anisotropy.[5] For the NiO/Fe system reported here, when the magnetic field is swept along the hard axis, the magnetization firstly rotates towards the easy direction (e.g., clockwise) and when the magnetic field is increased, it rotates back (counterclockwise). This indicates that the anisotropy in our system is not a simple uniaxial one. The anisotropy that would prevent the 360° reversal for the magnetic field applied at $\varphi = 50°$ must be of the unidirectional character. Furthermore, the longitudinal loops for all the directions

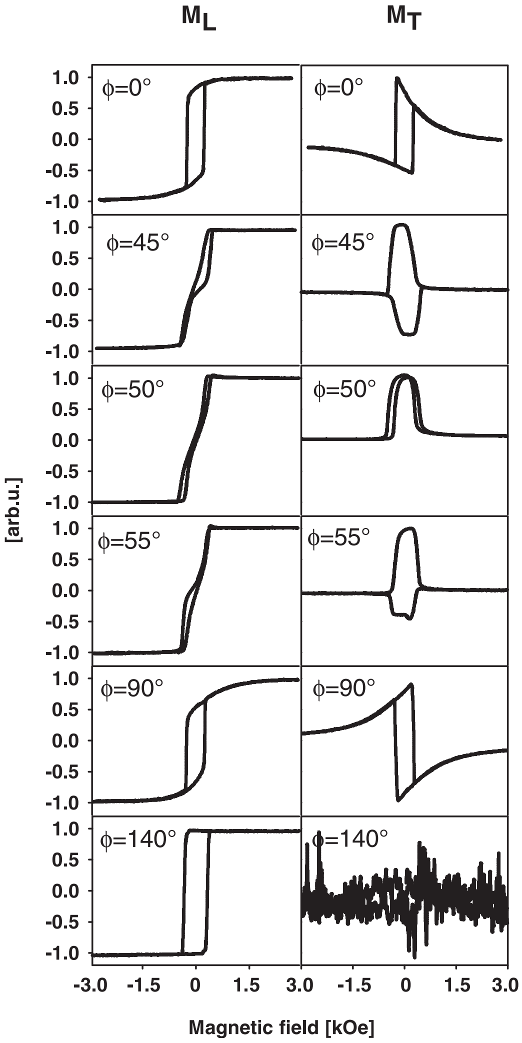

FIG. 6. The longitudinal (M_L) and transversal (M_T) components of the magnetization measured for different azimuthal angles (φ) for the "EB−" system after FC.

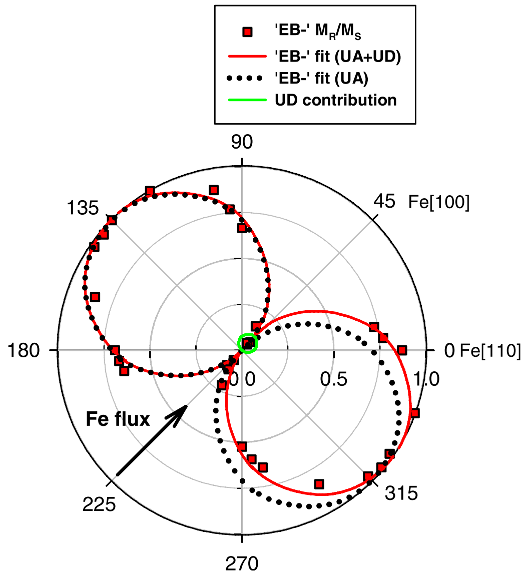

FIG. 7. The reduced remanence (M_R/M_S) as a function of the azimuthal angle (φ) derived from both branches of the hysteresis loops (squares). The dotted line presents the cosine dependence of the remanence for the simple uniaxial anisotropy while the red (dark grey) solid line for the uniaxial anisotropy accompanied by a small unidirectional term presented separately as the green (light grey) solid circle.

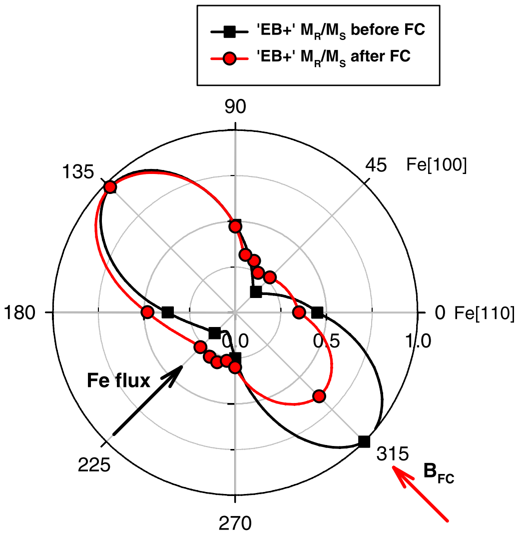

FIG. 8. The reduced remanence (M_R/M_S) as a function of the azimuthal angle (φ) derived from both branches of the hysteresis loops measured before (black squares) and after (red circles) FC. The lines are guides to the eye.

except for the easy one ($\varphi = 140°$) and the hard one ($\varphi = 50°$) are asymmetric. The asymmetrical magnetization reversal is theoretically expected to occur in the exchange-biased systems[27] and was experimentally observed[28] depending on the relative orientation of the external magnetic field and the unidirectional anisotropy axis. However, the discussed system did not exhibit any exchange bias after field cooling, which suggests that the unidirectional anisotropy of EB origin is negligible for this system. The strong asymmetry of the hysteresis loops with no field cooling applied was observed before in the similar system, i.e., in Fe/NiO/Ag(001),[15] and explained by some morphological effects.

The polar plot of the remanent magnetization could be fitted with a linear combination of the cosine functions (Fig. 7), a method used before to determine the direction of the easy anisotropy axes in single- and multi-layer systems.[29] For the case of pure uniaxial anisotropy, the theoretical azimuthal dependence of the remanence, ($M_R/M_S(\varphi) = M_R/M_S|\cos(\varphi\text{-}\varphi_{UA})|$, where φ_{UA} is the direction of the uniaxial anisotropy with respect to the Fe[110]), is shown in Fig. 7 as a dotted line. The curve was calculated using $\varphi_{UA} = 135°$, the direction expected for the growth induced uniaxial anisotropy. Although the agreement between the fit and the experimental data is good for the quarter between $\varphi = 90°$ and $\varphi = 180°$, the data points between $\varphi = 270°$ and $\varphi = 0°$ slightly deviate from the theoretical prediction in line with the asymmetric hysteresis loops atypical for the simple uniaxial anisotropy. A satisfactory fit was obtained by the introduction of a small unidirectional term, proportional to $\cos(\varphi\text{-}\varphi_{UD})$, where $\varphi_{UD} = 50°$ is the unidirectional anisotropy direction, presented separately in Fig. 7 as the green (light grey) solid circle and by using $\varphi_{UA} = 140°$. The obtained fit is presented in Fig. 7 as solid red (dark grey) line. This approach explains also the small loop shift observed with the magnetic field applied along $\varphi = 45°$ before field cooling (Fig. 3).

The magnetic behavior observed for the "EB+" sample is markedly different from the "EB−" case. Even for the as-grown sample, before FC, the magnetization reversal was not consistent with coherent rotation, in contrast to the 'EB−' system, as discussed in Sec. III A. The magnetic hysteresis loops measured for the as grown sample were elongated, suggesting a more complex behavior, which is also reflected in the polar plot of the reduced remanence (Fig. 8, black squares). For this case, it was not possible to fit the polar plot with a simple cosine angular dependence, thus the solid lines in Fig. 8 are only guides to the eye. The magnetization reversal was investigated after the sample was field cooled along $\varphi = 135°$ azimuth, which introduced the loop shift. The azimuthal dependence of the reduced remanence derived from the hysteresis loops measured in the biased state is also presented in Fig. 8 with the red circles. During these measurements, the sample was in the trained state ($H_{EB} = 100$ Oe), as multiple hysteresis loops were already measured after FC. The unidirectional anisotropy introduced along the field cooling direction (marked in Fig. 8 by a red arrow) is evident. The magnetization reversal for the "EB+" sample is not confined to the surface plane, as illustrated in Fig. 9, where all three magnetization components measured for different azimuthal angles are plotted. The magnetization for all the φ angles, except for the φ_{UD} one, rotates through the φ_{UD} direction for both branches of the hysteresis loop (i.e., the 360° rotation is prevented), as shown by the shape and sign of the transversal components. The M_P loops, which are identical for all the azimuthal angles, indicate that the magnetization points in two opposite polar directions for the reversal from the negative saturation to the positive saturation and back. Consequently, in a tentative picture, the magnetization reversal is not uniform for the entire Fe film but is a combination of the rotation through the unidirectional anisotropy axis for some parts of the film and the magnetization

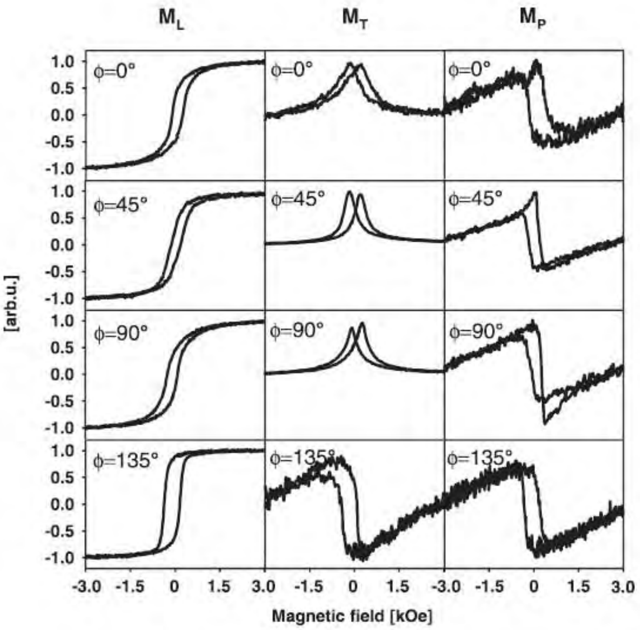

FIG. 9. The longitudinal (M_L), transversal (M_T), and polar (M_P) components of the magnetization measured for different azimuthal angles (φ) for the 'EB+' system.

switching of some other (possibly interfacial) parts having the out- of plane anisotropy.

C. Interface structure as revealed by CEMS

Characterization of the interfacial structure in the as-grown "EB−" system was performed based on the Mössbauer spectra measured for two samples, differing in the thicknesses of the ^{57}Fe probe layer used. The thick ^{57}Fe probe layer ("1_EB−") was used to assess the extent and composition of the interfacial oxide. The thin ^{57}Fe probe ("2_EB−"), which gave a better vertical resolution, helped to judge whether the composition of the interfacial iron oxide between Fe and NiO was uniform or not. In addition, the system was also analyzed in the biased state ("EB+").

The CEMS spectra obtained for "1_EB−," "2_EB−," and "EB+" samples together with the result of the deconvolution into spectral components are presented in Figs. 10 and 11. The hyperfine parameters which characterize the spectral components are listed in Table I.

Each spectral component corresponds to a specific type of atomic sites occupied by the ^{57}Fe atoms. The components are grouped by the value of the isomer shift (IS), which is given relative to α-Fe. IS near zero corresponds to the metallic Fe sites, while the significantly increased value of IS, to the Fe sites coordinated with oxygen.

To determine the composition of the interfacial layers in our samples, especially the amount of the oxidized Fe atoms, the relative weight of a given component should be related to the overall amount of ^{57}Fe atoms in each sample. The amount of atoms occupying a given atomic site is expressed as equivalents of the Fe(001) layer thickness (Å). Because in the preparation of the "EB−" samples also Fe_{nat} was used, we had to take into account the signal coming from the ^{57}Fe isotope present in the Fe_{nat} layer, where the natural abundance of the ^{57}Fe isotope is equal to 2.12%. The "EB+" sample was prepared without Fe_{nat}, so the amount of ^{57}Fe atoms present in this sample is simply equal to the Fe layer thickness, i.e., 24ML.

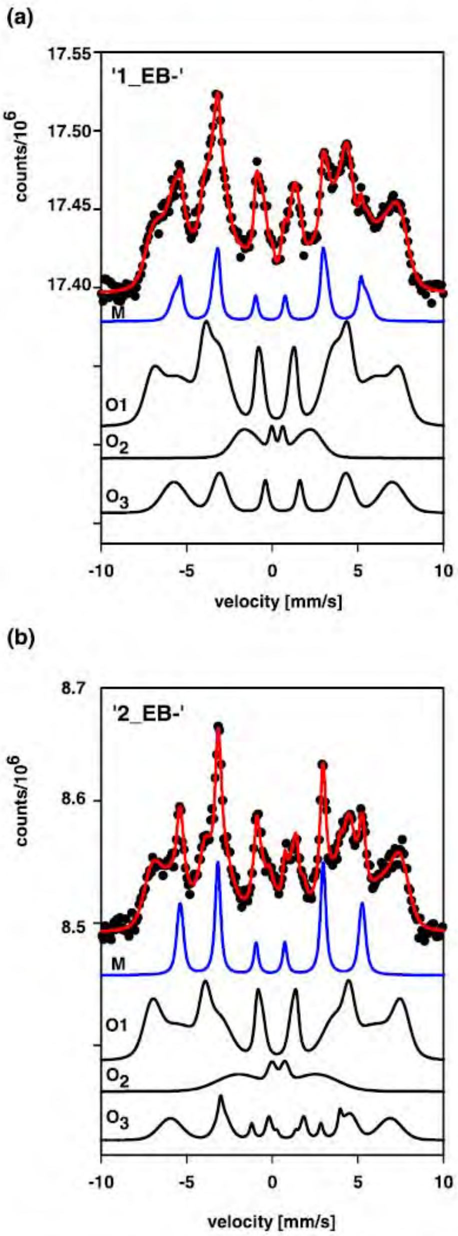

FIG. 10. CEMS spectra of the sample "1_EB−" (a) and "2_EB−" (b) with the result of the best fit. The spectral components: M, O_1, O_2 and O_3 are offset in the y-axis for clarity.

For the "1_EB−" sample the metallic site (component M in the Table I) constitutes only 14% of the signal, which corresponds to 2.4 Å of metallic ^{57}Fe. As described above, the Fe_{nat} film contains 1.3 Å equivalents of ^{57}Fe, and only 1.1 Å of ^{57}Fe atoms of a metallic character in the 16 Å thick (11.2ML) interfacial probe. The remaining interfacial ^{57}Fe atoms, equivalent to 14.9 Å have a non-metallic character. Based on the same considerations, the component M in the "2_EB−" spectrum originates only from the Fe_{nat} film and the oxidation is not limited only to the ^{57}Fe probe, but it extents also to the Fe_{nat} part of the sample.

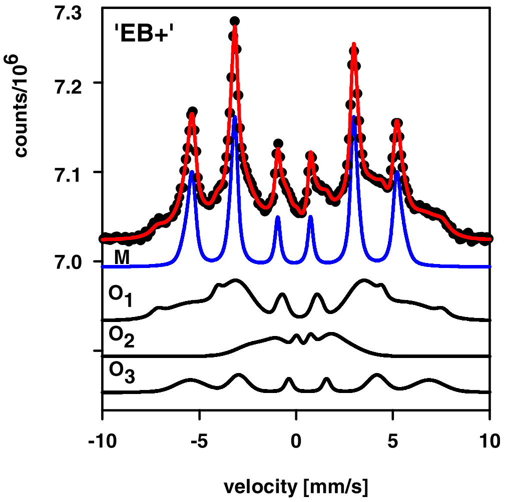

FIG. 11. CEMS spectra of the ‘EB+’ sample with the result of the best fit. The spectral components: M, O_1, O_2, and O_3 are offset in the y-axis for clarity.

The metallic site of the “EB+” spectrum has the relative weight of 40%, which corresponds to 13.7 Å of ^{57}Fe atoms. It shows that the interfacial layer, chemically modified with respect to the metallic Fe atoms is composed of 20.6 Å of Fe atoms. The comparison with the result obtained for the “1_EB−” sample shows the significantly thicker interfacial region, as a consequence of the thermal treatment applied during the FC procedure.

The main groups of the components in all the spectra (O_1, O_2, and O_3) correspond to the oxidized Fe atoms as identified by distinctly positive IS values ranging from 0.3 mm/s to 0.75 mm/s. The hyperfine pattern of the oxide components does not directly fit to any of the typical bulk iron oxide phases, such as wüstite, FeO, magnetite, Fe_3O_4 or hematite and maghemite, α- and γ-Fe_2O_3, respectively. This situation was already observed when Mössbauer spectroscopy was used for the identification of chemical composition of Fe/oxide interfaces,[14,24,30] where Fe atoms may have different oxidation and/or coordination state than the bulk. In such a situation, a model of the interfacial iron oxide atomic structure can be proposed by exploiting the local sensitivity of the hyperfine interactions and the similarity of the local coordination among different iron oxides. The base for most of the iron oxide crystalline structures is a close-packed lattice of oxygen ions. The octahedral and tetrahedral holes in the oxygen lattice are partially filled with the smaller iron cations, either Fe^{2+}, which favors octahedral coordination or Fe^{3+}, with no preference for the octahedral or tetrahedral coordination.[31] Depending on the oxidation state and the crystal structure, the hyperfine interaction parameters differ significantly, especially the magnetic hyperfine field, which is the key of phase analysis using Mössbauer spectroscopy. In the complex situation of a low dimensional oxide phase at the NiO/Fe interface, some general correlations between the oxidation/coordination state and hyperfine parameters apply, collected from dozens of iron compounds.[32] Especially, the isomer shift, that is sensitive to the valence electron density, and the quadrupole interaction, which reflects the symmetry of the charge distribution both of valence and lattice charges, are useful as fingerprints of the Fe atoms state.

TABLE I. Hyperfine parameters derived from the numerical fits of CEMS spectra for “1_EB−,” “2_EB−,” and “EB+” samples. Numbers in parentheses indicate the last digit uncertainty resulting from the least squares fit analysis.

Sample	Site	IS[a] (mm/s)	ε[b] (mm/s)	I_2/I_3[c]	Cp	B_{hf}[d] (T)	ΔB_{hf}[e] (T)	RW[f] (%)	F_O[g] (%)
“1_EB−”	M	0.00(2)	0.00(2)	4.0(5)	M^A	32.6(3)	0.0(7)	5(2)	—
					M^B	34(1)	1.5(8)	9(2)	—
	O_1	0.33(4)	0.00(3)	2.9(3)	O_1^A	36(1)	6.2(9)	43(5)	50
					O_1^B	44.8(3)	2.5(5)	16(5)	19
	O_2	0.39(6)	0.00(5)	0.5(6)	O_2	12(1)	3.5(1)	9(1)	10
	O_3	0.71(7)	0.01(5)	2.5(5)	O_3	39.5(7)	3.9(7)	18(5)	21
“2_EB−”	M	0.01(0)	0.02(0)	4.0(2)	M	33.0(0)	0.72(6)	20(1)	—
	O_1	0.36(1)	−0.01(1)	2.1(1)	O_1^A	36(1)	6.8(9)	33(2)	41
					O_1^B	45.2(1)	2.5(2)	20(2)	25
	O_2	0.42(7)	−0.03(5)	0.1(3)	O_2	15(1)	7.2(6)	11(1)	14
	O_3	0.74(2)	−0.18(2)	2.2(3)	${O_3}^A$	21.6(2)	0.0(6)	3(1)	4
					${O_3}^B$	39.8(4)	3.8(4)	13(1)	16
“EB+”	M	0.00(1)	0.00(1)	3.8(1)	M^A	32.7(1)	0.6(1)	27(1)	—
					M^B	34.5(9)	1.3(6)	13(1)	—
	O_1	0.29(5)	0.00(4)	3.9(5)	O_1^A	34.6(8)	7.8(9)	33(2)	55
					O_1^B	45.7(6)	1(1)	2(5)	3
	O_2	0.35(6)	−0.13(5)	1.8(6)	O_2	14(1)	5.2(8)	13(2)	22
	O_3	0.75(8)	0.05(5)	2.7(5)	O_3	38.2(6)	4.4(8)	12(1)	20

[a] IS is the average isomer shift with respect to α-Fe.

[b] ε is the average quadrupole interaction.

[c] I_2/I_3 is the ratio of the spectral areas of line 2 to the line 3 in the sextet.

[d] B_{hf} is the average hyperfine magnetic field.

[e] ΔB_{hf} is the Gaussian width of the B_{hf} distribution for the given component.

[f] RW is the relative weight of the component.

[g] F_O denotes the fraction of the corresponding atoms in the oxidic Fe_xO_y interfacial layer.

The isomer shifts of around 0.3–0.4 mm/s (sites O_1 and O_2) and 0.7 mm/s (site O_3) are characteristic for the Fe^{3+} and Fe^{2+} ions, respectively.[33] The total amount of Fe^{3+} atoms is equivalent to 11.8 Å for the "1_EB" sample and 16.5 Å for the "EB+" sample. In both samples, the amount of Fe^{2+} ions is smaller (3.1 Å and 4.1 Å for "1_EB−" and "EB+" samples, respectively). In order to better depict the composition of the iron oxide interfacial layers, the amount of atoms corresponding to each site was expressed in Table I as a percentage of the oxidic layer thickness F_O. The comparison of F_O parameters clearly shows that the relative amount of Fe^{2+} and Fe^{3+} ions are very similar in all the samples: Fe^{3+} ions constitute 79%, 80%, and 80% of the iron oxide layer in "1_EB−," "2_EB−," and "1_EB+" samples, respectively. Therefore, the formal composition of the iron oxide layer formed at the NiO/Fe interface may be expressed as $Fe^{3+}{}_4Fe^{2+}{}_1O_7$, where the number of oxygen atoms is adjusted based on the charge neutrality condition. The studied interfaces, being homogenous with respect to the chemical state, show a significant variation of the hyperfine magnetic field within the group of the Fe^{3+} components. The most abundant Fe^{3+} site (O_1^A) is characterized by the B_{hf} only slightly increased relative to the metallic Fe value (34–36 T). The second of the Fe^{3+} sites, the less abundant O_1^B component, is characterized by $B_{hf} \approx 45$ T, closer to values typical for the Fe^{3+} ions in oxides.[33] It is worth noting that the Gaussian width of the B_{hf} distribution for the O_1^A component is large (6–8 T) as compared to the well-defined O_1^B component ($\Delta B_{hf} \approx 2$ T), which suggest a significant heterogeneity of the local atomic environments represented by the component O_1^A. The considerable distribution of the hyperfine field around the central value is also observed for the O_2 component, characterized by the smallest hyperfine fields (12-15 T). In iron compounds, the hyperfine field at the Fe nucleus originates mainly from the imbalance of the *s* core electron spin density at the nucleus, mediated by the 3*d*-polarization effects (core contribution) and polarization of the 4*s* conduction electrons (conduction electron contribution), both known as the Fermi contact term.[33] The core contribution scales with the magnetic moment of a given atom (roughly-11 T per Bohr magneton[33]), while the conduction electron contribution depends on the magnetic moment of the neighboring atoms and, although smaller in magnitude, is difficult to predict.[34] The orbital and dipolar magnetic hyperfine fields are negligible for Fe^{3+}, resulting in the rough proportionality between the magnetic moment of the given atom and its total hyperfine magnetic field.[33] The diversity of the hyperfine parameters of the Fe^{3+} sites can thus be attributed to the differences in the magnetic moments of the corresponding atoms. The Fe^{3+} sites observed in our samples are similar to the ones found in nanomaterials, where a polymorph, intermediate between γ-Fe_2O_3 and α-Fe_2O_3, called ε-Fe_2O_3, has been identified.[35] A typical Mössbauer spectrum of ε-Fe_2O_3 consists of three sextets characterized by $B_{hf} = 44$ T, 38 T, and 25 T, corresponding to the magnetic moments of $3.9\mu_B$, $3.7\mu_B$, and $2.4\mu_B$.[35] The difference in the isomer shift between O_1 and O_2 components should be attributed to local coordinations of Fe atoms, variations of which is understandable in such a non-stoichiometric, low-dimensional iron oxide. The Fe^{3+} atoms described by the O_2 component are probably located in the atomic sites adjacent to anionic vacancies. This assumption is supported by the smaller hyperfine field values with wide distributions. Additionally, in the "EB+" sample, the O_2 site has a non-zero quadrupole splitting parameter (ε), which reflects the lower symmetry of the local anionic environment. The coordination of Fe^{3+} ions (octahedral or tetrahedral) is not easy to identify based on the Mössbauer spectra, however, there is a distinct tendency for the IS to be close to 0.2 mm/s for the tetrahedral sites and above 0.35 mm/s for the octahedral Fe^{3+} sites. Moreover, taking into account that the Fe-oxide is formed at the interface with the NiO fcc phase, the observed IS values point rather to the octahedral coordinations.

The hyperfine field experienced by the Fe^{2+} atoms (O_3 component) equals to 38–39T, which is similar to the value found for the octahedral sites in the FeO-wüstite phase below its Néel temperature.[36] The observation of the Fe^{2+} octahedral sites magnetically ordered at room temperature is not surprising when we consider the proximity of the Fe^{3+} sites of high magnetic moment. This observation points to the picture where Fe^{2+} and Fe^{3+} sites are intermixed, as it is, for example, in magnetite, rather than being separated in the form of distinct phases or layers. Such a picture is further confirmed by the identical results of the quantitative composition analysis from the CEMS results for the samples with the thick ("1_EB−") and thin ("2_EB−") probe layers.

A comment is needed to the "1_EB−" and "EB+" spectra that contain two metallic components. The component M^A, which is present in all the spectra ($B_{hf} = 32.6$ T-33.0 T) is typical for the α-Fe and originates from the Fe atoms away from the interface. The additional metallic component (M^B) is distinguished by its slightly higher hyperfine field, reaching 34.5 T. Its hyperfine parameters resemble the NiFe characteristics, an alloy which is often formed at the NiO-Fe interface as a result of the oxidation- reduction reactions.[37,38] In the Mössbauer spectra, a hyperfine field variation with the amount of Ni in the FeNi alloy is observed, from around 34 T for 10% of Ni down to 28 T for high Ni concentrations, except for the concentration around 30% of Ni, where the specimens are paramagnetic at room temperature.[39,40] However, in our NiO/$Fe^{3+}{}_4Fe^{2+}{}_1O_7$/Fe system, NiO is separated from metallic Fe by at least 20 Å of iron oxide. Taking into account that a MgO-oxide layer as thin as 10 Å prevents the NiO reduction in the Fe/MgO/NiO trilayer,[9] we find it improbable that the FeNi alloy was formed in our sample. Thus, we conclude that the increased hyperfine field of component M^B is related to a metallic Fe layer polarized by the high- magnetic moment interfacial iron oxide. The thickness of this layer can be approximated from the "EB+" spectra and equals to 4.4 Å.

Due to the proximity of iron and nickel oxides, the formation of a mixed iron- nickel oxide at the NiO/Fe interface should be considered. Unfortunately, we are not able to unambiguously distinguish such oxides from the pure iron oxide, because the substitution of Fe atoms by Ni does not change the Mossbauer spectrum significantly, as it is the case for the magnetite (Fe_3O_4) and nickel ferrite

($NiFe_2O_4$),[41] that could be formed at the iron oxide/NiO interface.[42,43] On the other hand, a possible diffusion of the Fe atoms into the NiO lattice would be detected as Fe^{2+} ions with a small hyperfine field (around 22 T) or Fe^{3+} ions with $B_{hf} \approx 47$ T[44] and indeed, the component O_3^A detected in the "2_EB−" sample can be identified as Fe^{2+} ions inside the NiO lattice. The relative intensity of this component corresponds to only 0.2 Å of Fe and this small intensity explains why it was detected only for the "2_EB−" sample, for which the small probe thickness gives the best interfacial sensitivity.

In total, the oxidic phase at the NiO/Fe interface was found to be formed by an equivalent of 14.9 Å and 20.6 Å of Fe, for the "1-EB−" and "EB+" samples, respectively. However, it is necessary to point out that almost the entire probe in the "1-EB−" sample was oxidized, so the assessment of the oxide thickness is based on the assumption that the $Fe^{3+}_{4}Fe^{2+}_{1}O_7$/Fe interface is sharp. This assumption is motivated by the similarity of the chemical composition of the thick ("1_EB−") and thin ("2_EB−") probe, i.e., absence of any distinct intermediate iron oxide phase. To calculate the resulting thickness of the iron oxide layer, we take into account a typical interlayer distance for the iron oxide of the given stoichiometry (2.1 Å of Fe_3O_4 is formed from 1 Å of Fe), which makes 31 Å of $Fe^{3+}_{4}Fe^{2+}_{1}O_7$ for the "EB−" sample and 43 Å for the "EB+" sample. The increase of the amount of the oxidic phase as a result of the thermal treatment is related to the oxidation-reduction reactions characteristic for many metal/oxide systems,[37] enhanced by the increased temperature. Thermodynamically, the formation of iron oxide is more favorable than the formation of nickel oxide,[37] thus spreading of the iron oxide layer as a result of the temperature treatment is expected to be accompanied by a reduction of nickel oxide and/or formation of the mixed iron-nickel oxide. As discussed above, the existence of a mixed iron- nickel oxide phase cannot be excluded in our system. Although it was not directly confirmed, based on the significant expansion of the iron oxide layer we suggest that the NiO was partially reduced as a result of the thermal treatment. The suggested structure of the interfacial layers for the as-deposited sample ("EB−") and thermally treated sample ("EB+") is presented in Fig. 12.

Beside the structural characterization, the Mössbauer spectra carry some information on the magnetic order in the probe layer, which is encrypted in the relative intensities of the second (I_2) and third (I_3) line of a Zeeman sextet. The ratio $R = I_2/I_3$ is related to an average angle between the magnetization direction and the direction of the γ quanta, $\theta = \arccos[(4\text{-}R)/(4+R)]^{1/2}$. In the geometry of our CEMS experiment, where the γ quanta travel along the sample normal, $R = 4$ yields $\theta = 90°$, which means that the magnetization related to the metallic components M in '1_EB−' and '2_EB−' lies in plane. For the O1 sites R equals to 2.9, 2.1 and 3.9 for "1_EB−," "2_EB−," and "EB+" samples, respectively, which reflects a canted magnetization and yields the average canting angle β measured from the surface equal to 24°, 34°, and 7°, respectively. For the O2 sites, the R values are significantly lower, equal to 0.5 and 0.1 for the "1-EB−" and "2-EB−" samples and 1.8 for the "EB+" sample, which means that the corresponding magnetization points 62°, 77°, and 38° out of the sample plane, respectively. For the Fe^{2+} sites of the "EB−" samples, the magnetization canting is similar to the O_1 sites: 29° for "1_EB−" and 33° for "2_EB−." In contrast, for the biased "EB+" sample, the O_3 sites canting is 26°, which is significantly more than 7° observed for the O_1 site. The small canting is also observed for the metallic site in the 'EB+' system, reaching 9° out of the sample plane. Such canting of the magnetic moments in the thin films, where the shape anisotropy forces them to lie in the film plane must be related to some other dominating anisotropy contributions. In our NiO/Fe bilayers, we relate the observed canting of the Fe spins to the exchange coupling with the NiO film. As a result of the exchange interactions, the Fe magnetic moments are forced to align along the magnetic anisotropy axis of NiO. The anisotropy in NiO films depends on the in-plane epitaxial strain.[45] The domains with the spin axis along the [+/−1 +/−2 +/−1] and [2+/−1+/−1] directions pointing 24° out of plane are preferentially stabilized when NiO is subjected to the compressive strain (e.g., NiO grown on Ag(001)[46]). When the NiO film is stretched (e.g., NiO grown on MgO(001)), the [+/−1 +/−1 +/−2] domains are preferentially stabilized, which point 54° out of plane.[45] It is not obvious to determine the size and sign of the strain of the NiO film on top of the $Fe^{3+}_{4}Fe^{2+}_{1}O_7$ phase here investigated. For NiO epitaxially grown on Fe(001), the lattice mismatch of +2.8% points to an in-plane contraction that would stabilize the 24° out-of-plane domains in NiO. However, NiO grown on FeO(001) should experience a −3.9% expansion, which in turn would stabilize the NiO domains pointing 54° out of plane. The imperfect crystalline structure of our $Fe^{3+}_{4}Fe^{2+}_{1}O_7$ layer probably influenced the atomic arrangement of the NiO film grown on it; in this way, a mixed domain structure was stabilized, which in turn magnetically frustrated the $Fe^{3+}_{4}Fe^{2+}_{1}O_7$ film. Consequently, it is not surprising that the iron magnetization directions do not perfectly match the anisotropy axis of an ideal NiO layer. The observed frustration might be also related to the competing effects of the exchange coupling and growth- induced anisotropy. The canting observed also for the metallic sites in the "EB+" system might be related to the stronger coupling with NiO thanks to its larger magnetocrystalline anisotropy related to NiO thickness. This effect is also involved in the establishing of the exchange bias.

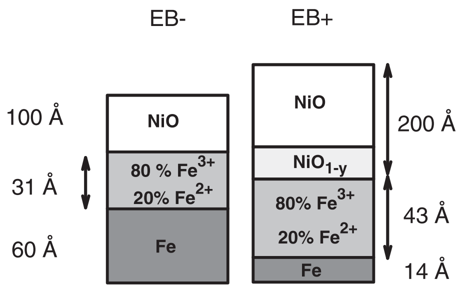

FIG. 12. The schematic representation of the "EB−" and "EB+" samples, based on the results of the Mössbauer measurements.

The $Fe^{3+}_{4}Fe^{2+}_{1}O_7$ oxide phase, 31 Å and 43 Å thick in "EB−" and "EB+," respectively, was found at the interface of our NiO/Fe bilayer. This contrasts with the iron oxide structure formed at the Fe(001) that is exposed to molecular oxygen,[47,48] where the iron oxide mostly includes the Fe^{2+} cations. Leibbrandt *et al.* reported the stoichiometry of the iron oxide prepared at room temperature to be $Fe_{0.95+/-0.7}O$.[47] What is more, at RT the thickness of the iron oxide layer saturates around 10 Å.[47] In a similar study,[48] a 10^4 Langmuir (L) exposure to molecular oxygen (60 min at 2×10^{-6} mbar) was necessary to form a 20 Å oxide layer with a Fe^{3+} concentration of around 43%. Lower oxygen exposures led to the iron oxide layer composed of Fe^{2+} ions only, corresponding to FeO. For intermediate oxygen exposures, Fe^{3+} cations were found but only near the film surface. Annealing at 200 °C, reduced the iron oxide back to the FeO form.[48] The recent molecular dynamics study of the Fe oxidation process also showed a gradation of the iron oxide stoichiometry across the Fe_xO_y oxide thickness not exceeding 20 Å, where y/x ~1.3–1.5 was observed near the Fe surface and y/x ~ 0.7–0.8 in the iron oxide interior.[48] Analyzing the preparation procedure used in our study, we find that the Fe(001) surface was exposed to the molecular oxygen at 1.3×10^{-7} mbar for around 30 s before the Ni evaporation started, which corresponds to 3 L. Finazzi *et al.*,[12] in their study of the chemical effects at the buried NiO/Fe interface explained the formation of a Fe^{3+} rich interfacial oxide phase by assuming that Ni dissociates oxygen molecules and lowers the system work function.[49] The reason why the thickness of the iron oxide layer found in our study is larger than the one reported by Finazzi *et al.*[12] should be attributed to the pre-adsorbed oxygen used in their study, which forms the stable Fe(001)-p(1x1)O structure protecting the Fe surface against further oxidation.

D. Magnetic properties of the NiO/Fe bilayers in view of their interface structure

Characterization of the interface structure in our NiO/Fe system led to the structural model presented in Fig. 12, which helps to understand the observed magnetic behavior described in Secs. III A and III B. The nominal NiO/Fe bilayers must be treated as $NiO/Fe^{3+}{}_4Fe^{2+}{}_1O_7/Fe$ trilayers. The consequences are twofold. Firstly, not the NiO/Fe interface, which is absent, but rather two other: $NiO/Fe^{3+}{}_4Fe^{2+}{}_1O_7$ and $Fe^{3+}{}_4Fe^{2+}{}_1O_7/Fe$ are responsible for the exchange bias. Second, the magnetic structure at the interface formed by the described mixed iron oxide is not obvious. An antiferromagnetic order, similar to FeO or α-Fe_2O_3 cannot be excluded, however, more probably its nature is ferrimagnetic, like Fe_3O_4 or γ-Fe_2O_3, as it is composed of unequal magnetic sites. The ferrimagnets can be parts of the exchange bias systems, equally with either ferromagnets or antiferromagnets.[4] Hysteresis loops shifted after field cooling were observed for Fe-Fe_3O_4 bilayers,[50] nanoparticles,[51] and even for the magnetite alone[52,53] but at the temperatures below 200 K. Since for our system the field-cooling induced loop shift is observed at room temperature we infer that the bias is introduced by the exchange coupling with the NiO layer. Nevertheless, as the exchange bias is an interfacial effect,[1,5] the ferromagnetic spins that are coupled to NiO must be located in the $Fe^{3+}{}_4Fe^{2+}{}_1O_7$ layer. The hysteresis loops shifts observed in our system even before the field cooling (both for "EB−" and "EB+") suggest that the magnetic moments of Fe are coupled to some population of the rigid spins that break the reversal symmetry in the system. We attribute these rigid spins to the frustrated magnetic structure of the $Fe^{3+}{}_4Fe^{2+}{}_1O_7$ layer having large anisotropy, similarly to Fe_3O_4[53] or ε-Fe_2O_3.[35] During the field cooling, if the NiO anisotropy is high enough (the "EB+" case), the uncompensated Ni spins present at the $NiO/Fe^{3+}{}_4Fe^{2+}{}_1O_7$ interface pin some fraction of the Fe spins in the field cooling direction. Due to strong exchange coupling within the $Fe^{3+}{}_4Fe^{2+}{}_1O_7$ film, the unidirectional anisotropy is transferred through the iron oxide film to the Fe metallic layer, which exhibits a hysteresis loop shift. The observed training is related to the evolution of the disordered Fe spins in the $Fe^{3+}{}_4Fe^{2+}{}_1O_7$ layer towards equilibrium. The coercivity increase, as compared to the single Fe films, may be also explained by the coupling of Fe film to the $Fe^{3+}{}_4Fe^{2+}{}_1O_7$ layer of a higher anisotropy. The frustrated magnetic structure of $Fe^{3+}{}_4Fe^{2+}{}_1O_7$ may also pin the propagating domain walls in the Fe layer increasing its coercivity.[54] On the other hand, in both "EB−" and "EB+" the coercivity decreased after field cooling. In view of the interface structure this effect should be attributed to changes in the composition of the iron oxide layer upon thermal treatment, especially marked by the lowered amount of the Fe^{3+} cations with a high magnetic moment (component O_1^B, Table I).

IV. CONCLUSIONS

A combined study of the magnetism and structure in the epitaxial NiO/Fe(001) system was performed. The iron oxide phase with a formal stoichiometry $Fe^{3+}{}_4Fe^{2+}{}_1O_7$, as thick as 31 Å, was identified at the NiO/Fe interface in the as-deposited samples. The composition of the interfacial iron oxide layer was similar to magnetite (whose stoichiometry might be expressed as: $Fe^{3+}{}_{3.5}Fe^{2+}{}_{1.75}O_7$), with a deficit of the Fe^{2+} cations and an abundance of the Fe^{3+} cations, for each oxygen atom. The iron oxide layer was found to have canted magnetic structure, as a result of the exchange coupling with the NiO film. The two systems were compared: one giving the exchange bias ("EB+" 100ML NiO/24ML Fe) and the other one, where the exchange bias was not observed ("EB−" 50ML NiO/50MLFe). The 'EB+' system exhibited training of the exchange bias, related to the interfacial disorder introduced by the $Fe^{3+}{}_4Fe^{2+}{}_1O_7$ phase. For both, the magnetic anisotropy was a combination of the growth- induced uniaxial anisotropy (dominating) and the unidirectional anisotropy introduced by the iron oxide interfacial layer. The magnetization reversal was found to proceed via simple in- plane rotation for the "EB−" system. For the "EB+" case, the reversal was incoherent, affected by the strong coupling with the NiO layer.

ACKNOWLEDGMENTS

This work was supported in part by the National Science Center (NCN), Poland (Grant No. 2011/02/A/ST3/00150) and by the MPD and TEAM Programs of the Foundation for Polish Science co-financed from the EU European Regional Development Fund. Support from the Italian MIUR through the FIRB Project RBAP115AYN "Oxides at the nanoscale: multifunctionality and applications" is also gratefully acknowledged.

[1] C. Tsang, R. E. Fontana, T. Lin, D. E. Heim, V. S. Speriosu, B. A. Gurney, and M. L. Williams, IEEE Trans. Magn. **30**, 3801 (1994).
[2] S. S. P. Parkin, K. P. Roche, M. G. Samant, P. M. Rice, R. B. Beyers, R. E. Scheuerlein, E. J. O'Sullivan, S. L. Brown, J. Bucchigano, D. W. Abraham, Yu. Lu, M. Rooks, P. L. Trouilloud, R. A. Wanner, and W. J. Gallagher, J. Appl. Phys. **85**, 5828 (1999).
[3] W. H. Meiklejohn and C. P. Bean, Phys. Rev. **102**, 1413 (1956).
[4] J. Nogués and I. K. Schuller, J. Magn. Magn. Mater. **192**, 203 (1999).
[5] F. Radu and H. Zabel, Springer Tracts Mod. Phys. **227**, 97 (2008).
[6] M. Finazzi, L. Duò, and F. Ciccacci, Surf. Sci. Rep. **64**, 139 (2009).
[7] P. Luches, V. Bellini, S. Colonna, L. Di Giustino, F. Manghi, S. Valeri, and F. Boscherini, Phys. Rev. Lett. **96**, 106106 (2006).
[8] W. Kim, E. Jin, J. Wu, J. Park, E. Arenholz, A. Scholl, C. Hwang, and Z. Q. Qiu, Phys. Rev. B **81**, 174416 (2010).
[9] R. de Masi, D. Reinicke, F. Müller, P. Steiner, and S. Hüfner, Surf. Sci. **516**, L515 (2002).
[10] K. Arai, T. Okuda, A. Tanaka, K. Fukumoto, T. Hasegawa, T. Nakamura, T. Matsushita, T. Muro, A. Kakizaki, and T. Kinoshita, J. Appl. Phys. **110**, 084306 (2011).
[11] A. Hochstrat, Ch. Binek, and W. Kleemann, Phys. Rev. B **66**, 092409 (2002).
[12] M. Finazzi, A. Brambilla, L. Duò, G. Ghiringhelli, M. Portalupi, F. Ciccacci, M. Zacchigna, and M. Zangrando, Phys. Rev. B **70**, 235420 (2004).
[13] L. Duò, A. Brambilla, P. Biagioni, M. Finazzi, A. Scholl, G.-H. Gweon, J. Graf, and A. Lanzara, Surf. Sci. **600**, 4160 (2006).
[14] E. Młyńczak, K. Freindl, N. Spiridis, and J. Korecki, J. Appl. Phys. **113**, 024320 (2013).
[15] P. Luches, S. Benedetti, A. di Bona, and S. Valeri, Phys. Rev. B **81**, 054431 (2010).
[16] J. A. Stroscio, D. T. Pierce, and R. A. Dragoset, Phys. Rev. Lett. **70**, 3615 (1993).
[17] Q. Zhan, Ch. Van Haesendonck, S. Vandezande, and K. Temst, Appl. Phys. Lett. **94**, 042504 (2009).
[18] Y. Park, E. E. Fullerton, and S. D. Bader, Appl. Phys. Lett. **66**, 2140 (1995).
[19] P. Vavassori, Appl. Phys. Lett. **77**, 1605 (2000).
[20] Recoil 1.05 Mössbauer Analysis Software for Windows, © 1998, 2002, Ken Lagarec.
[21] J. L. Costa- Krämer, J. L. Menéndez, A. Cebollada, F. Briones, D. García, and A. Hernando, J. Magn. Magn. Mater. **210**, 341 (2000).
[22] D. Alders, L. H. Tjeng, F. C. Voogt, T. Hibma, G. A. Sawatzky, C. T. Chen, J. Vogel, M. Sacchi, and S. Iacobucci, Phys. Rev. B **57**, 11623 (1998).
[23] P. Luches, L. Pasquini, S. Benedetti, S. Valeri, R. Rüffer, and F. Boscherini, Appl. Phys. Lett. **101**, 082412 (2012).
[24] J. Gurgul, K. Freindl, A. Kozioł-Rachwał, K. Matlak, N. Spiridis, T. Ślęzak, D. Wilgocka-Ślęzak, and J. Korecki, Surf. Interface Anal. **42**, 696 (2010).
[25] S. Brems, K. Temst, and C. Van Haesendonck, Phys. Rev. Lett. **99**, 067201 (2007).
[26] M. Gester, C. Daboo, R. J. Hicken, S. J. Gray, A. Ercole, and J. A. C. Bland, J. Appl. Phys. **80**, 347 (1996).
[27] B. Beckmann, U. Nowak, and K. D. Usadel, Phys. Rev. Lett. **91**, 187201 (2003).
[28] J. Camarero, J. Sort, A. Hoffmann, J. M. García-Martín, B. Dieny, R. Miranda, and J. Nogués, Phys. Rev. Lett. **95**, 057204 (2005).
[29] F. Q. Zhu and C. L. Chien, J. Appl. Phys. **97**, 10J110 (2005).
[30] P. Luches, S. Benedetti, L. Pasquini, F. Boscherini, M. Zając, J. Korecki, R. Rüffer, and S. Valeri, Nucl. Instrum. Methods Phys. Res. B **268**, 361 (2010).
[31] R. M. Cornell and U. Schwertmann, *The Iron Oxides* (Wiley-Vch Verlag GmbH & Co. KGaA, Weinheim 2003).
[32] C. McCammon, "Mössbauer Spectroscopy of Minerals," in *Mineral Physics & Crystallography: A Handbook of Physical Constants*, edited By T. J. Ahrens (American Geophysical Union, Washington, D. C. 1995), p. 332.
[33] N. N. Greenwood and T. C. Gibb, *Mössbauer Spectroscopy* (Chapman and Hall LTD, London 1971).
[34] S. Ohnishi, A. J. Freeman, and M. Weinert, Phys. Rev. B. **28**, 6741 (1983).
[35] J. Tuček, R. Zbořil, A. Namai, and S. Ohkoshi, Chem. Mater. **22**, 6483 (2010).
[36] C. Wilkinson, A. K. Cheetham, G. J. Long, P. D. Battle, and D. A. O. Hope, Inorg. Chem. **23**, 3136 (1984).
[37] T. J. Regan, H. Ohldag, C. Stamm, F. Nolting, J. Lüning, J. Stöhr, and R. L. White, Phys. Rev. B **64**, 214422 (2001).
[38] P. Luches, M. Liberati, and S. Valeri, Surf. Sci. **532**, 409 (2003).
[39] C. E. Johnson, M. S. Ridout, and T. E. Cranshaw, Proc. Phys. Soc. **81**, 1079 (1963).
[40] J. F. Valderruten, G. A. Pérez Alcázar, and J. M. Grenèche, J. Phys.: Condens. Matter **20**, 485204 (2008).
[41] M. De Marco, X. W. Wang, R. L. Snyder, J. Simmins, S. Bayya, M. White, and M. J. Naughton, J. Appl. Phys. **73**, 6287 (1993).
[42] N. Keller, M. Guyot, A. Das, M. Porte, and R. Krishnan, Solid State Commun. **105**, 333 (1998).
[43] R. F. C. Farrow, M. J. Carey, R. F. Marks, P. M. Rice, and D. J. Smith, Appl. Phys. Lett. **77**, 1191 (2000).
[44] V. G. Bhide and G. K. Shenoy, Phys. Rev. **143**, 309 (1966).
[45] J. Li, E. Arenholz, Y. Meng, A. Tan, J. Park, E. Jin, H. Son, J. Wu, C. A. Jenkins, A. Scholl, H. W. Zhao, C. Hwang, and Z. Q. Qiu, Phys. Rev. B **84**, 012406 (2011).
[46] S. Altieri, M. Finazzi, H. H. Hsieh, H.-J. Lin, C. T. Chen, T. Hibma, S. Valeri, and G. A. Sawatzky, Phys. Rev. Lett. **91**, 137201 (2003).
[47] G. W. R. Leibbrandt, G. Hoogers, and F. H. P. M. Habraken, Phys. Rev. Lett. **68**, 1947 (1992).
[48] R. Subbaraman, S. A. Deshmukh, and S. K. R. S. Sankaranarayanan, J. Phys. Chem. C **117**, 5195 (2013).
[49] M. Sambi, R. Sensolo, G. A. Rizzi, M. Petukhov, and G. Granozzi, Surf. Sci. **537**, 36 (2003).
[50] D. V. Dimitrov, A. S. Murthy, G. C. Hadjipanayis, and C. P. Swann, J. Appl. Phys. **79**, 5106 (1996).
[51] Q. K. Ong, A. Wei, and X.-M. Lin, Phys. Rev. B **80**, 134418 (2009).
[52] D. T. Margulies, F. T. Parker, F. E. Spada, R. S. Goldman, J. Li, R. Sinclair, and A. E. Berkowitz, Phys. Rev. B **53**, 9175 (1996).
[53] C. Gatel, E. Snoeck, V. Serin, and A. R. Fert, Eur. Phys. J. B **45**, 157 (2005).
[54] C. Leighton, J. Nogués, B. J. Jönsson-Åkerman, and I. K. Schuller, Phys. Rev. Lett. **84**, 3466 (2000).